

行政院原子能委員會
委託研究計畫研究報告

環境效應對 SOFC 玻璃陶瓷接合劑高溫機械性質之影響
**Environmental Effects on the Mechanical Properties of
Glass-Ceramic Sealant in Solid Oxide Fuel Cell**

計畫編號：1032001INER025

受委託機關（構）：國立中央大學

計畫主持人：林志光 教授

聯絡電話：03-4267340

E-mail address：t330014@cc.ncu.edu.tw

核研所聯絡人員：吳思翰、劉建國

報告日期：103 年 12 月

目錄

	頁碼
中文摘要	1
英文摘要	2
1. INTRODUCTION.....	4
1.1 Solid Oxide Fuel Cell	4
1.2 Glass Sealant	5
1.3 Joint of Glass-Ceramic Sealant, and Metallic Interconnect	7
1.4 Effect of Environmental Atmosphere	9
1.5 Purposes.....	111
2. MATERIALS AND EXPERIMENTAL PROCEDURES	12
2.1 Materials and Specimen Preparation	12
2.2 Mechanical Testing.....	13
2.3 Microstructural Analysis	14
3. RESULTS AND DISCUSSION	15
3.1 Non-aged Joint of Glass-Ceramic Sealant and Metallic Interconnect.....	16
3.2 100 h-aged Joint of Glass-Ceramic Sealant and Metallic Interconnect.....	18
3.3 1000 h-aged Joint of Glass-Ceramic Sealant and Metallic Interconnect.....	20
3.4 Effects of Thermal Aging in Reducing Environment	22
3.5 Comparison of Joint Strength at Oxidizing and Reducing Environment	24
4. CONCLUSIONS	26
REFERENCES	27
TABLES	32
FIGURES	34

中文摘要

本研究目的在探討還原環境對於玻璃陶瓷和金屬連接板接合件的接合強度及破壞模式的影響，所使用的玻璃陶瓷為核能研究所開發一款代號為 GC-9 的材質，金屬連接板則是使用代號為 Crofer 22 H 的商用肥粒鐵系不銹鋼。藉由製作兩款三明治試片，分別量測接合件在室溫與 800 °C 還原環境下的剪力及張力強度，同時評估還原環境時效處理對接合件強度的影響，並比較在還原環境與氧化環境下接合件所受之影響。結果顯示，經一千小時還原環境時效處理的剪力試片，在常溫下接合強度比未經時效處理之試片增加 24%，而在高溫下則下降 19%；張力試片的接合強度亦有相同之趨勢，與未時效相比較，時效處理後接合強度在常溫下增加與高溫下減少的幅度分別為 47%與 51%。時效處理後常溫接合強度增加的主因可能為：(1) 時效熱處理的過程中，改變 GC-9 玻璃陶瓷基材中缺陷的大小、形貌；(2) 時效熱處理時有應力鬆弛的現象；(3) 時效熱處理後，GC-9 玻璃陶瓷結晶化程度提高。而在時效處理後，高溫下接合強度降低的主因為時效熱處理時，在 GC-9 玻璃陶瓷基材中的玻璃相與結晶相之間形成微孔洞所導致。由微結構及破斷面分析結果發現，接合件試片有四種破壞模式：(1) 破裂發生在玻璃陶瓷基材的內部；(2) 脫層現象發生於玻璃陶瓷基材與鉻酸鋇層的界面；(3) 脫層現象發生於金屬連接板與氧化鉻層的界面；(4) 破裂發生於玻璃陶瓷/鉻酸鋇/氧化鉻的混和層內。將微結構及破斷面分析結果與接合強度做比對，發現當破裂只發生於玻璃陶瓷基材的內部時通常伴隨的較高的接合強度，而破裂發生於界面或混和層時會有較低的接合強度。在還原環境與氧化環境下，未時效試片的接合強度與破壞模式並未有明顯差異，而在一千小時長時效處理後，還原環境與氧化環境皆會降低試片之接合強度，下降的幅度皆為 19%。

Abstract

The objective of this study is to investigate the effect of reducing environment on the mechanical properties of a joint between a glass-ceramic sealant and an interconnect steel. A technique is developed for measuring the joint strength between glass-ceramic and metallic interconnect under tensile or shear loading in reducing environment at room temperature and 800 °C. The applied materials are a GC-9 glass-ceramic developed at the Institute of Nuclear Energy Research (INER) and a commercial Crofer 22 H ferritic stainless steel. Comparison of oxidizing and reducing environment effects on mechanical properties of a joint are also presented for variously, thermally aged conditions. Both tensile and shear joint strengths are increased at room temperature and decreased at 800 °C after a reducing aging treatment. A reducing aging treatment at 800 °C for 1000 h enhances the joint strength of shear loading at room temperature by 24% and degrades it at 800 °C by 19%. A reducing aging treatment at 800 °C for 1000 h increases the joint strength of tensile loading at room temperature by 47% and deteriorates it at 800 °C by 51%. Promotion of joint strength at room temperature may be related to changes in the flaw size and morphology, relaxation of residual stresses, and a greater extent of crystallization during aging treatment. Degradation of joint strength at 800 °C is probably due to formation of micro-voids between crystalline and glassy phases after aging treatment. Through fractography analysis, fracture mode of the joint is correlated with the measured fracture strength. Four types of fracture modes are identified for the joint specimens. Firstly, fracture occurs within the glass-ceramic layer. Secondly, delamination takes place at the interface between the GC-9 glass-ceramic sealant and a

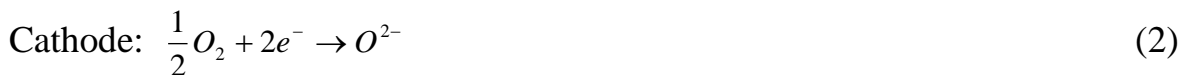
chromate layer. Thirdly, delamination occurs at the interface between the metal substrate and a Cr_2O_3 layer. Fourthly, fracture involves cracking in the interfacial mixed layer of glass-ceramic/chromate/chromia. A greater joint strength is accompanied by cracking within the glass-ceramic layer, while a lower joint strength corresponds to fracture involving interfacial delamination or cracking in the interfacial mixed layer of glass-ceramic/chromate/chromia. The joint strength and fracture mode are comparable between the given reducing and oxidizing environments for non-aged specimens. Thermal aging treatments in both given environments have detrimental effects on the joint strength at 800 °C. Compared to the shear strength of the non-aged specimens, 19% of reduction in strength is both observed for the specimens exposed to the given reducing and oxidizing environments.

1. INTRODUCTION

1.1 Solid Oxide Fuel Cell

Solid oxide fuel cells (SOFCs) are energy conversion devices which produce electricity by the electrochemical reaction between fuel and an oxidant. They directly convert chemical energy into electrical power without an intermediate step of conversion to heat such that the efficiency is higher than that of the power generation systems in conventional power plants. Among the fuel cells developed, SOFCs are the most efficient type. The efficiency of SOFCs with an integrated steam turbine system even can reach about 90% [1]. Compared with other fuel cells, the most important features of SOFC are (1) that components are made of solids, (2) that the utilization of solid oxides as the electrolyte which can prevent leakage or evaporation, and (3) that electrochemical reactions occur without noble catalysts and solid oxides possess highly ionic conductivity at a high operation temperature of 600 °C-1000 °C. Among the SOFCs developed, planar SOFC attracts more attention due to its lower fabricating cost, higher current density, and lower operating temperature [2].

Figure 1 shows the operating principle of an SOFC using hydrogen as fuel [3]. The electrochemical reactions involved are expressed below:



Fuel such as hydrogen is fed into the anode side where it is oxidized by reacting with oxygen ions to produce water and release electrons to the external electrical circuit. Oxidant flows through the cathode side such that oxygen is transformed into oxygen ions as a result of receiving electrons from the external circuit. By means of the thrust of differences in potential and concentration, oxygen ions migrate to the anode through oxygen vacancies in the electrolyte. The electrolyte conducts these ions between the electrodes by maintaining the overall electrical charge balance. Finally, the flow of electrons in the external circuit generates the electrical power, providing for electrical appliance.

Figure 2 shows the structural scheme of a planar SOFC stack [3]. A unit cell is composed of a positive electrode-electrolyte-negative electrode (PEN) plate, interconnects, sealants, and a nickel mesh. The interconnects separate fuel and oxidant gasses and connect individual cells in series in order to obtain sufficient power density. They must be stable in both oxidized and reduced environments, and be compatible with other SOFC components for long-term

operation at high temperatures. Between an interconnect and PEN plate, a nickel mesh is inserted to work as both an electrical connector and fuel gas manifold. In addition, high temperature hermetic sealants are needed and play an important role in planar SOFCs to prevent fuel and oxidant from mixing and leakage during operation. Undesired chemical interaction and mismatch of coefficient of thermal expansion (CTE) between sealant and interconnect will generate damages of stack and decrease the electrochemical performance [4-6].

1.2 Glass Sealant

Sealants are required to maintain the electrical performance of SOFC by avoiding a mixing of fuel and air. Therefore, one of the key issues in development of planar SOFC is the technique of sealing adjacent components to ensure gas tightness. SOFC sealants must have good resistance to both oxidizing and reducing environments and good chemical compatibility with adjacent components. There are several designs of sealants developed for SOFC. They can be classified into compressive sealing and rigid sealing [7]. The compressive sealing such as mica-based sealants does not require a rigid bond with the other SOFC components so that the requirement of CTE match between neighboring components is not as demanded as that in rigid seals. However, they need externally applied forces to compress the fuel cell stack for tight sealing. Rigid seals such as glass-ceramics form a joint that is non-deformable at room temperature. They are susceptible to breaking when subjected to tensile stresses which are generated during non-equilibrium thermal events due to thermal expansion mismatches and brittle properties. However, they do not require an application of constant load during operation and have an excellent sealing performance. Recently, a new joining approach known as bonded compliant seal (BCS) has been developed for planar SOFC stacks [8]. This new sealing design relies on a thin, deformable metal foil that is bonded to the neighboring metallic and ceramic components. The flexible metal is able to decouple the effects of differential thermal expansion between the metallic support structure and the ceramic cell by “trapping” much of stress as elastic or plastic strain within the foil. Consequently the cell stresses in this type of seal are predicted to be much lower than other designs. The BCS is prospective to show excellent hermeticity and high mechanical integrity under thermal cycling and mechanical vibration, while relaxing thermal mismatch stresses in the ceramic cell [8]. Since an exact match of CTE between adjacent components is not required, it provides that a much wider range of alloy compositions can be considered for use in the planar SOFC interconnect. However, more work is needed to understand the effects of the BCS design variables on the stresses and strains that arise in the

components, particularly foil stiffness and geometry [9].

Glass sealants are commonly used in planar SOFC stacks because of easy fabrication and application. An important factor for selection of suitable glass sealants is the glass transition temperature (T_g), because the key mechanism of the glass sealant at operating condition is viscosity [7,10]. A rigid sealant must offer sufficient viscosity and good wetting behavior to form a well adherent bond during joining process, but it should not soften too much to flow during operation for a gas-tight seal. Therefore, T_g of the glass system used as a sealant in SOFCs must be lower than the operating temperature; otherwise, the brittle behavior of a glass at temperature below T_g makes it breakable.

Glass-ceramics are a composite which consists of amorphous and crystalline phases. During operation and sintering process, the amorphous glassy phase transforms into crystalline phases. The mismatch of CTE between these two phases may generate cracks, microvoids or fracture by thermal stress. However, the viscosity and flowability of the amorphous phase could relax the thermal stress caused by thermal mismatch at operation. Crystallization of a glass is sometimes dependent on its composition and thermal events so that it is important to have suitable viscosity and wetting behavior during bonding process and to have sufficient integrity during operation. Therefore, crystallization of glass sealants is an important factor related to thermal stress distribution which may generate some defects during operation. To satisfy necessary requirements, some additives are used to adjust the chemical and physical properties of glass sealants. An overview of the effects achieved by small amounts of additives is shown in Table 1 [11].

Many compositions of glass and glass-ceramic sealants for planar SOFC have been developed. Phosphate, borosilicate, boroaluminosilicate, silicate glasses and glass-ceramics have been developed and evaluated for use in planar SOFC [7,12,13]. In the case of barium-containing glass-ceramics for SOFCs, CTE is increased by crystallization and formation of barium silicate (BaSiO_3) [7]. Crystallization of a barium-containing glass is faster than that of one containing other alkaline-earth metal elements due to a lower activation energy of barium [7]. Barium is used as a network modifier in the glass. BaO/SrO can reduce T_g and glass crystallization temperature (T_c) along with raising the CTE [14]. In the study of Choi and Bansal [15], mechanical properties of some glass sealants with different reinforcements were investigated. The strength of BaO-CaO- Al_2O_3 - SiO_2 (BCAS) glass can be improved by reinforcing with alumina platelets. Zhao et al. [10] characterized the mechanical properties for glass-ceramic sealants of various compositions and with reinforcements of metallic or ceramic fillers. In that study [10], indentation was conducted after the joining process and additional aging at operation temperature. The results indicated that the elastic modulus, hardness, and fracture toughness increased with increasing aging time for some

materials but decreased for the others [10]. It reveals that the mechanical properties are dependent on thermal events.

A new glass-ceramic sealant (designated as GC-9) containing BaO, B₂O₃, Al₂O₃, and SiO₂ for intermediate-temperature planar SOFC (IT-pSOFC) at 700 °C-750 °C has been developed at the Institute of Nuclear Energy Research (INER). The properties of CTE, viscosity, crystallization, and chemical interaction between this sealant and other planar SOFC components (electrolyte, electrode, interconnect, and frame) have been investigated [16-18]. Mechanical properties of GC-9 at various temperatures have been studied by Chang [19]. In the study of Chang [19], GC-9 samples were sintered at 850 °C and aged at 750 °C for 4 and 100 h, designated as non-aged and aged, sintered GC-9 glass-ceramic, respectively, for generating different degrees of crystallization. Results showed that the extent of crystallization was increased with a longer aging time up to 100 h, but the types of crystalline phases were not changed. Strength of both types of GC-9 glass-ceramic increased with temperature due to a crack healing effect at temperature below T_g , as compared to the room-temperature strength [19]. Even though mechanical strength of the aged GC-9 was increased, the ability for relaxing thermal stresses was degraded at high temperature as a result of a less amount of amorphous phase. The strength and stiffness of both aged and non-aged GC-9 glass-ceramics were decreased at temperature above T_g . A research of Yeh [20] further studied the mechanical properties of 1000 h-aged, sintered GC-9 glass-ceramic in comparison with those of Chang [19]. A longer aging time of 1000 h generated additional crystalline phases in the sintered GC-9 glass-ceramic [20]. Because of a greater extent of crystallization, an improvement of flexural strength and stiffness of the aged GC-9 glass-ceramic over the non-aged one was observed at temperature higher than 700 °C [20].

1.3 Joint of Glass-Ceramic Sealant, and Metallic Interconnect

Joining glass-ceramic sealants with metallic interconnects is very common when a rigid type of sealing is applied to IT-pSOFC. Figure 3 [12] shows the locations where seals are used in a planar SOFC stack with metallic internal gas manifolds and metallic interconnects. Common seals include: (a) cell to metal frame; (b) metal frame to metal interconnect; (c) frame/interconnect pair to electrically insulating spacer; (d) stack to base manifold plate [12]. Seals (b) and (d) can be referred to as a joint of glass-ceramic sealant and metallic interconnect.

Generation of thermal stresses cannot be avoided during cyclic operation of SOFC leading the seals to be subjected to tensile and shear stresses [21-23]. Once the stresses exceed the corresponding strength of the joint, the

seals may fail leading to degradation of cell performance. For this reason, it is necessary to investigate the mechanical properties of the joint of glass-ceramic sealant and metallic interconnect for assessment of the structural reliability of an SOFC. The mechanical properties of a joint do not belong to that of a single material due to the multi-layer structure while they are interfacial properties between dissimilar materials. Any interaction between the glass-ceramic sealant and interconnect may influence the mechanical properties of the joint. The results of Chou et al. [24] showed that the joint strength at room temperature drastically reduced after aging in air (850°C/500h) due to formation of SrCrO₄ at the outer sealing edges exposed to air. Besides, joint strength slightly increased after aging in wet reducing environment (850°C/250h) [24]. Unfortunately, interactions such as undesirable chromate formation [24] and electrical short-circuiting [25] are difficult to avoid if ferritic chromia-forming alloys are applied as the interconnect.

The joint strength between glass-ceramic sealants and metallic interconnects in SOFCs have been characterized using various testing techniques. Malzbender et al. [26] characterized the shear strength of the joint between a glass-ceramic sealant (BCAS) and a metallic interconnect (Crofer 22 APU) at the SOFC operation temperature by a symmetric shear test. In addition to shear strength, shear modulus and viscosity of the joint were also determined by a rheological model. At the operation temperature, the as-joined specimens exhibited viscous shear deformation while the viscous shear deformation became more difficult for additionally crystallized specimens [26]. In the study of Weil et al. [27], a modified rupture testing technique was developed by placing a sealed disk specimen in a test fixture and pressurizing the backside of the sample until rupture of seal. An anode-supported bilayer made of nickel oxide-5 mol% yttria stabilized zirconia and 5 mol% yttria stabilized zirconia (NiO-5YSZ/5YSZ) and eight different ferritic stainless steels, five of which had a chromia scale and three of which had an alumina scale, were sealed using a G-18 paste to make sealed disk specimens [27]. In addition to testing as-joined specimens, aging tests were carried out by exposing the sealed disk specimens to ambient air at 750 °C for various hold times. Cyclic thermal testing was performed between room temperature and 750 °C for a number of cycles. The results revealed that in both the as-joined and exposure tested conditions, alumina-forming ferritic steel substrates offered greater bond strength with G-18 [27]. Composition and thickness of the reaction zone between the metal's oxide scale and G-18 glass also influenced the joint strength [27]. The barium chromate layer that developed on the chromia-forming steels exhibited poorer thermal expansion match and tended to grow to a greater thickness than the celsian zone observed on the alumina-formers [27].

Smeacetto et al. [28] evaluated the tensile joint strength between a

glass-ceramic (SACN, $\text{SiO}_2\text{-Al}_2\text{O}_3\text{-CaO-Na}_2\text{O}$) and a metallic interconnect (Crofer 22 APU) at room temperature. It was observed that fracture always occurred within the glass-ceramic and never at the interface of the joint [28]. Another study by Stephens et al. [29] investigated the interfacial strength between the G18 glass-ceramic and Crofer 22 APU substrate at temperatures ranging from 25 °C to 800 °C under both tensile and shear loading. However, two different failure modes were observed in the tensile tests, glass bulk failure mode referring to failure occurring through the glass layer, and interfacial failure mode referring to failure occurring at the glass-metal interface [29]. In the study of Chen [30], the joint strength of GC-9 and Crofer 22 H was investigated under both tensile and shear loading at room temperature and 800 °C. For both tensile and shear joints, the joint strength at room temperature was greater than that at 800 °C [30]. The fracture sites for the tensile joint are within the GC-9 layer at room temperature and 800 °C, while those for the shear joint are at the metal/chromia and glass/chromate interfaces, respectively [30]. Yeh [20] further investigated the effect of interconnect with LSM coating on shear and tensile joint strength at 800 °C. There is a significant decrease in shear and tensile joint strength for samples with LSM coating because of generation of microvoids and microcracks in the chromate layer during sintering process [20]. The results of Chen [30] and Yeh [20] indicate that both tensile and shear joint strengths are lower than the flexural strength of GC-9 so that it is attributed to initiation and propagation of cracks at the interfaces.

1.4 Effect of Environmental Atmosphere

As mentioned above, interactions between the joining components may degrade the mechanical properties of a joint. Therefore, it is necessary to investigate chemical compatibility as well as mechanical integrity of sealant-interconnect joined structures. The joining behavior of various sealants with Cr-containing ferritic stainless steels under simulated SOFC environments have been studied [4,11,24,25,28,31-36]. Some studies were carried out using a single exposure atmosphere, either air (or moist air) representing the cathode-side environment, or a reducing atmosphere simulating the anode-side environment. Recently, some reports [4,11,25] were conducted under dual-atmosphere conditions that closely simulate the joint exposure condition during SOFC operation to determine the interaction between seal and interconnect.

In the study of Yang et al. [31], a BCAS-based glass-ceramic and a ferritic stainless steel (AISI446) were selected as an example to explore the chemical compatibility issue in SOFCs. A glass tape was sandwiched between two interconnects. For investigating the effect of oxide layer on the joining

quality, some AISI446 samples were initially heat treated in vacuum or air at 800 °C for 2 h. Their results indicated that the interaction between glass-ceramic and interconnect is dependent on the exposure condition [31]. At the edge of a joint, where oxygen was accessible, often formed was a BaCrO₄ layer, while in the interior of the joint, chromium or chromia dissolved into glass to form a thin layer of chromium-rich solid solution [31]. In addition, the interaction in the interior of the joint often resulted in the formation of pores which can be avoided through a pre-oxidized treatment [31]. Menzler et al. [32] characterized the interaction of Crofer 22 APU or JS-3 steel with a BCAS-based glass-ceramic under three different atmospheric conditions (air, humidified air, and humidified hydrogen) at 800 °C for durations between 1 and 500 h. It appeared that air or humidified air had no detrimental effect, with respect to adhesion, cracking, and enhanced interdiffusion, on the joint. In contrast, interaction under humidified hydrogen leads to internal oxidation in the steel [32]. In addition, the corrosion intensity of the JS-3 steel was lower than that of the Crofer 22 APU due to containing a less amount of silica and alumina.

Haanappel et al. [25] developed a test method to assess the suitability of combinations of sealing and interconnect under simulated conditions of SOFC stacking. Experiments were conducted with sandwich samples composed of two metallic interconnects, which were joined together by a glass paste. One of the interconnects has a small hole allowing desired gas to spread into the inner part of the sample [25]. Therefore, inner and outer sides can both be exposed to different gases. Each interconnect was connected to Pt-wires to measure the electrical resistance of the sample. The electrical resistance of the sample with air or humidified hydrogen at both sides showed no degradation. In contrast, the insulation capacity was obviously affected by the presence of a dual environment (one side exposed to air and the other side exposed to humidified hydrogen) because of the formation of iron-rich oxide which resulted in “short-circuiting” between the two metallic sheets [25]. In a further study of Haanappel et al. [11], the interaction of several sealants with various ferritic steels was investigated. In that study [11], the influence of small amounts of additives to both the glass-ceramic sealant and the steel on the electrical and chemical behavior was characterized. Their results indicated that internal oxidation, sometimes accompanied with iron-rich oxide, only occurred in the case of glass-ceramic containing minor amounts of PbO [11]. The rate of corrosion strongly depends on the steel composition. With increasing Si content, the rate of corrosion clearly increased, and thus probably reduced the time for occurrence of short-circuiting [11]. Batfalsky et al. [4] took apart the SOFC stacks after operation to observe and elucidate the mechanism responsible for performance degradation or failure. The stack test results in that study [4] were consistent with those of model experiments tailored to verify the interaction effect on a laboratory scale [11,25]. Their

results revealed that severe corrosion of the steel occurred along the seal rims. Near the three-phase boundary of air/sealant/steel, conductive iron-containing oxide nodules, which are related to the short-circuiting, were observed. These oxide nodules finally resulted in stack failure [4]. In addition, the results showed that applying a thin yttria stabilized zirconia (YSZ) layer on the steels could suppress the unfavorable chemical interaction [4].

1.5 Purposes

The high operation temperature enables SOFCs to obtain a superior efficiency of energy conversion while accompanying concerns such as degradation of materials which results from undesirable reactions between components. The thermal stresses caused by considerable CTE mismatch between components and thermal gradients affect the structural durability of SOFC. Excessive thermal stresses may lead to fracture of components endangering the mechanical integrity of an SOFC stack. In an SOFC stack, it is difficult to replace rigid sealants when they fail or fracture because they are bonded to several components, such as interconnects and PENs. Therefore, a systematic investigation of mechanical properties of joints between the glass-ceramic sealant and metallic interconnect at room temperature and operation temperature is essential for development of a reliable SOFC stack.

For those steels and glass-ceramics developed for use in planar SOFC, effects of environment on their joint characteristics, such as electrical performance, chemical properties, and long-term stabilities, have been widely investigated [4,11,24,25,28,31-36]. However, there are only a limited number of studies focused on the effect of environment on the mechanical properties of the joint between interconnect and sealant [20,30,37,38]. In those studies [20,30,37,38], the joint strength and creep behavior under oxidizing environment have been investigated. However, information about the effect of reducing environment on the joint strength is still lack. For these reasons, the objective of this study is to investigate the effect of reducing environment on the mechanical properties of a joint between a glass-ceramic sealant and an interconnect steel. Two loading modes, tensile and shear forces, are applied to characterize the mechanical properties of the joint at both room temperature and 800 °C in wet hydrogen. In addition, some samples are also tested after aging at 800 °C in wet hydrogen to simulate the SOFC working environment. Fractographic and microstructural analyses are conducted with scanning electron microscopy (SEM) and correlated with the mechanical testing results. It is hoped that results of the current study and previous work [20,30,37,38] can provide some useful information for assessing the structural integrity of planar SOFC stacks.

2. MATERIALS AND EXPERIMENTAL PROCEDURES

2.1 Materials and Specimen Preparation

As mentioned in Section 1.3, glass-ceramic sealants are applied as a rigid sealing to bond each layer together and prevent direct mixing of air and fuel SOFC stack. Among the four sealing locations shown in Fig. 3 [12], sealing of a metallic frame to a metallic interconnect (S2) or of a stack to a base manifold plate (S4) is regarded as a joint of glass-ceramic sealant and metallic interconnect. In order to simulate the conditions of a joint subjected to thermal stresses at room temperature and operating temperature, two types of sandwich-like specimens (metal/sealant/metal) are designed in this study for determining the mechanical properties of the joint and investigating the interfacial reactions.

In the present work, the metallic parts of the joint specimens are made of a commercial ferritic stainless steel, Crofer 22 H (ThyssenKrupp VDM GmbH, Werdohl, Germany), which is a heat-resistant alloy developed for application in SOFCs. Chemical compositions and mechanical properties of the Crofer 22 H alloy are listed in Tables 2 and 3 [39], respectively. For Crofer 22 H, the yield strength, ultimate tensile strength, and Young's modulus are decreased but the elongation is increased with an increase in temperature, as shown in Table 3 [39]. The GC-9 glass sealant used was developed at INER for intermediate-temperature planar SOFC. The major chemical composition of the GC-9 glass sealant includes 34 mol% BaO, 34 mol% SiO₂, 9.5 mol% B₂O₃, 12 mol% CaO, 5 mol% La₂O₃, 4.5 mol% Al₂O₃, and 1 mol% ZrO₂ [40]. It was made by mixing the constituent oxide powders followed by melting at 1550 °C for 10 h. After melting, it was poured into a mold preheated to 680 °C to produce GC-9 glass ingots. The GC-9 glass ingots were then annealed at 680 °C for 8 h and cooled down to room temperature. GC-9 glass powders were made by crushing the as-cast glass ingots and sieving with 325 mesh sieves. The average size of the glass powder is 45 μm. Slurries were made by adding into the GC-9 powders the desired amounts of solvent (alcohol), binder (ethyl celluloid), and plasticizer (polyethylene glycol). Table 4 [20] lists the average biaxial flexural strength of the sintered GC-9 glass at various temperatures.

Figure 4 shows the scheme of two types of joint specimens for tensile test (Fig. 4(a)) and shear test (Fig. 4(b)), respectively. The as-received metal plates were cut into slices in the dimensions of 95 mm x 25 mm x 2.5 mm. A pin hole was drilled in each steel slice for applying pin loading. It is effective to minimize bending and twisting effects during a test by means of pin loading. For shear specimens, an edge of each steel slice was milled from the original thickness of 2.5 mm to 1 mm with an area of about 8 mm x 25 mm. After

machining, a GC-9 glass slurry was spread on the joining region of each steel slice to make a half-specimen. The apparent joining areas are 25 mm x 2.5 mm and 25 mm x 6 mm for tensile and shear specimens, respectively. The glass slurry was made of a mixture of glass powder dispersed in ethanol. The half-specimen was then put in a furnace at 70 °C to dry the slurry. A joint specimen was assembled by placing one half-specimen onto another half-specimen to form a Crofer 22 H/GC-9/ Crofer 22 H sandwich specimen through appropriate heat treatments. In the assembling process, the joint specimens were firstly held at 500 °C for 1 h and heated to 900 °C followed by a hold time of 4 h. The heating rate at each heating step in the given assembling process is 5 °C/min. For investigating the effect of environmental atmosphere on the joining quality, some samples were aged in a reducing atmosphere of wet hydrogen (H₂-7 vol% H₂O) at 800 °C for 100 h or 1000 h. The aging treatment was carried out in a furnace attached with a quartz tube filled with desired gas. Photograph of this environmental furnace is shown in Fig. 5. The reducing atmosphere is generated using helium as a carrier gas to pass through water at 90 °C and then mix with pure hydrogen. During the heating step, the helium is used to purge the quartz tube continuously. After reaching 800 °C, the wet hydrogen gas (H₂-7 vol% H₂O) starts to flow into the quartz tube for aging treatment. To avoid water condensation, gas lines are wrapped with a heating tape to maintain at a certain, warm temperature.

2.2 Mechanical Testing

For determination of mechanical properties of the joint at room temperature and 800 °C, the specimens were tested under uni-axial loading on a commercial closed-loop servo-hydraulic test machine (MTS 810). In order to minimize bending and twisting during test, pin loading was applied in the tests. In order to understand the effect of reducing environment on the mechanical properties, a stainless steel tube (AISI 310), which was designed in house and made by a local machine shop, was attached to the specimen for mechanical test in wet hydrogen environment. The tube encloses the specimen in a gas-tight condition, as shown in Fig. 6. Photograph of the experimental setup for mechanical test is given in Fig. 7. During the test, hydrogen with 7 vol% H₂O gas flows in and out of the attached tube to keep the entire tube filled with wet hydrogen gas. All of the mechanical tests at both room temperature and 800 °C are conducted in the given wet hydrogen environment using such an attachment for the specimen. For tests at 800 °C, a compact furnace was used to heat the central portion of the specimen and attachment as shown in Fig. 6. For the high-temperature tests, the specimens were heated to 800 °C with a rate of 5 °C/min and held for 15 min to reach thermal equilibrium before mechanical

testing. During the heating step, the attached stainless tube was flushed with helium gas. When temperature reached 800 °C, the tube was then filled with wet hydrogen. The mechanical tests were conducted by means of displacement control with a loading rate of 0.5 mm/min. For each case, about 3-5 specimens were repeatedly tested and the average strength was determined.

2.3 Microstructural Analysis

After mechanical testing, fracture surface of each specimen was examined with an optical microscope to determine the true joining area. In order to investigate the characteristics of interfaces in the joint, some samples were cut along the longitudinal direction to observe the cross sections. The cross sections were finely polished to optical finish. SEM was also used to examine the interfacial morphology between the glass-ceramic sealant and metallic interconnect. The energy dispersive spectrometer (EDS) module was used for composition analysis in order to understand the elemental distribution in the glass-ceramic sealant and metallic interconnect. The fracture behavior and mode of the joint under tensile stress and shear stress were then characterized.

3. RESULTS AND DISCUSSION

Glass-ceramic sealants suffer thermal stresses of tensile and shear modes during operation as a result of CTE mismatch between glass-ceramic sealants and other components in a planar SOFC stack [21]. Unfortunately, the thermal stresses caused by CTE mismatch are unavoidable because the glass-ceramic sealants are rigidly bonded with adjacent components. Once the critical stresses in the sealants reach a critical value, the glass-ceramic sealants may fail due to the fracture of bulk material or interfacial delamination between the joining surfaces. In order to avoid these problems, there are two approaches: (a) improving the mechanical properties of glass-ceramic sealants; (b) enhancing the interfacial bonding strength between glass-ceramic sealants and metallic interconnects.

In the present work, suitability of the GC-9 glass-ceramic for use in planar SOFC is investigated. Sandwich-like (metal/GC-9/metal) specimens are used to determine the tensile and shear joint strength at room temperature and 800 °C. Formation of adhesive oxide layers is the main mechanism of interfacial joining between the glass-ceramic and metallic interconnect. The bonding strength of the joint originates from the mutual Van Der Waals force of the formed oxide layers. The high-temperature joining mechanism of the GC-9 glass-ceramic and Crofer 22 APU alloy involves formation of two oxide layers with a Cr_2O_3 layer on the surface of Crofer 22 APU connected with a BaCrO_4 layer on the surface of GC-9 [17]. A spinel ($(\text{Cr,Mn})_3\text{O}_4$) layer is formed between these two oxide layers. Figure 8 shows the location of each oxide layer between Crofer 22 H and GC-9 glass-ceramic.

In the following discussion, some of the results in an oxidizing environment have been reported in the thesis of Chen [30]. As sealants used in SOFC are exposed to both oxidizing and reducing environments during operation, it is important to understand the environmental effect on the joint strength at elevated temperature, especially for planar SOFCs which are expected to last for tens of thousands of hours with repeated thermal cycles. In the study of Chen [30], effect of thermal aging in an oxidizing environment on the joint strength was investigated under shear loading at 800 °C. Compared to the shear strength of unaged specimens, a 17-19% reduction of strength was observed for the aged ones. In this study, some of the joined specimens were aged in wet hydrogen at 800 °C for 100 h or 1000 h to assess the effect of aging treatment on the mechanical integrity of the joint. After aging treatment, the aged specimens were tested at both room temperature and 800 °C in a reducing environment.

3.1 Non-aged Joint of Glass-Ceramic Sealant and Metallic Interconnect

After sintering, the non-aged specimens were tested under tensile or shear loading in H₂-7 vol% H₂O at room temperature and 800 °C. Typical force-displacement curves for the non-aged shear specimens tested at room temperature and 800 °C are shown in Fig. 9. The force-displacement curve at room temperature exhibits a typical pattern of brittle fracture with fracture taking place at the linear portion. However, the force-displacement curve at 800 °C exhibits a non-linear failure mode. As the testing temperature of 800 °C is higher than the softening temperature (745 °C) of the GC-9 glass-ceramic, the failure behavior at 800 °C changes from a brittle mode to a ductile one.

The average shear strength of the non-aged joint specimens tested at room temperature and 800 °C are shown in Fig. 10. In Fig. 10, the height of a solid bar indicates the average strength value and the attached error bar represents the standard deviation for each given condition. For the shear loading mode, the average joint strength is 6.8 MPa at room temperature and decreases to 4.2 MPa at 800 °C. The standard deviation is 1.4 MPa and 0.3 MPa, respectively. Figure 11 shows the failure patterns in the non-aged shear specimens tested at room temperature and 800 °C. There are two Crofer 22 H slices in Fig. 11(a); the upper one is separated from the glass-ceramic after testing and the lower one is still adhered with the GC-9 glass-ceramic. There is a shining region in the middle of the upper Crofer 22 H slice, and there is a corresponding darker region in the lower half on the surface of the GC-9 with a shape similar to the shining region. The darker region is the chromia layer which is peeled from the metal substrate. Hence, a metallic luster of the metal substrate appears in the shining region. Note that BaCrO₄ chromate also appears at the periphery of the shining region in Fig. 11(a). However, this phenomenon is not observed in Fig. 11(b). No such shining region is observed on the upper Crofer 22 H slice in Fig. 11(b), but a slightly bright region is observed on the top surface of the Crofer 22 H slice. The composition of the slightly bright region is identified to be the GC-9. Again, BaCrO₄ chromate appears at the periphery of the slightly bright region in Fig. 11(b). Evidences of microstructural observation for selected regions in the fracture surfaces of Fig. 11(a) and 11(b) are provided as follows. Optical and SEM micrographs of two outlined regions of the fracture surface without adhered glass-ceramic in the upper micrograph of Fig. 11(a) are shown in Fig. 12. As Cr, Fe, and O elements are detected in Fig. 12(b), the shining region is indeed the metal substrate. By means of EDX analysis, Cr, Ba, and O elements are detected in Fig. 12(c), indicating that this region is a BaCrO₄ chromate layer. Such microstructural features of SEM for the metal substrate and BaCrO₄ chromate are similar to those observed by Chen [30]. The EDX results of Fig. 12(b) and

12(c) are shown in Fig. 13. Accordingly, for the non-aged shear specimens tested at room temperature, delamination occurs at the interfaces between the glass-ceramic substrate and chromate and between the metal substrate and chromia. For the non-aged shear specimens tested at 800 °C, delamination occurs mostly within the glass-ceramic layer and occasionally at the interface between the glass-ceramic substrate and chromate because the glass-ceramic substrate is softer at 800 °C.

Typical force-displacement curves for the non-aged tensile specimens tested in H₂-7 vol% H₂O at room temperature and 800 °C are shown in Fig. 14. The force-displacement curves at room temperature and 800 °C both exhibit a typical linear brittle fracture pattern. Figure 15 shows the tensile strength of the non-aged joint specimens tested in H₂-7 vol% H₂O at room temperature and 800 °C. For the tensile loading mode, the average joint strength at room temperature is about 31.3 MPa and drops to about 11.9 MPa at 800 °C. The standard deviation for room temperature and 800 °C is 4.4 MPa and 4.7 MPa, respectively. The fracture patterns of non-aged tensile specimens tested at room temperature and 800 °C are not as diverse as those of shear specimens. Figure 16 shows the typical failure patterns of tensile specimens tested at room temperature and 800 °C. Optical and SEM micrographs of an outlined region in the upper micrograph of Fig. 16(a) are shown in Fig. 17. Needle-shape crystalline phases (α -Ba (Al₂Si₂O₈)) are observed in Fig. 17(c), indicating the fracture surface is covered with a glass-ceramic layer. Figure 18 shows the optical and SEM micrographs of an outlined region in the lower micrograph of Fig. 16(b). High-magnification SEM micrographs of the glass-ceramic features are presented in Fig. 18(c). These fractography observations indicate that delamination occurs within the glass-ceramic layer for the tensile specimens tested in H₂-7 vol% H₂O at room temperature. Figures 19 and 20 show the SEM micrographs of the upper and lower parts of Fig. 16(b), respectively. Similar to the results of the tensile specimens tested at room temperature, fracture also occurs within the glass-ceramic layer for tensile specimens tested in H₂-7 vol% H₂O at 800 °C.

In order to investigate the characteristics of interfaces in the joint, some non-aged tensile specimens were cut along the longitudinal direction after the assembling process to observe the cross sections. Cross-sectional microstructures of the interface between GC-9 and Crofer 22 H are shown in the SEM micrographs of Fig. 21 with back-scattered electron (BSE) mode. In Fig. 21, the vertical direction is the direction of applied force during the test. During the joining process, the specimens are subjected to a compressive loading such that some glass-ceramic is squeezed out of the edge of joining area (Fig. 21). As shown in Fig. 21(a), the upper zone is the Crofer 22 H, while the lower region is the glass-ceramic sealant. In Fig. 21(b), a light gray region between Crofer 22 H and GC-9 is observed. Note that the light gray region is not formed uniformly. It is thicker at the edge of the joining area,

which is expected to be exposed to more oxygen during the assembling process, compared to that formed at the central region of the joint. Through EDS analysis, element distributions in these zones are confirmed and shown in Fig. 22. A high intensity of Cr and Fe is found in the region of Crofer 22 H, as expected. As shown in Fig. 22(b), 22(c), and 22(e), a high intensity of Cr, Ba, and O is found in the light gray region, indicating that this region is a BaCrO₄ chromate layer. As mentioned before, the main mechanism of interfacial joining between the glass-ceramic and metallic interconnect is formation of two oxide layers with a Cr₂O₃ layer on the surface of Crofer 22 APU connected with a BaCrO₄ chromate layer on the surface of GC-9 [17]. As shown in Fig. 21(c), a chromia oxide (Cr₂O₃) layer on the metal side is seen and has a thickness about 0.2 μm. However, the BaCrO₄ chromate layer is barely found in the SEM micrographs at the central region of the joint. It is implied that the BaCrO₄ chromate layer is too thin to be observed due to a less amount of oxygen available in the inner central region. Similar observations of formation of a chromate layer at the outer sealing edges are also reported in the study of Chou et al. [24].

3.2 100 h-aged Joint of Glass-Ceramic Sealant and Metallic Interconnect

After a 100-h aging treatment, the aged specimens were tested under tensile or shear loading in H₂-7 vol% H₂O at room temperature and 800 °C. The force-displacement curves for the 100 h-aged shear specimens tested in H₂-7 vol% H₂O at room temperature and 800 °C exhibit a typical pattern of brittle fracture and a non-linear failure mode, respectively (Fig. 23). For the 100 h-aged tensile specimens tested in H₂-7 vol% H₂O at room temperature and 800 °C, the force-displacement curves both exhibit a typical pattern of brittle fracture (Fig. 24.).

The average shear strength of the 100 h-aged joint specimens tested at room temperature and 800 °C is shown in Fig. 25. For the 100 h-aged shear specimens, the average joint strength is 8.2 MPa at room temperature and decreases to 2.3 MPa at 800 °C due to a high-temperature softening mechanism. The standard deviation is 1.4 MPa and 0.3 MPa, respectively. Figure 26 shows the failure patterns in the 100 h-aged shear specimens tested in H₂-7 vol% H₂O at room temperature and 800 °C. As shown in each of Fig. 26(a) and 26(b), the upper Crofer 22 H slice is peeled from the glass-ceramic layer after testing and the lower one is still adhered with the GC-9 glass-ceramic/BaCrO₄ chromate layer. Figures 27 and 28 show the SEM micrographs of the upper and lower parts of Fig. 26(a), respectively. A slightly bright region is observed on the fracture surface of the upper Crofer 22 H slice in Fig. 26(a). Optical and SEM micrographs of an outlined region

of the fracture surface without adhered glass-ceramic in the upper micrograph of Fig. 26(a) are shown in Fig. 27. As Cr, Ba, Fe, and O elements are detected in Fig. 27(b), the region observed is indeed a chromia layer with some residual BaCrO₄ chromate. Optical and SEM micrographs of an outlined region in the lower micrograph of Fig. 26(a) are shown in Fig. 28. Aggregated particles and few needle-shape crystals are observed in Fig. 28(b). As aggregated particles are buried in the residual glass of GC-9 glass-ceramic, it is difficult to identify their phases. Needle-shape crystals are the crystalline phase, alpha-Ba(Al₂Si₂O₈). By means of EDX analysis, Si, Ba, and O elements are detected in Fig. 28(b), indicating that this region is a GC-9 glass-ceramic layer. Accordingly, for the 100 h-aged shear specimens tested at room temperature, delamination occurs mostly at the interfacial mixed layer of glass-ceramic/chromate/chromia. Figures 29 and 30 show the SEM micrographs of the upper and lower parts of Fig. 26(b), respectively. By means of EDS analysis, Cr and O elements are mainly detected in Fig. 29(b). However, some Mn and Ba elements are also found here, revealing that the Crofer 22 H slice is covered with a chromia layer and some spinel phases ((Cr,Mn)₃O₄). In Fig. 30(b), O, Si, and Ba are detected for a high level of content such that the region observed is indeed a glass-ceramic layer. However, Cr is also found in this area. The possible reasons are as follows. (1) Delamination occurs at the interfacial mixed layer of glass-ceramic/chromate/chromia with a thin BaCrO₄ chromate layer formed in the center of the joining area such that O, Si, Ba, and Cr are all detected in the observed area. (2) Chromium vapor species provide a source of chromium for interfacial diffusion between the glass-ceramic layer and metallic interconnect such that Cr is found at the fracture surface. These observations indicate that fracture occurs within the interfacial mixed layer of glass-ceramic/chromate/chromia for the 100 h-aged shear specimens tested at 800 °C.

Figure 31 shows the tensile strength of the 100 h-aged joint specimens tested in H₂-7 vol% H₂O at room temperature and 800 °C. The average joint strength under tensile loading at room temperature is about 46.6 MPa and reduces to about 3.2 MPa at 800 °C. Again, this is due to a high-temperature softening effect. The standard deviation for the results of room temperature and 800 °C is 5.0 MPa and 0.3 MPa, respectively. The failure patterns of the 100 h-aged tensile specimens tested in H₂-7 vol% H₂O at room temperature and 800 °C are shown in Fig. 32. A white region is visible at the right portion of the upper and lower micrographs in Fig. 32(a). Microstructure of the GC-9 glass-ceramic is observed in this white region. Figures 33 and 34 show the SEM micrographs of the upper and lower parts of Fig. 32(a), respectively. By means of EDX analysis, the regions observed in Figs. 33(b) and 34(b) are metal substrate and chromia, respectively. Therefore, for the 100 h-aged tensile specimens tested at room temperature, delamination occurs at the

interfaces between the metal substrate and chromia and within the glass-ceramic layer. SEM micrographs of the upper and lower parts of Fig. 32(b) are shown in Figs. 35 and 36, respectively. The microstructures in the upper and lower micrographs of the 100 h-aged tensile specimens tested at 800 °C are similar to those of the 100 h-aged shear specimens tested at 800 °C. EDX analysis results are also similar to those for 100 h-aged shear specimens tested at 800 °C indicating that fracture occurs within the interfacial mixed layer of glass-ceramic/chromate/chromia for the 100 h-aged tensile specimens tested at 800 °C.

Figure 37 shows the cross-sectional SEM micrographs (BSE mode) of the interface of Crofer 22H/GC-9 in a 100 h-aged tensile specimen. A non-uniform chromate layer at the interface is observed in Fig. 37(a). Again, the BaCrO₄ chromate layer is too thin to be observed at the interior region of the joint. In comparison of the cross-sectional micrographs (Figs. 21 and 37) between non-aged and 100 h-aged specimens, an internal Cr-oxidation zone is found in the steel (Fig. 37(b)). As shown in Fig. 37(c), the thickness of the chromia oxide (Cr₂O₃) layer on the metal side is about 0.2 μm. Below the chromia oxide (Cr₂O₃) layer in Fig. 37(c), some needle-shape crystals are buried in the amorphous phase, indicating that this layer is a glass-ceramic. However, Cr is also detected here, presumably, due to an interfacial diffusion between the glass-ceramic layer and metallic interconnect. Note that the internal oxidation is mostly located at the triple-phase boundary of metal/glass-ceramic sealant/wet hydrogen atmosphere. Similar observations of internal oxidation at the triple-phase boundary are also reported in the study of Menzler et al. [32]. The internal metal oxidation may be attributed to an interaction of hydrogen/water vapor with the double oxide layer to form hydroxides or other volatile species [32]. Additionally, not only the aluminum and silicon in the interconnect but also the elements in the glass-ceramic possibly enhance the internal oxidation [11,32]. It is known that the SOFC operating conditions such as atmosphere, temperature, and time affect the interfacial stability. In general, air atmosphere promotes chromate phase formation and humidified hydrogen atmosphere promotes iron- and chromium-containing phase formation at the interface [11].

3.3 1000 h-aged Joint of Glass-Ceramic Sealant and Metallic Interconnect

The 1000 h-aged specimens were also tested under tensile or shear loading in H₂-7 vol% H₂O at room temperature and 800 °C. Again, the force-displacement relationship of the 1000 h-aged specimens at room temperature and 800 °C is similar to that of the non-aged specimens. Figures 38 and 39 show typical shear and tensile force-displacement curves,

respectively, for the 1000 h-aged joint specimens tested at room temperature and 800 °C. Figure 40 shows the shear strength of the 1000 h-aged joint specimens tested in H₂-7 vol% H₂O at room temperature and 800 °C. For the 1000 h-aged shear specimens, the average joint strength is 8.4 MPa at room temperature and decreases to 3.4 MPa at 800 °C due to a high-temperature softening mechanism. The standard deviation is 1.2 MPa and 0.3 MPa, respectively. Typical failure patterns in the 1000 h-aged shear specimens tested at room temperature and 800 °C are shown in Fig. 41. Figures 42 and 43 show the SEM micrographs of the upper and lower parts of Fig. 41(a), respectively. Needle-shape crystalline phases are observed in Fig. 42(b). In Fig. 43(b), microstructure of the GC-9 glass-ceramic is also observed. These fractography observations indicate that the delamination occurs within the glass-ceramic for the 1000 h-aged shear specimens tested in H₂-7 vol% H₂O at room temperature. SEM micrographs of the upper and lower parts of Fig. 41(b) are shown in Figs. 44 and 45, respectively. Through EDS analysis, Si, Ba, and O elements are detected in both Figs. 44(b) and 45(b) such that fracture occurs within the GC-9 glass-ceramic layer for the 1000 h-aged shear specimens tested at 800 °C. Microstructural features of the GC-9 glass-ceramic such as needle-shape crystals and aggregated particles are observed in Figs. 44(b) and 45(b). In addition, a considerable amount of micro-voids are found between the aggregated particles and glassy phase in the aged samples.

Tensile strength of the 1000 h-aged joint specimens tested in H₂-7 vol% H₂O at room temperature and 800 °C is presented in Fig. 46. Under a tensile loading mode, the average joint strength at room temperature is 46.0 MPa and drops to 5.8 MPa at 800 °C because of a high-temperature softening effect. The standard deviation is 9.4 MPa and 2.2 MPa, respectively, for the room temperature and 800 °C. Typical failure patterns of the 1000 h-aged tensile specimens tested in H₂-7 vol% H₂O at room temperature and 800 °C are shown in Fig. 47. The glass-ceramic features are clearly observed in the upper and lower parts of Fig. 47(a) such that the fracture occurs within the GC-9 glass-ceramic layer for the 1000 h-aged tensile specimens tested at room temperature. Figures 48 and 49 show the SEM micrographs of the upper and lower parts of Fig. 47(b), respectively. Similar to that observed in the 1000 h-aged shear specimens tested at 800 °C, needle-shape crystals, aggregated particles, micro-voids between the aggregated particles, and glassy phase are observed in Fig. 49(b). Furthermore, EDS analysis results indicate the existence of Si, Ba, and O elements in both Figs. 48(b) and 49(b). In this regard, fracture occurs within the GC-9 glass-ceramic layer for the 1000 h-aged tensile specimens tested at 800 °C.

Cross-sectional microstructures at the interface of Crofer 22 H/GC-9 in a 1000 h-aged tensile specimen are shown in Fig. 50. Again, a non-uniform chromate layer and an internal Cr-oxidation zone of steel at the interface are

observed in the cross-sectional micrograph (Fig. 50(a)). However, thickness of the chromia oxide (Cr_2O_3) layer is changed compared to that observed in the 100 h-aged specimens. After a 1000-h aging treatment, the thickness of the chromia layer becomes non-uniform at interface (Fig. 50(b)). The reason is not clear, probably due to depletion of chromia that provides chromium vapor species for interfacial diffusion of chromium [31].

3.4 Effects of Thermal Aging in Reducing Environment

In previous sections, the results of joint strength, fracture modes, and load-displacement relationship for all the given testing conditions in H_2 -7 vol% H_2O are presented. Table 5 lists the average shear strength, standard deviation, and corresponding fracture site for various thermal aging conditions. Results of tensile test are listed in Table 6. As described above, four types of fracture site are observed in the joint specimens. Fracture occurring in the GC-9 substrate is designated as “A” in Tables 5 and 6. Fracture occurring at the interface between the GC-9 substrate and BaCrO_4 layer is designated as “B.” Fracture occurring at the interface between the metal substrate and Cr_2O_3 layer is designated as “C.” Fracture occurring at the interfacial mixed layer of glass-ceramic/chromate/chromia is designated as “D.” If fracture involves two sites, these two fracture sites are marked together. For the shear specimens tested at room temperature, it is seen that the shear joint strength is lower if the fracture involves interfacial delamination or cracking in the mixed layer. For the shear specimens tested at 800 °C, fracture occurring within the glass-ceramic layer accompanies a greater joint strength. Fracture mostly takes place within the glass-ceramic layer for joint specimens tested under tensile loading. For tensile loading mode, 100 h-aged specimens tested at 800 °C has the lowest joint strength with a D type of fracture site, indicating a lower tensile joint strength for fracture involving delamination at the interfacial mixed layer. A similar phenomenon was found in Ref. [29]. As described in Ref. [29], for the joint specimens of a G-18 glass and Crofer 22 APU tested under tensile loading, an interfacial fracture mode generated a lower joining strength in comparison with the case of fracture taking place within the bulk glass sealant. For both tensile and shear loading modes, fracture all occurs within the glass-ceramic layer after 1000-h aging treatment in H_2 -7 vol% H_2O . It reveals that the interfacial bonding strength between different layers is greater than the sealant strength. In this regard, the GC-9 glass-ceramic layer is the weakest layer to resist both shear and tensile loading for joint specimens subjected to a long-term thermal aging treatment in a reducing environment.

The load-displacement relationship obtained at room temperature and 800 °C for the 100 h-aged specimens is not exactly similar to that of the

non-aged specimens. The fracture displacement of 100 h-aged shear specimens at 800 °C is smaller than that at room temperature, while it is larger for non-aged specimens. A similar tendency is observed for the 1000 h-aged specimens under shear loading. In comparison of the force-displacement curves between non-aged and aged specimens, it is seen that the fracture displacement of aged specimens becomes larger at room temperature and smaller at 800 °C. Water in glass has a great influence on a variety of properties for glass. For instance, water increases the rates of structural relaxation and crystallization of glass [41-43]. In addition, water reduces the viscosity of the glass [41-43]. Therefore, fracture displacement of the aged specimens tested at 800 °C is lower than that of the non-aged specimens. Note that the aged specimens were heat treated in H₂-7 vol% H₂O at 800 °C for 100 h or 1000 h.

As the service life of planar SOFCs is expected for 40,000 h or more, it is important to know the effect of reducing environment on the mechanical integrity of the joint. The shear strength of the joint specimens aged in H₂-7 vol% H₂O at 800 °C for 0 h, 100 h, and 1000 h is plotted in Fig. 51. In general, a thermal aging treatment enhances the average shear joint strength at room temperature but deteriorates it at 800 °C. Compared to the shear strength of the unaged specimens, about 21%-24% of increase in strength is observed for the aged specimens tested at room temperature and 19%-45% of reduction in strength for the aged ones tested at 800 °C. Figure 52 shows the tensile strength of the joint specimens aged in H₂-7 vol% H₂O at 800 °C for 0 h, 100 h, and 1000 h. For the tensile specimens, the trend is similar to that in shear specimens. The average tensile joint strength for aged specimens increases in about 47%-49% at room temperature and decreases in 51%-73% at 800 °C. A tendency of increasing joint strength at room temperature after thermal aging in a reducing environment was also found in Ref. [24]. Some explanations for the observed behavior are given as follows. Firstly, it could be related to changes in defect morphology and/or size due to aging treatment [24]. As the sealing glass is devitrified into a polycrystalline multi-phase mixture, changes in the flaw size and morphology may occur in the aging treatment, leading to a reduction in the size of the critical defect for failure during the test [24]. Secondly, it could be related to the relief of residual stresses during the aging treatment. Thirdly, with a longer aging time during operation, devitrification may reduce the residual glass content in the sealant while boosting the ceramic crystalline content. A greater extent of crystallization in the aged specimens is expected to generate a higher strength in the glass-ceramic substrate. As shown in Fig. 53, the extent of main crystalline phase, alpha-Ba(Al₂Si₂O₈), is estimated by calculating the average area proportion of the darker gray needles in fifteen SEM micrographs for each aged condition. As a result, the area proportion of the crystalline alpha-Ba(Al₂Si₂O₈) phase is approximately 23%, 32%, and 32%, in the non-aged, 100 h-aged, and 1000

h-aged GC-9, respectively. Accordingly, the joint strength at room temperature is enhanced for the aged specimens. However, the study of Liu et al. [44] indicates that micro-voids due to CTE difference between the ceramic and glass phases are formed in the aged samples during a cooling process. In Fig. 53, the extent of micro-voids is also calculated for each aged GC-9. The porosity ratio for the non-aged, 100 h-aged, and 1000 h-aged GC-9 is thus determined as 15%, 22%, and 22%, respectively. It might be the reason why the joint strength is decreased at 800 °C for the aged specimens.

3.5 Comparison of Joint Strength at Oxidizing and Reducing Environment

As mentioned above, sealants used in SOFC are exposed to both oxidizing and reducing environments during operation, it is important to understand the environmental effect on the joint properties. Figure 54 shows the comparison of shear joint strength at room temperature and 800 °C for joint specimens tested in H₂-7 vol% H₂O and in air. For the shear specimens tested in air, the average joint strength is 6.6 MPa at room temperature and decreases to 4.7 MPa at 800 °C. The corresponding standard deviation is 1.6 MPa and 0.3 MPa, respectively. The comparison of tensile joint strength at room temperature and 800 °C for joint specimens tested in H₂-7 vol% H₂O and in air is shown in Fig. 55. The average tensile strength tested in air is 23 MPa at room temperature and decreases to 12.7 MPa at 800 °C. The corresponding standard deviation each is 3.3 MPa. Note that the data of air are taken from Ref. [30]. The softening behavior of the glass-ceramic sealant at 800 °C is observed in both H₂-7 vol% H₂O and air. As shown in Figs. 54 and 55, the average joint strength for non-aged specimens in oxidizing environment is slightly higher than that in reducing environment except for the tensile strength at room temperature. However, in consideration of the standard deviation and batch effects, the joint strength may be seen as comparable between the two given environments for non-aged specimens.

Typical failure patterns for the non-aged shear specimens tested in air at room temperature and 800 °C are shown in Fig. 56 [30]. A shining region is observed in the middle of the lower Crofer 22 H substrate and a corresponding chromia layer is peeled from the lower substrate, as shown in Fig. 56(a) [30]. It indicates that delamination between the chromia layer and the Crofer 22 H substrate dominates the failure at room temperature. For the non-aged shear specimens tested in air at 800 °C (Fig. 56(b)), it is seen that in addition to delamination at interfaces, fracture even takes place in the glass-ceramic layer [30]. Typical failure patterns of the tensile specimens tested in air at room temperature and 800 °C are shown in Fig. 57 [30]. For the tensile specimens, fracture takes places in the glass-ceramic layer at both

room temperature and 800 °C [30]. For the non-aged specimens, fracture modes are comparable between the two given environments. However, the color observed on the fracture surface shows some differences in those tested at 800 °C. As shown in the lower part of Figs. 11(b) and 56(b), the peripheral region of the glass-ceramic is yellowish for an oxidizing environment, while it changes to green for a wet reducing environment. A major issue with chromia forming alloys is the evaporation of chromium species at elevated temperatures. The main volatile species formed from evaporation of Cr₂O₃ in atmospheres containing O₂ and H₂O are CrO₃, CrO₂(OH)₂, and CrO₂(OH) [45]. These species are formed by the following reactions:

(4)

(5)

As shown in Eqs. (4) and (5), the partial pressure of volatile chromium species is dependent on the partial pressure of oxygen and water vapor. At very low water vapor pressures, the CrO₃ will be the predominant volatile chromium species [45]. Atmospheric air is normally moist to some extent which leads to predominant formation of CrO₂(OH)₂ [45]. As described above, chromium species are not the same between these two testing environments. Additionally, chromium evaporation takes place at high temperature such that color changes only observed in the non-aged specimens tested at 800 °C.

Figure 58 shows the shear strength of the joint specimens aged in H₂-7 vol% H₂O or air at 800 °C for 0 h and 1000 h. The average joint strength is 4.7 MPa and 3.8 MPa, respectively, for non-aged and 1000 h-aged specimens, which are thermally aged and tested in air. The corresponding standard deviation is 0.3 MPa and 0.5 MPa, respectively. As shown in Fig. 58, both aging treatments have similar detrimental effects on the joint strength at 800 °C. Compared to the shear strength of the non-aged specimens, 19% of reduction in strength is observed for the specimens exposed to both the given reducing and oxidizing environments. The mechanism causes reduction of strength in the oxidizing atmosphere is similar to that in the reducing atmosphere. Note that fracture occurs within the glass-ceramic layer for both types of 1000 h-aged specimens. As mentioned before, some micro-voids are formed in the aged samples because of CTE mismatch between the ceramic and glass phases such that fracture takes place in the glass-ceramic substrate. However, a thicker chromate layer formed in the oxidizing environment may play a role in reduction of strength. Since the chromate layer of high CTE ($22-23 \times 10^{-6} \text{ }^\circ\text{C}^{-1}$) becomes thicker as compared to the non-aged specimens, high thermal stresses are expected to generate cracks during cooling after an oxidizing aging treatment [30].

4. CONCLUSIONS

- (1) In the current study, a technique for measuring the joint strength between glass-ceramic and metallic interconnect in reducing environment at room temperature and 800 °C is developed.
- (2) Both tensile and shear joint strengths are increased at room temperature and decreased at 800 °C after a long-term reducing aging treatment in H₂-7 vol% H₂O. A reducing aging treatment at 800 °C for 1000 h enhances the joint strength of shear loading at room temperature by 24% and degrades it at 800 °C by 19%. A reducing aging treatment at 800 °C for 1000 h increases the joint strength of tensile loading at room temperature by 47% and deteriorates it at 800 °C by 51%.
- (3) For the shear specimens tested in H₂-7 vol% H₂O at 800 °C, fracture occurring within the glass-ceramic layer accompanies a greater joint strength. For a lower shear joint strength, fracture involves interfacial delamination or cracking in the interfacial mixed layer of glass-ceramic/chromate/chromia.
- (4) For the tensile specimens tested in H₂-7 vol% H₂O, a greater joint strength corresponds to fracture occurring only in the glass-ceramic sealant layer. For a lower tensile joint strength, fracture involves cracking in the interfacial mixed layer of glass-ceramic/chromate/chromia.
- (5) Promotion of joint strength at room temperature may be related to changes in the flaw size and morphology, relaxation of residual stresses, and a greater extent of crystallization during aging treatment. Degradation of joint strength at 800 °C is probably due to formation of micro-voids between crystalline and glassy phase after aging treatment.
- (6) The joint strength and fracture mode are comparable between a reducing environment and an oxidizing environment for non-aged specimens. However, the color observed on the fracture surface is different between the two given environments because of chromium evaporation at high temperature. In addition, aging treatments in both given environments have detrimental effects on the joint strength at 800 °C. Compared to the shear strength of the non-aged specimens, 19% of reduction in strength at 800 °C is both observed for the specimens exposed in 1000 h to the given reducing and oxidizing environment, respectively.

REFERENCES

1. A. Choundhury, H. Chandra, and A. Arora, "Application of Solid Oxide Fuel Cell Technology for Power Generation-A Review," *Renewable and Sustainable Energy Reviews*, Vol. 20, pp. 430-442, 2013.
2. K. Kendall, N. Q. Minh, and S. C. Singhal, "Cell and Stack Designs," Chapter 8 in *High Temperature Solid Oxide Fuel Cells: Fundamentals, Design and Applications*, edited by S. C. Singhal and K. Kendall, Elsevier, Kidlington, UK, 2003.
3. W. Z. Zhu and S. C. Deevi, "A Review on the Status of Anode Materials for Solid Oxide Fuel Cells," *Materials Science and Engineering*, Vol. A362, pp. 228-239, 2003.
4. P. Batfalsky, V. A. C. Haanappel, J. Malzbender, N. H. Menzler, V. Shemet, I. C. Vinke, and R. W. Steinbrech, "Chemical Interaction Between Glass-Ceramic Sealants and Interconnect Steels in SOFC Stacks," *Journal of Power Sources*, Vol. 155, pp. 128-137, 2006.
5. Y. Zhao and J. Malzbender, "Elevated Temperature Effects on the Mechanical Properties of Solid Oxide Fuel Cell Sealing Materials," *Journal of Power Sources*, Vol. 239, pp. 500-504, 2013.
6. A. Nakajo, J. Kuebler, A. Faes, U. F. Vogt, Hans J. Schindler, L.-K. Chiang, S. Modena, J. van Herle, and T. Hocker, "Compilation of Mechanical Properties for the Structural Analysis of Solid Oxide Fuel Cell Stacks. Constitutive Materials of Anode-Supported Cells," *Ceramics International*, Vol. 38, pp. 3907-3927, 2012.
7. J. W. Fergus, "Sealants for Solid Oxide Fuel Cells," *Journal of Power Sources*, Vol. 147, pp. 46-57, 2005.
8. K. S. Weil, J. S. Hardy, and B. J. Koeppel, "New Sealing Concept for Planar Solid Oxide Fuel Cells," *Journal of Materials Engineering and Performance*, Vol 15, pp. 427-432, 2006.
9. K. S. Weil and B. J. Koeppel, "Thermal Stress Analysis of the Planar SOFC Bonded Compliant Seal Design," *International Journal of Hydrogen Energy*, Vol. 33, pp. 3976-3990, 2008.
10. Y. Zhao, J. Malzbender, and S. M. Gross, "The Effect of Room Temperature and High Temperature Exposure on the Elastic Modulus, Hardness and Fracture Toughness of Glass Ceramic Sealants for Solid Oxide Fuel Cells," *Journal of the European Ceramic Society*, Vol 31, pp. 541-548, 2011.

11. V. A. C. Haanappel, V. Shemet, S. M. Gross, Th. Koppitz, N. H. Menzler, M. Zahid, and W. J. Quadackers, "Behaviour of Various Glass-Ceramic Sealants with Ferritic Steels under Simulated SOFC Stack Conditions," *Journal of Power Sources*, Vol. 150, pp. 86-100, 2005.
12. P. A. Lessing, "A Review of Sealing Technologies Applicable to Solid Oxide Electrolysis Cells," *Journal of Materials Science*, Vol. 42, pp. 3465-3476, 2007.
13. K. S. Weil, "The State-of-the-Art in Sealing Technology for Solid Oxide Fuel Cells," *JOM*, Vol. 58, pp. 37-44, 2006.
14. G. Kaur, O. P. Pandey, and K. Singh, "Interfacial Study Between High Temperature $\text{SiO}_2\text{-B}_2\text{O}_3\text{-AO-La}_2\text{O}_3$ (A = Sr, Ba) Glass Seals and Crofer 22APU for Solid Oxide Fuel Cell Applications," *International Journal of Hydrogen Energy*, Vol. 37, pp. 6862-6874, 2012.
15. S. R. Choi and N. P. Bansal, "Mechanical Properties of SOFC Seal Glass Composites," *Ceramic Engineering and Science Proceedings*, Vol. 26, pp. 275-283, 2005.
16. C.-K. Liu, T.-Y. Yung, and K.-F. Lin, "Effect of La Addition on the Thermal and Crystalline Properties of $\text{SiO}_2\text{-B}_2\text{O}_3\text{-Al}_2\text{O}_3\text{-BaO}$ Glasses," *Proceedings of the Annual Conference of the Chinese Ceramic Society (CD-ROM)*, 2007. (in Chinese)
17. C.-K. Liu, T.-Y. Yung, S.-H. Wu, and K.-F. Lin, "Study on a $\text{SiO}_2\text{-B}_2\text{O}_3\text{-Al}_2\text{O}_3\text{-BaO}$ Glass System for SOFC Applications," *Proceedings of the MRS_Taiwan Annual Meeting (CD-ROM)*, 2007. (in Chinese)
18. C.-K. Liu, T.-Y. Yung, and K.-F. Lin, "Isothermal Crystallization Properties of $\text{SiO}_2\text{-B}_2\text{O}_3\text{-Al}_2\text{O}_3\text{-BaO}$ Glass," *Proceedings of the Annual Conference of the Chinese Ceramic Society (CD-ROM)*, 2008. (in Chinese)
19. H.-T. Chang, "High-Temperature Mechanical Properties of a Glass Sealant for Solid Oxide Fuel Cell," Ph.D. Thesis, National Central University, 2010.
20. J.-H. Yeh, "Analysis of High-Temperature Mechanical Durability for the Joint of Glass Ceramic Sealant and Metallic Interconnect for Solid Oxide Fuel Cell," M.S. Thesis, National Central University, 2011.
21. C.-K. Lin, T.-T. Chen, Y.-P. Chyou, and L.-K. Chiang, "Thermal Stress Analysis of a Planar SOFC Stack," *Journal of Power Sources*, Vol. 164, pp. 238-251, 2007.

22. A.-S. Chen, "Thermal Stress Analysis of a Planar SOFC Stack with Mica Sealants," M.S. Thesis, National Central University, 2007.
23. C.-K. Lin, L.-H. Huang, L.-K. Chiang, and Y.-P. Chyou, "Thermal Stress Analysis of a Planar Solid Oxide Fuel Cell Stacks: Effects of Sealing Design," *Journal of Power Sources*, Vol. 192, pp. 515-524, 2009.
24. Y.-S. Chou, J. W. Stevenson, and P. Singh, "Effect of Pre-Oxidation and Environmental Aging on the Seal Strength of a Novel High-Temperature Solid Oxide Fuel Cell (SOFC) Sealing Glass with Metallic Interconnect," *Journal of Power Sources*, Vol. 184, pp. 238-244, 2008.
25. V. A. Haanappel, V. Shemet, I. C. Vinke and W. J. Quadackers, "A Novel Method to Evaluate the Suitability of Glass Sealant-Alloy Combinations under SOFC Stack Conditions," *Journal of Power Sources*, Vol. 141, pp. 102-107, 2005.
26. J. Malzbender, J. Mönch, R. W. Steinbrech, T. Koppitz, S. M. Gross and J. Remmel, "Symmetric Shear Test of Glass-Ceramic Sealants at SOFC Operation Temperature," *Journal of Materials Science*, Vol. 42, pp. 6297-6301, 2007.
27. K. S. Weil, J. E. Deibler, J. S. Hardy, D. S. Kim, G.-G. Xia, L. A. Chick, and C. A. Coyle, "Rupture Testing as a Tool for Developing Planar Solid Oxide Fuel Cell Seals," *Journal of Materials Engineering and Performance*, Vol. 13, pp. 316-326, 2004.
28. F. Smeacetto, M. Salvo, M. Ferraris, V. Casalegno, P. Asinari, and A. Chrysanthou, "Characterization and Performance of Glass-Ceramic Sealant to Join Metallic Interconnects to YSZ and Anode-Supported-Electrolyte in Planar SOFCs," *Journal of the European Ceramic Society*, Vol. 28, pp. 2521-2527, 2008.
29. E. V. Stephens, J. S. Vetrano, B. J. Koepfel, Y. Chou, X. Sun, and M. A. Khaleel, "Experimental Characterization of Glass-Ceramic Seal Properties and their Constitutive Implementation in Solid Oxide Fuel Cell Stack Models," *Journal of Power Sources*, Vol. 193, pp. 625-631, 2009.
30. J.-Y. Chen, "Analysis of Mechanical Properties for the Joint of Metallic Interconnect and Glass Ceramic in Solid Oxide Fuel Cell," M.S. Thesis, National Central University, 2010.
31. Z. Yang, K. D. Meinhardt, and J. W. Stevenson, "Chemical Compatibility of Barium-Calcium-Aluminosilicate Sealing Glasses with the Ferritic Stainless Steel Interconnect in SOFCs," *Journal of the Electrochemical Society*, Vol. 150, pp. A1095-A1101, 2003.

32. N. H. Menzler, D. Sebold, M. Zahid, S. M. Gross, and T. Koppitz, "Interaction of Metallic SOFC Interconnect Materials with Glass–Ceramic Sealant in Various Atmospheres," *Journal of Power Sources*, Vol. 152, pp. 156-167, 2005.
33. F. Smeacetto, M. Salvo, M. Ferraris, J. Cho, and A. R. Bocaccini, "Glass–Ceramic Seal to Join Crofer 22 APU Alloy to YSZ Ceramic in Planar SOFCs," *Journal of the European Ceramic Society*, Vol. 28, pp. 61-68, 2008.
34. V. A. Haanappel, V. Shemet, I. C. Vinke, S. M. Gross, T. Koppitz, N. H. Menzler, M. Zahid, and W. J. Quadackers, "Evaluation of the Suitability of Various Glass Sealant-Alloy Combinations under SOFC Stack Conditions," *Journal of Materials Science*, Vol. 40, pp. 1583-1592, 2005.
35. Z. Yang, J. W. Stevenson, and K. D. Meinhardt, "Chemical Interactions of Barium–Calcium–Aluminosilicate-Based Sealing Glasses with Oxidation Resistant Alloys," *Solid State Ionics*, Vol. 160, pp. 213-225, 2003.
36. Z. Yang, G. Xia, K. D. Meinhardt, K. S. Weil, and J. W. Stevenson, "Chemical Stability of Glass Seal Interfaces in Intermediate Temperature Solid Oxide Fuel Cells," *Journal of Materials Engineering and Performance*, Vol. 13, pp. 327-334, 2003.
37. J.-W. Tian, "Analysis of Thermal Stress and Mechanical Properties for the Components of Solid Oxide Fuel Cell," M.S. Thesis, National Central University, 2009.
38. K.-L. Lin, "Analysis of Creep Properties of Glass Ceramic Sealant and Its Joint with Metallic Interconnect for Solid Oxide Fuel Cells," M.S. Thesis, National Central University, 2012.
39. Y.-T. Chiu, "Creep and Thermo-Mechanical Fatigue Properties of Ferritic Stainless Steels for Use in Solid Oxide Fuel Cell Interconnect," Ph.D. Thesis, National Central University, 2012.
40. C.-K. Liu, T.-Y. Yung, K.-F. Lin, R.-Y. Lee, and T.-S. Lee, Glass-Ceramic Sealant for Planar Solid Oxide Fuel Cells, United States Patent No. 7,897,530 B2, 2011.
41. M. Tomozawa, H. Li, and K. M. Davis, "Water Diffusion, Oxygen Vacancy Annihilation and Structural Relaxation in Silica Glasses," *Journal of Non-Crystalline Solids*, Vol. 179, pp. 162-169, 1994.
42. S. Fujita, A. Sakamoto, and M. Tomozawa, "Behavior of Water in Glass During Crystallization," *Journal of Non-Crystalline Solids*, Vol. 320, pp.

56-63, 2003.

43. T. Jin, M. O. Naylor, J. E. Shelby, and S. T. Misture, "Galliosilicate Glasses for Viscous Sealants in Solid Oxide Fuel Cell Stacks: Part III, Behavior in Air and Humidified Hydrogen," *International Journal of Hydrogen Energy*, Vol. 38, pp. 16308-16319, 2013.
44. W. Liu, X. Sun, and M. A. Khaleel, "Predicting Young's Modulus of Glass/Ceramic Sealant for Solid Oxide Fuel Cell Considering the Combined Effects of Aging, Micro-Voids and Self-Healing," *Journal of Power Sources*, Vol. 185, pp. 1193-1200, 2008.
45. P. Alnegren, "Oxidation Behavior of Selected FeCr Alloys in Environments Relevant For Solid Oxide Electrolysis Applications," M.S. Thesis, Chalmers University, 2012.

TABLES

Table. 1 Effects of the presence of small amounts of additives in the glass-ceramic sealant [9]

Compound	Effect
La ₂ O ₃ , Nd ₂ O ₃ , Y ₂ O ₃	Increase CTE, T_g , and Melting temperature (T_m); control viscosity
B ₂ O ₃	Reduce CTE and surface tension; improve flux
ZnO, PbO	Reducing agent, improve flux
Al ₂ O ₃	Retard crystallization, improve flux
Cr ₂ O ₃ , V ₂ O ₅	Reduce surface tension
NiO, CuO, CoO, MnO	Improve adhesion
TiO ₂ , ZrO ₂ , SrO	Promote crystallization
Sb ₂ O ₅	Oxidizing agent

Table. 2 Chemical composition of Crofer 22 H alloy (in wt.%)

Fe	C	Cr	Mn	Si	Ti	Nb
Bal.	0.007	22.93	0.43	0.21	0.07	0.51
Cu	S	P	Al	W	La	
0.02	<0.002	0.014	0.02	1.94	0.08	

Table. 3 Average of mechanical properties for Crofer 22 H alloy [39]

Temperature (°C)	Yield strength (MPa)	Ultimate tensile strength (MPa)	Young's modulus (GPa)	Elongation (in 12 mm) (%)
25	406	567	205	27
600	286	359	181	29
650	241	295	161	30
700	204	219	142	39
750	140	147	88	54
800	120	123	86	55

Table. 4 Average biaxial flexural strength (σ_f) for variously aged GC-9 glass at different temperatures [20]

	Aged condition	Temperature				
		25 °C	650 °C	700 °C	750 °C	800 °C
σ_f (MPa)	Non-aged	38	50	47	33	18
	100 h-aged	38	49	53	54	32
	1000 h-aged	45	59	49	57	36

Table. 5 Average shear strength, standard deviation, and fracture site of variously aged joint specimens tested in H₂-7 vol% H₂O

Test temperature (°C)	Aged condition	Average shear strength (MPa)	Standard deviation (MPa)	Fracture site*
25	Non-aged	6.8	1.4	B+C
25	100 h-aged	8.2	1.4	D
25	1000 h-aged	8.4	1.2	A
800	Non-aged	4.2	0.3	A+B
800	100 h-aged	2.3	0.3	D
800	1000 h-aged	3.4	0.3	A

*A: in glass-ceramic sealant layer; B: at the interface between the glass-ceramic substrate and BaCrO₄ layer; C: at the interface between the metal substrate and Cr₂O₃ layer; D: at the interfacial mixed layer of glass-ceramic/chromate/chromia.

Table. 6 Average tensile strength, standard deviation, and fracture site of variously aged joint specimens tested in H₂-7 vol% H₂O

Test temperature (°C)	Aged condition	Average tensile strength (MPa)	Standard deviation (MPa)	Fracture site*
25	Non-aged	31.3	4.4	A
25	100 h-aged	46.6	5.0	A+C
25	1000 h-aged	46.0	9.4	A
800	Non-aged	11.9	4.7	A
800	100 h-aged	3.2	0.3	D
800	1000 h-aged	5.8	2.2	A

FIGURES

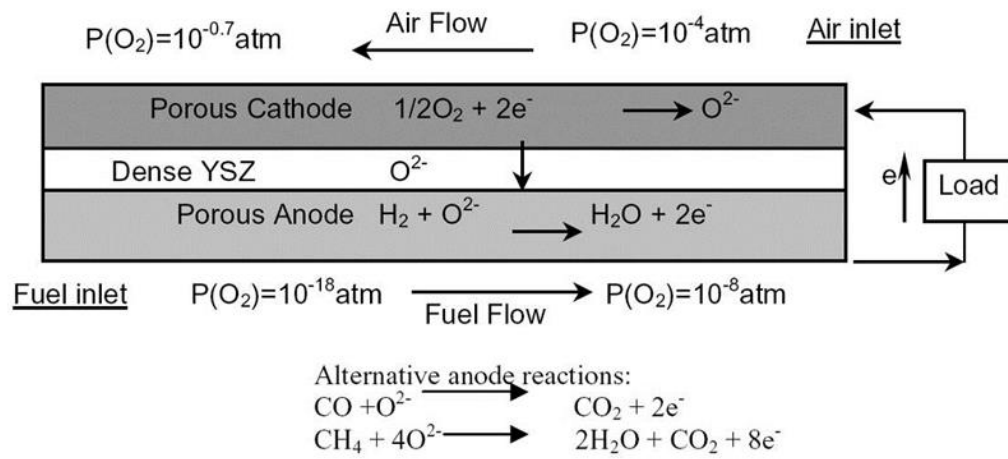


Fig. 1 Operating principle of a single SOFC unit using hydrogen as fuel. [3]

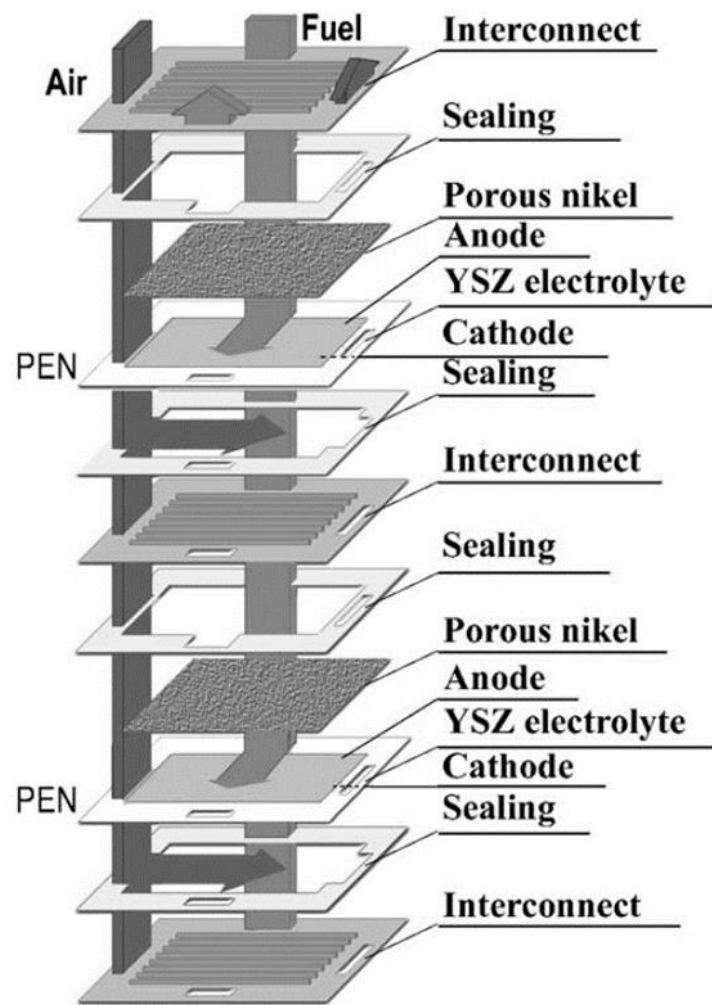


Fig. 2 Structural scheme of a planar SOFC stack. [3]

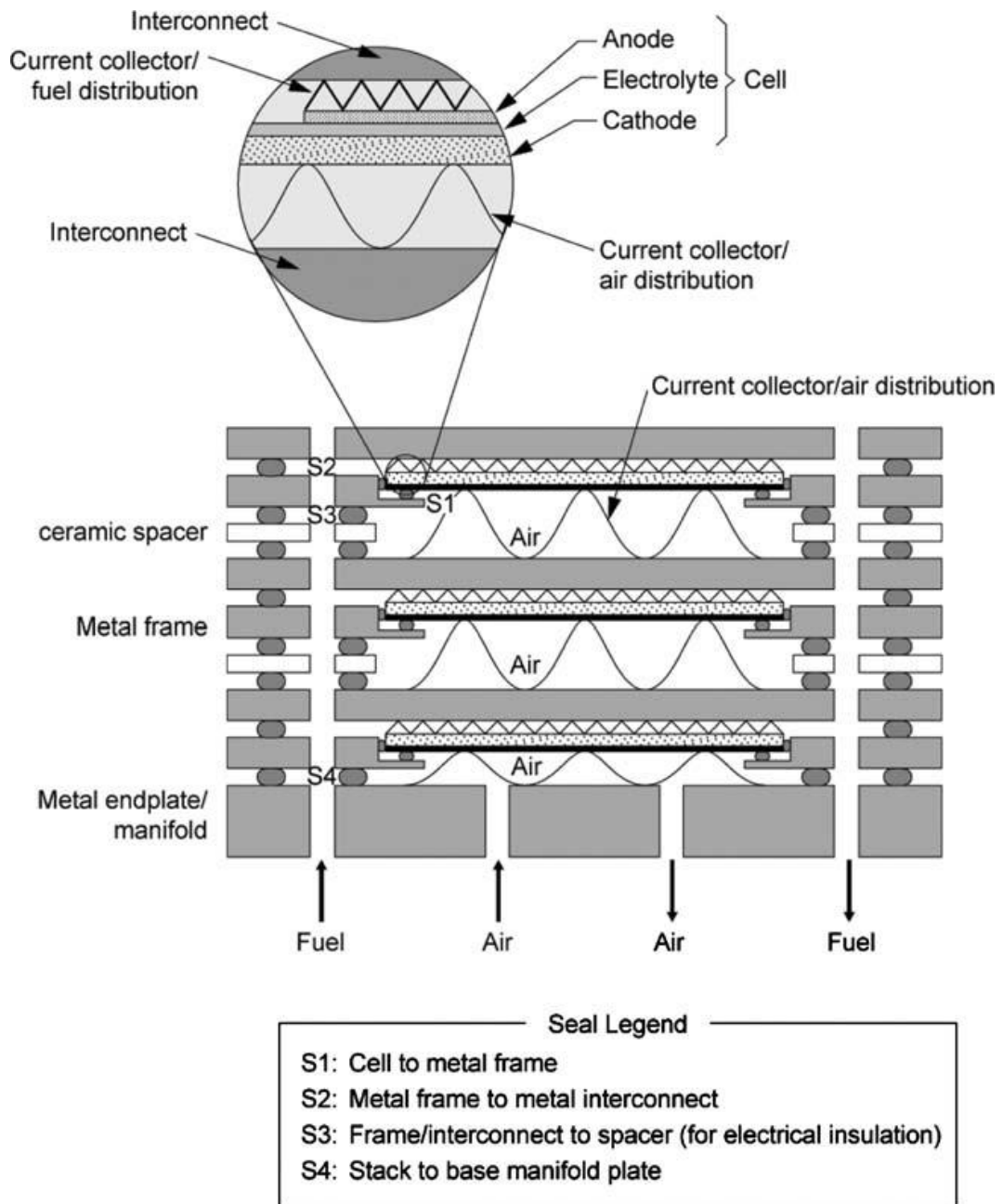
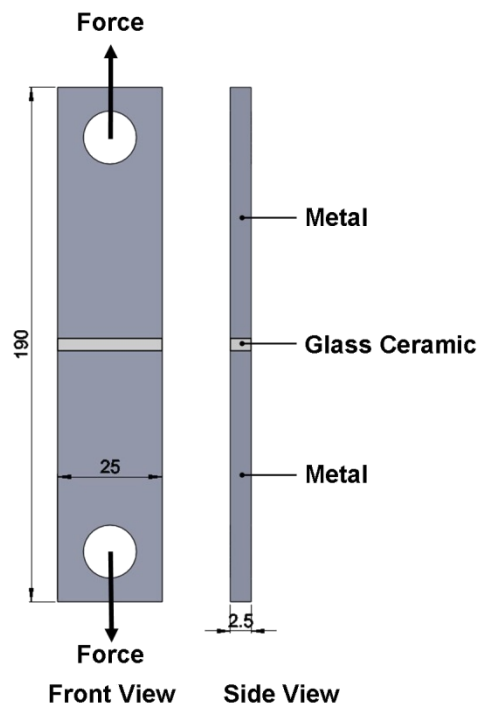
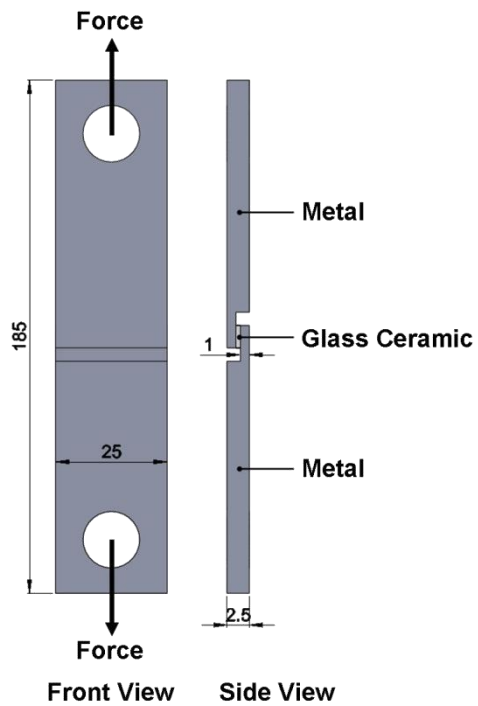


Fig. 3 Scheme of seals used in a planar SOFC stack with metallic interconnects and metallic internal gas manifold channels. [12]



(a)



(b)

Fig. 4 Scheme of two types of joint specimens: (a) tensile specimen; (b) shear specimen. (Dimensions: mm)

Quartz tube

Furnace



Fig. 5 Photograph of the environmental furnace for aging treatment.

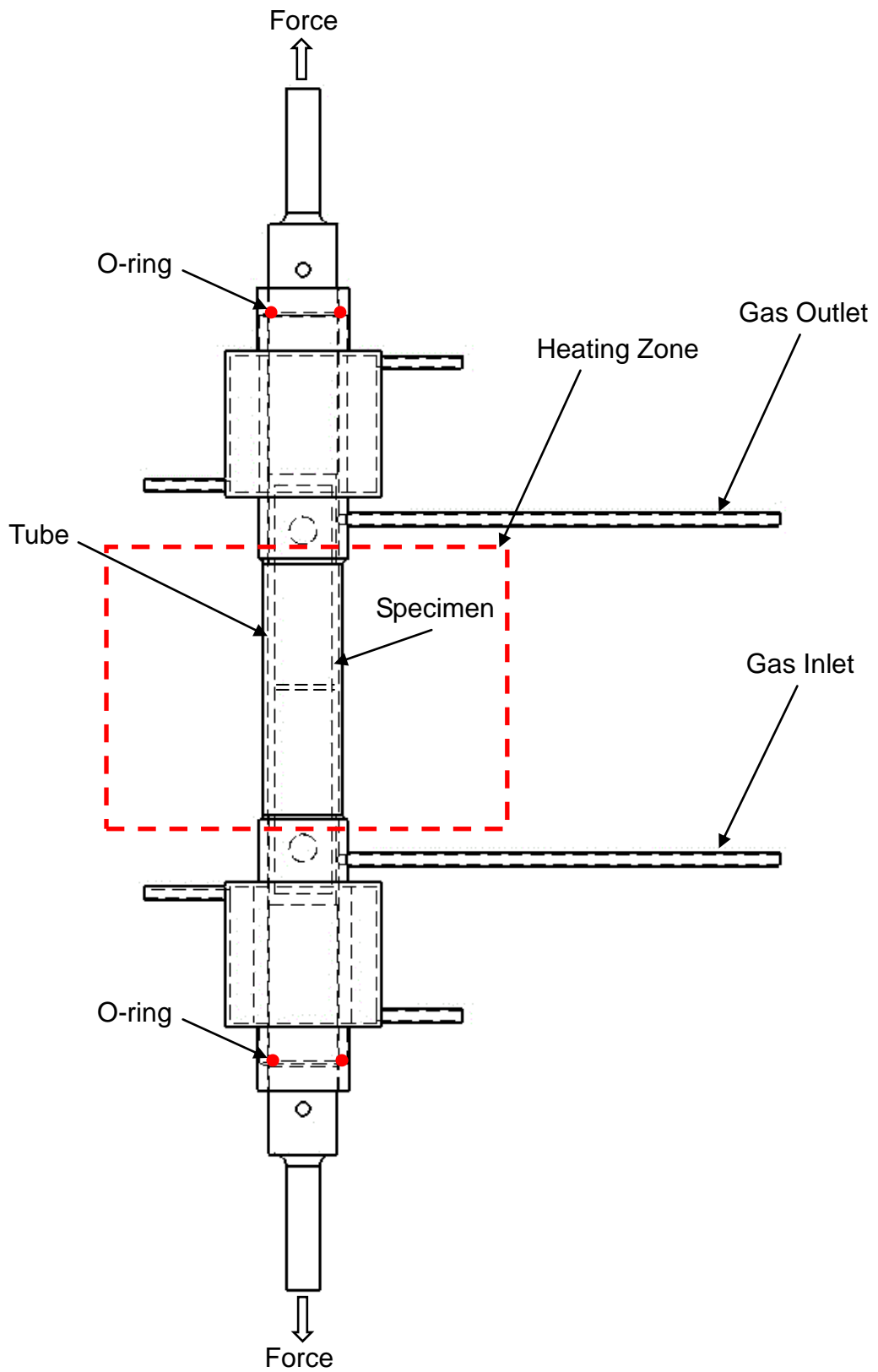


Fig. 6 Schematic of specimen enclosed by a gas-tight tube in mechanical test.

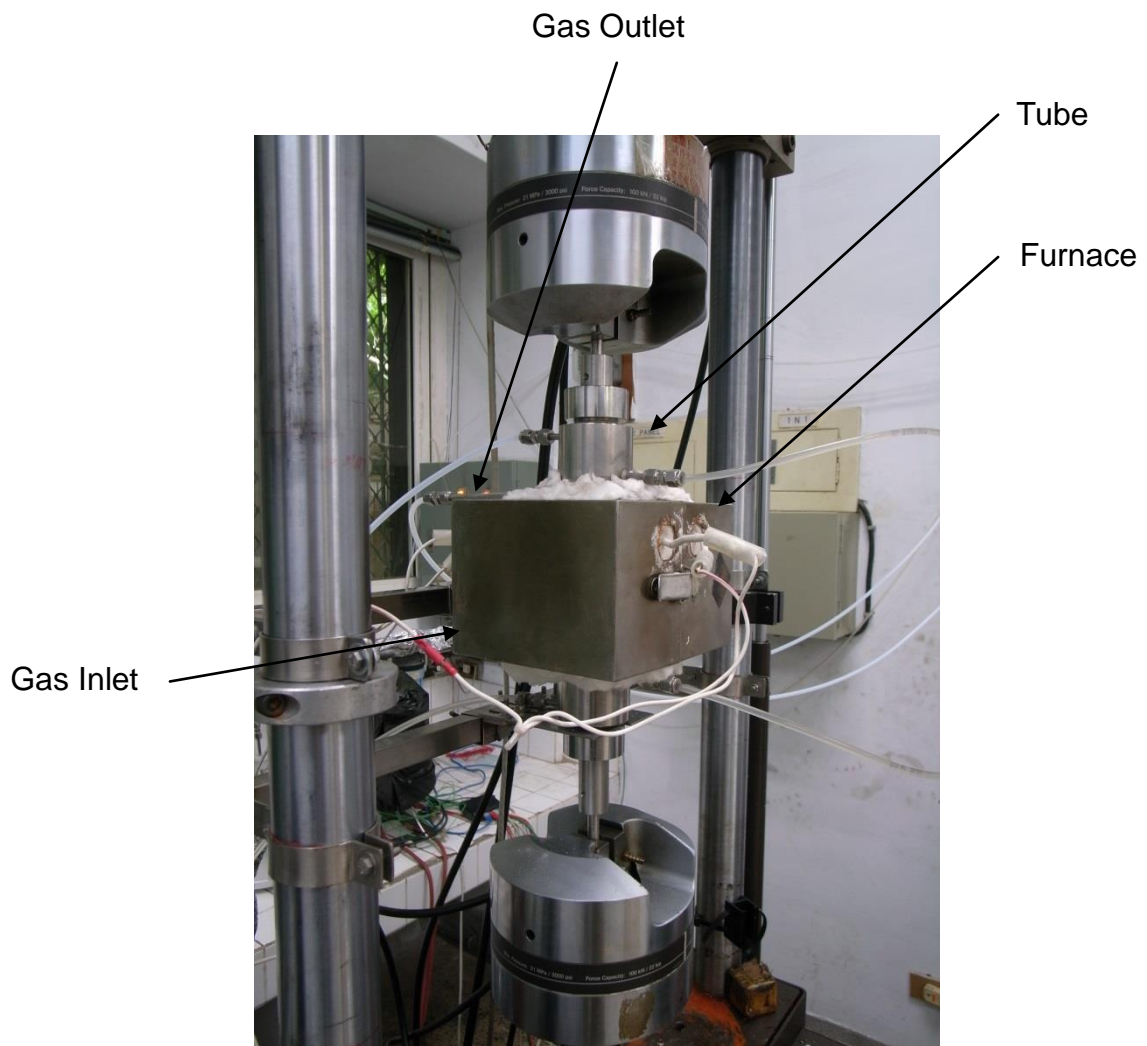


Fig. 7 Photograph of experimental setup for mechanical test.

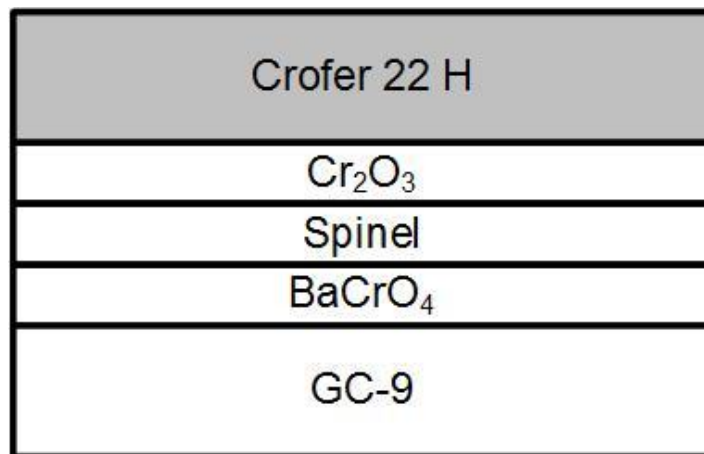


Fig. 8 Schematic of oxide layers between Crofer 22 H and GC-9 glass-ceramic.

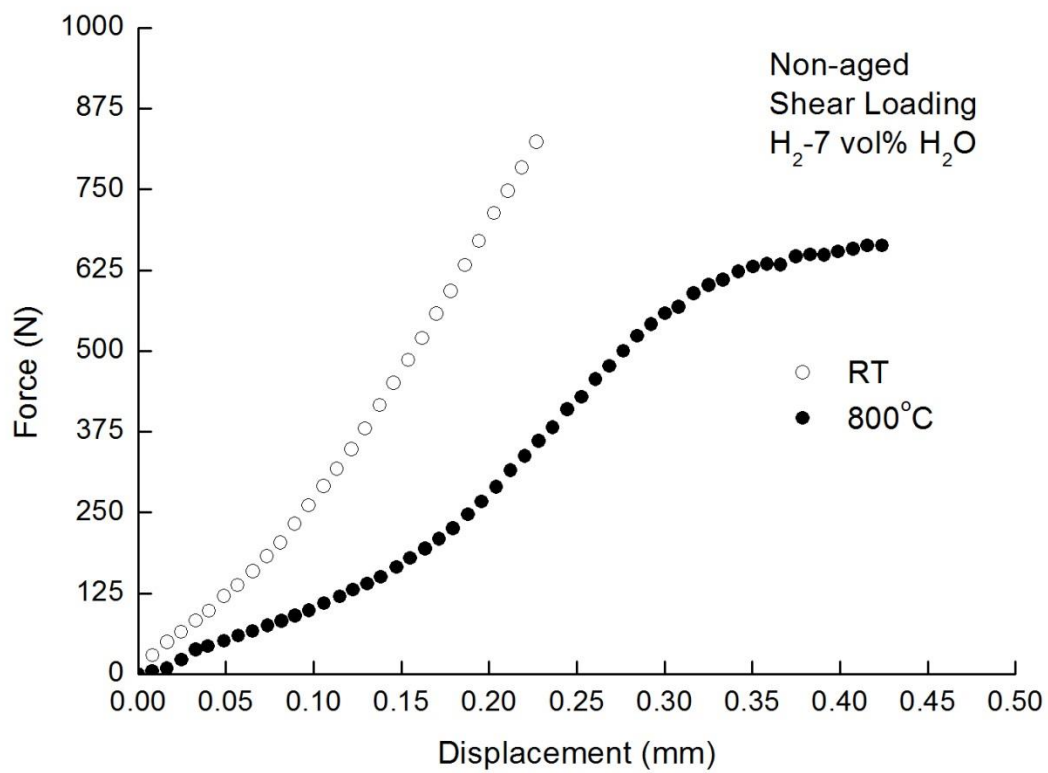


Fig. 9 Typical force-displacement curves of the non-aged joint specimens tested under shear loading in H₂-7 vol% H₂O at room temperature and 800 °C.

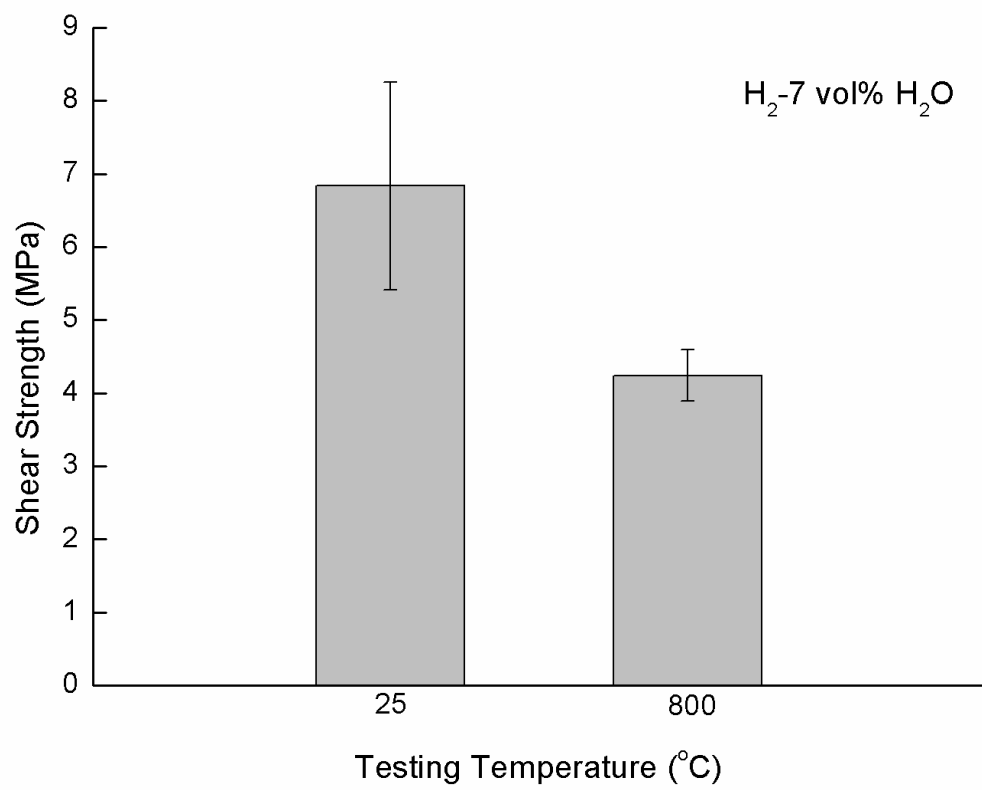
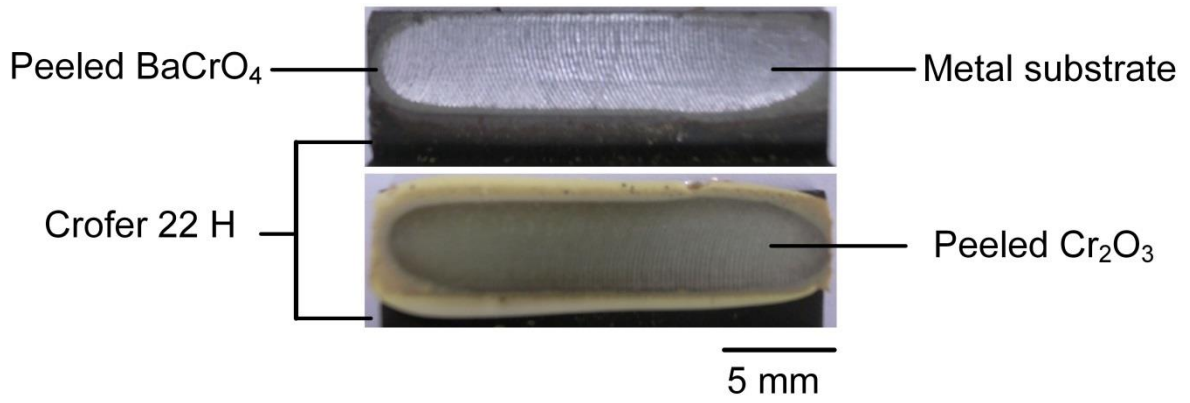
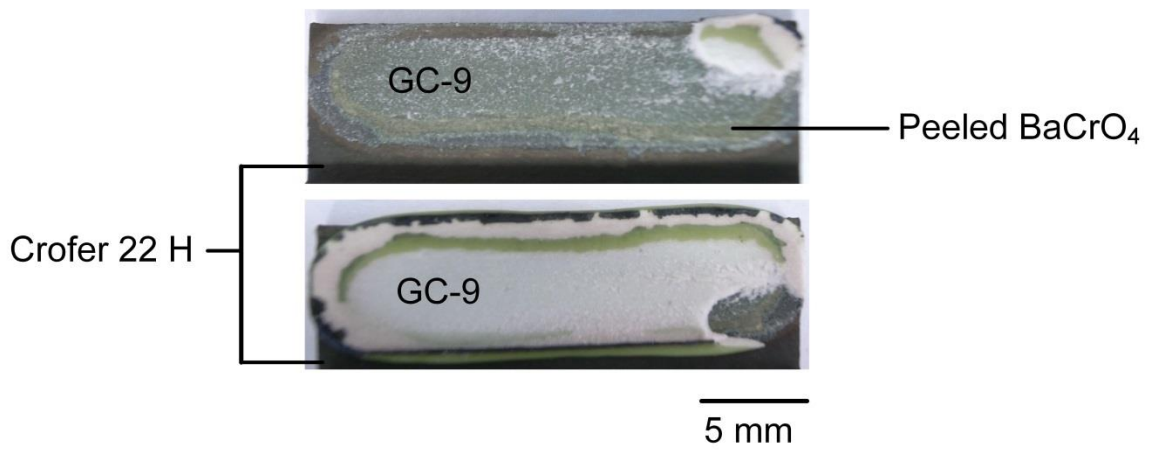


Fig. 10 Shear strength of non-aged joint specimens tested in H₂-7 vol% H₂O at room temperature and 800 °C.

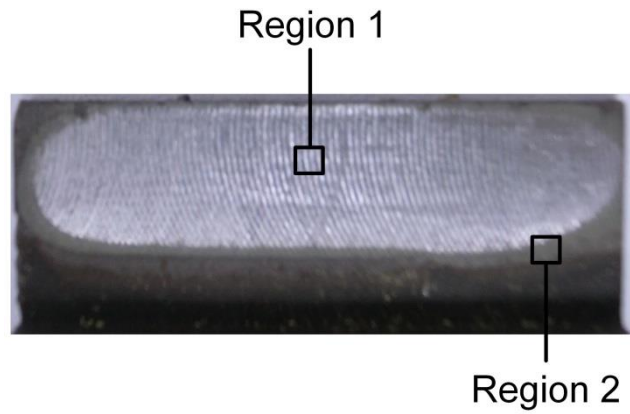


(a)

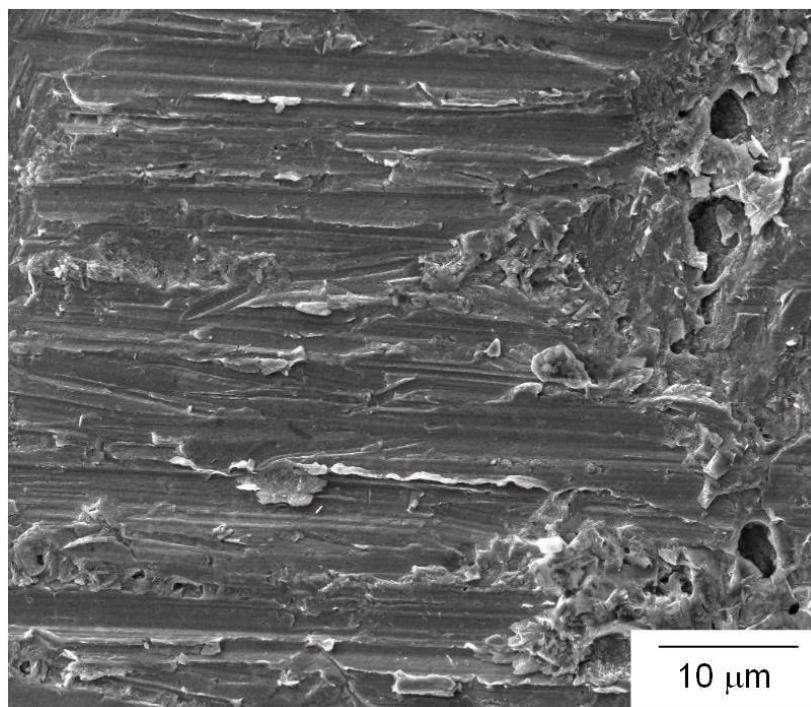


(b)

Fig. 11 Failure patterns of non-aged shear specimens tested in H₂-7 vol% H₂O at (a) room temperature and (b) 800 °C.

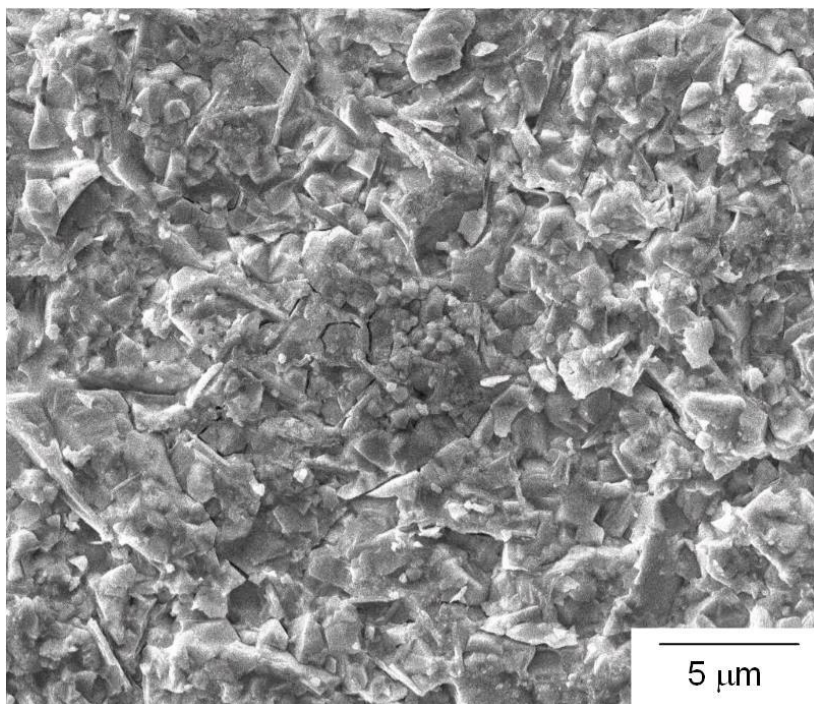


(a)



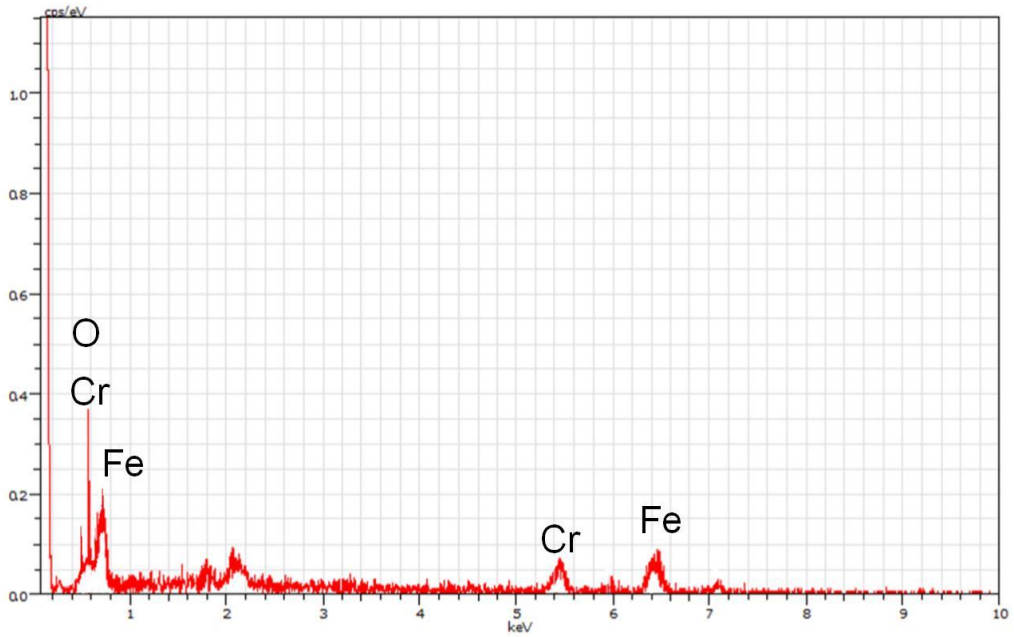
(b)

Fig. 12 A fracture surface region of the non-aged shear specimen shown in the upper part of Fig. 11(a): (a) optical micrograph showing the observed regions of SEM; (b) SEM micrograph of region 1 (metal substrate); (c) SEM micrograph of region 2 (BaCrO_4 chromate).

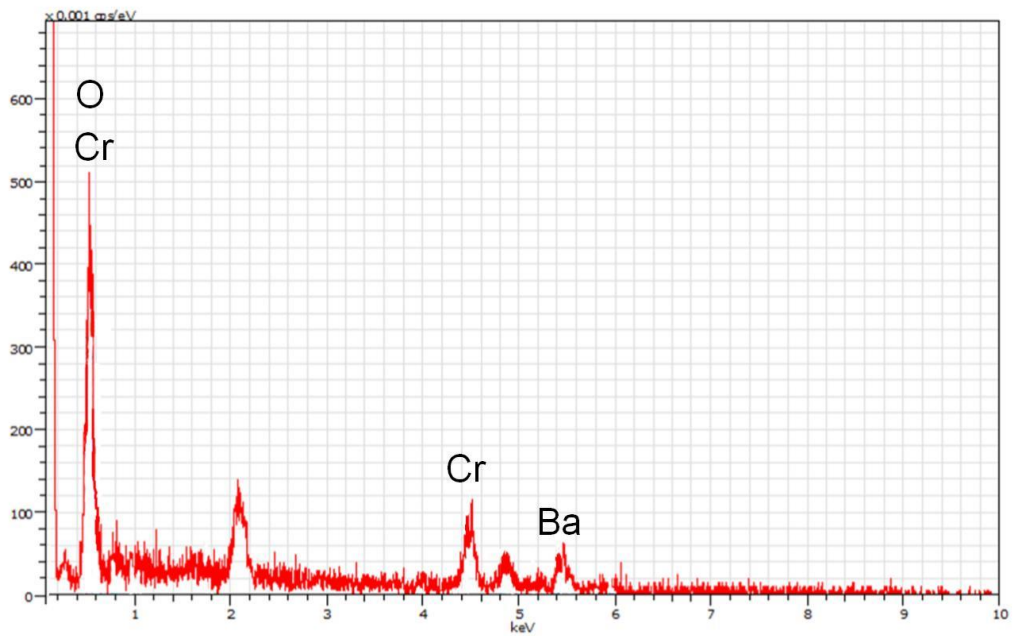


(c)

Fig. 12 (continued)



(a)



(b)

Fig. 13 EDS analysis results of the fracture surface of a non-aged shear joint specimen: (a) metal substrate (in Fig.12(b)); (b) BaCrO₄ chromate layer (in Fig. 12(c)).

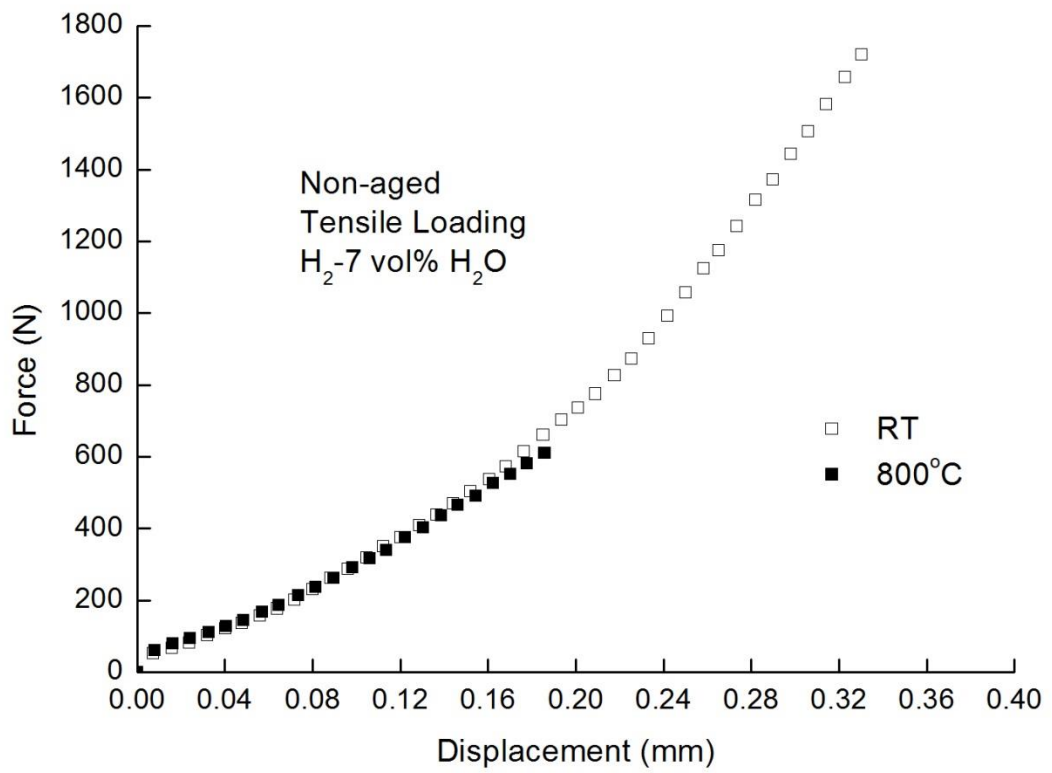


Fig. 14 Typical force-displacement curves of the non-aged joint specimens tested in H₂-7 vol% H₂O under tensile loading at room temperature and 800 °C.

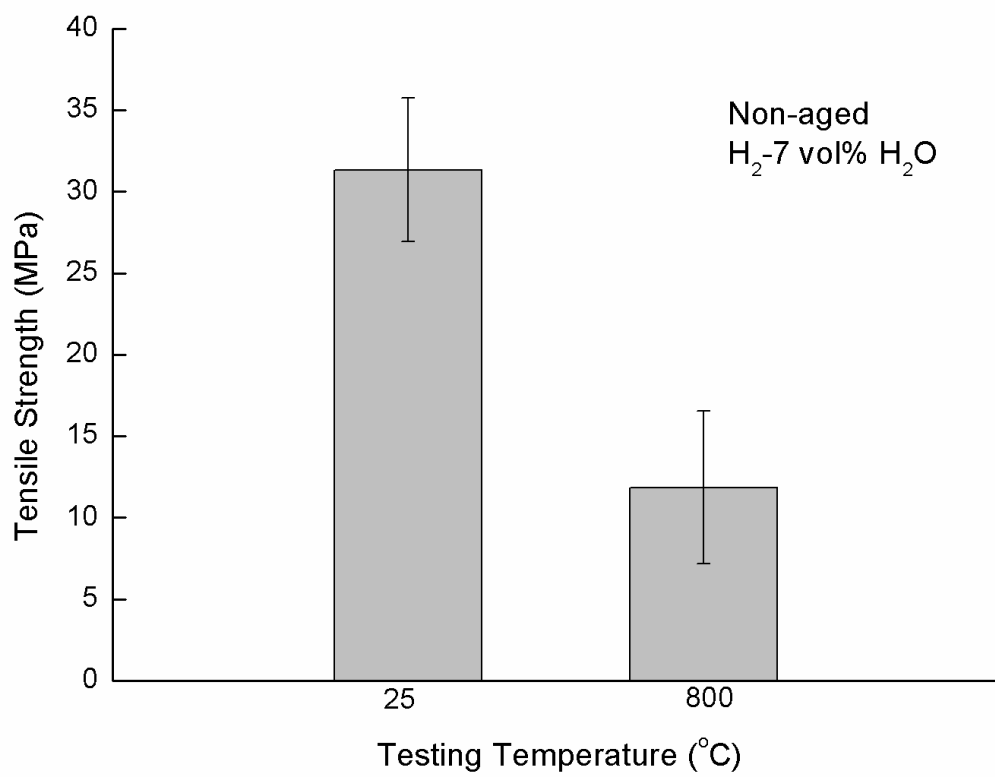
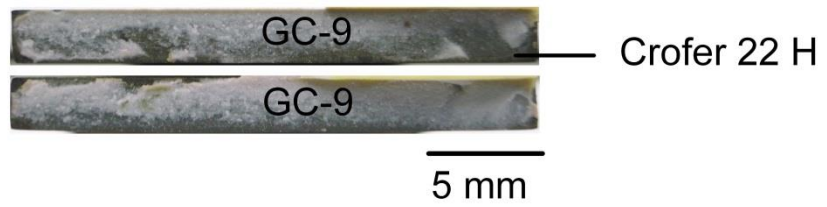
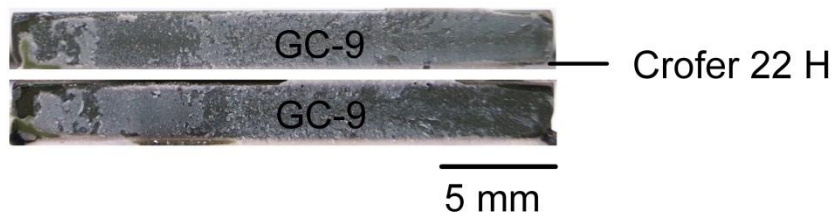


Fig. 15 Tensile strength of non-aged joint specimens tested in H₂-7 vol% H₂O at room temperature and 800 °C.



(a)

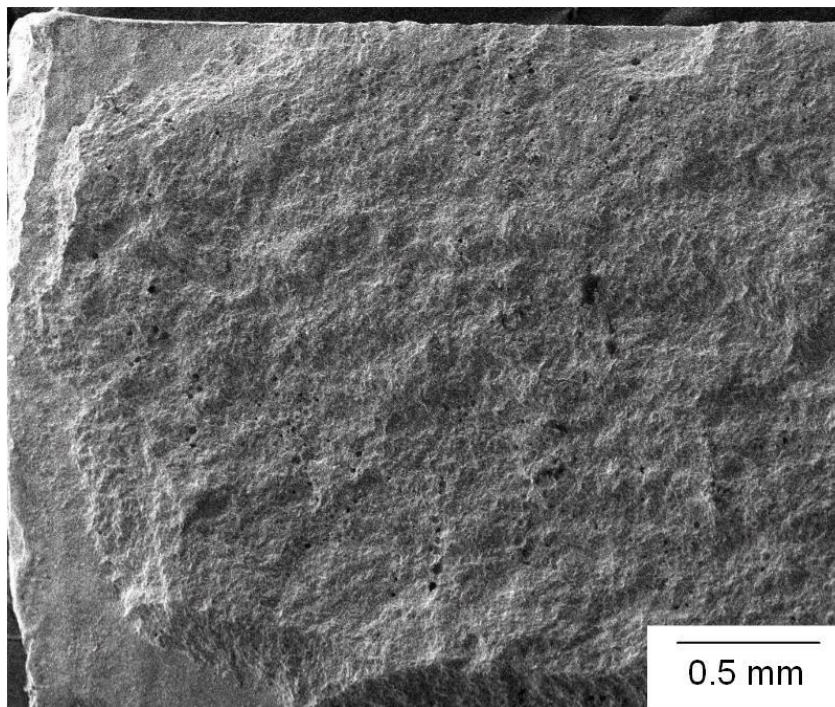


(b)

Fig. 16 Failure patterns of non-aged tensile specimens tested in H_2 -7 vol% H_2O at (a) room temperature and (b) 800 °C.

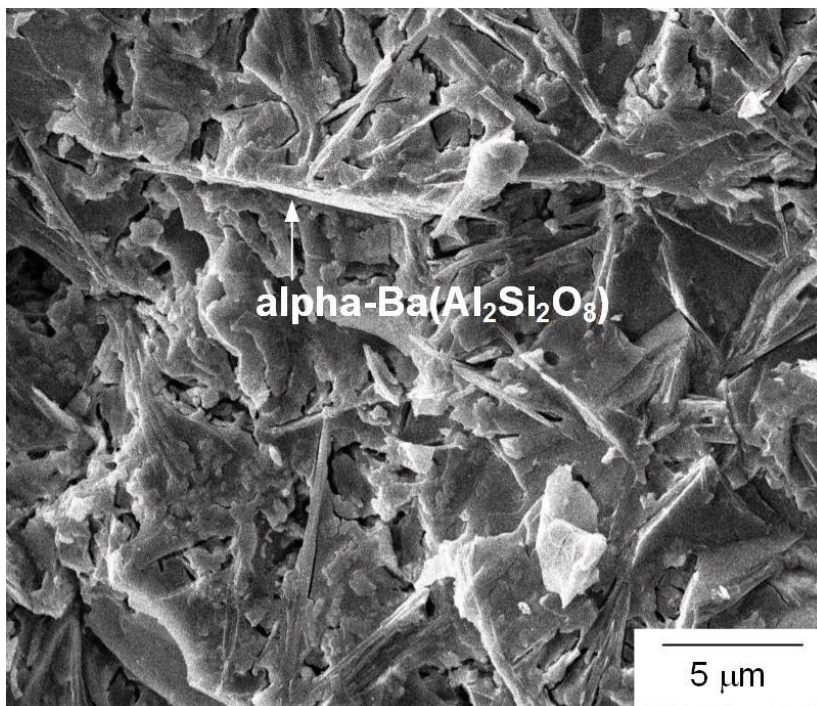


(a)



(b)

Fig. 17 A fracture surface region of the non-aged tensile specimen shown in the upper part of Fig. 16(a): (a) optical micrograph showing the observed region of SEM; (b) SEM micrograph of the outlined region (glass-ceramic layer); (c) microstructure of GC-9 glass-ceramic.

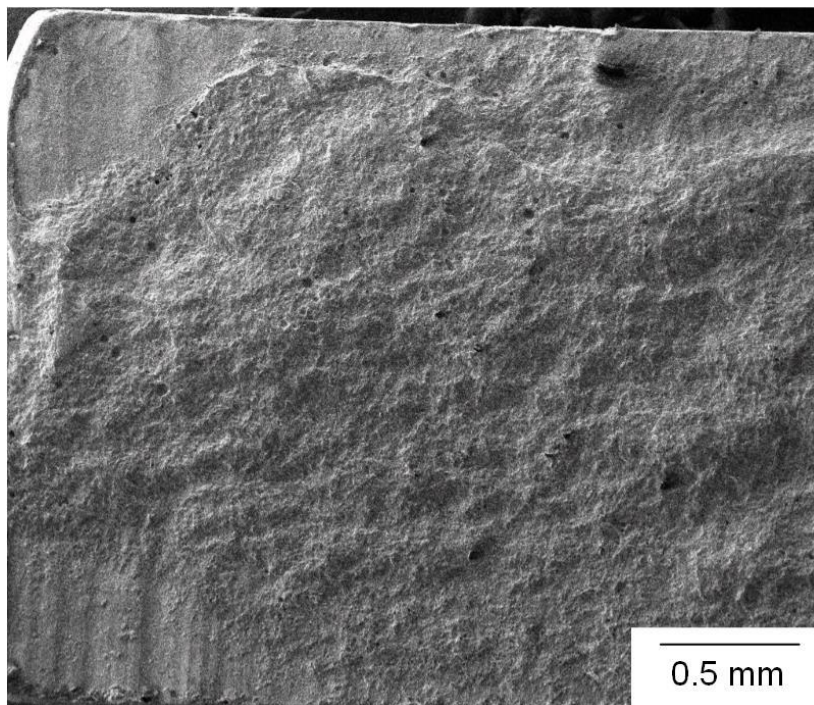


(c)

Fig. 17 (continued)

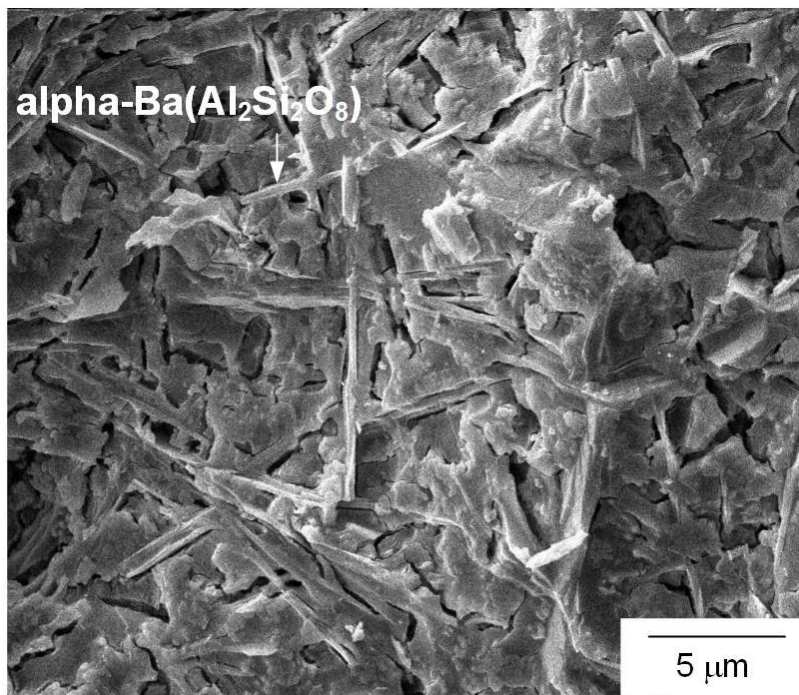


(a)



(b)

Fig. 18 A fracture surface region of the non-aged tensile specimen shown in the lower part of Fig. 16(a): (a) optical micrograph showing the observed region of SEM; (b) SEM micrograph of the outlined region (glass-ceramic layer); (c) microstructure of GC-9 glass-ceramic.



(c)

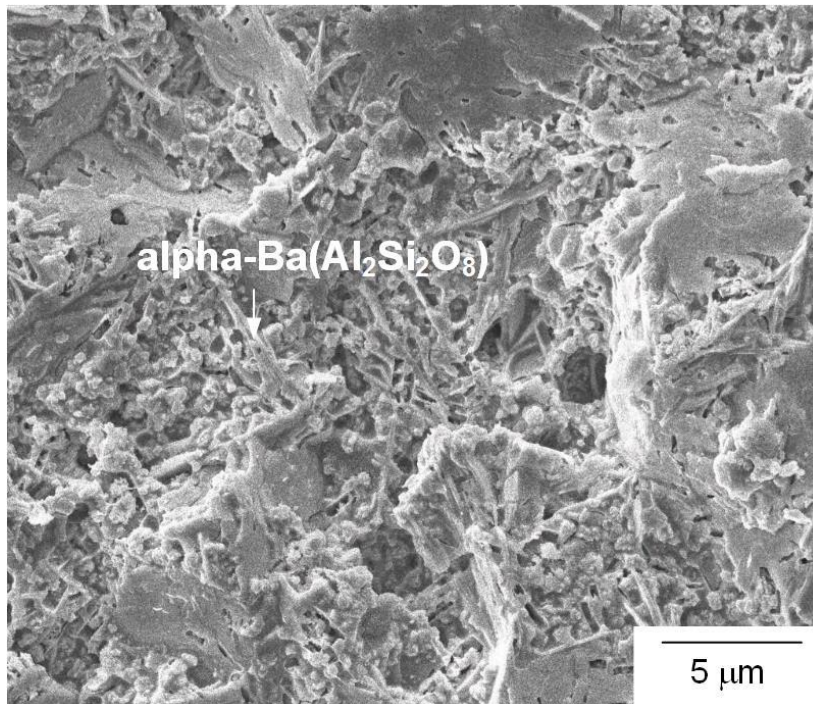


Fig. 19 A fracture surface region of the non-aged tensile specimen shown in the upper part of Fig. 16(b): (a) optical micrograph showing the observed region of SEM; (b) microstructure of GC-9 glass-ceramic.

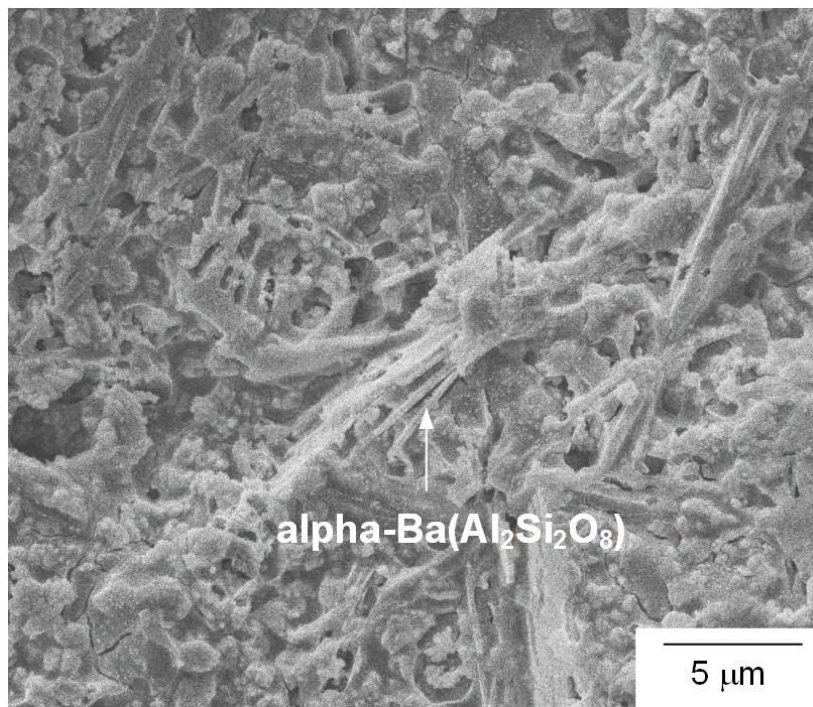
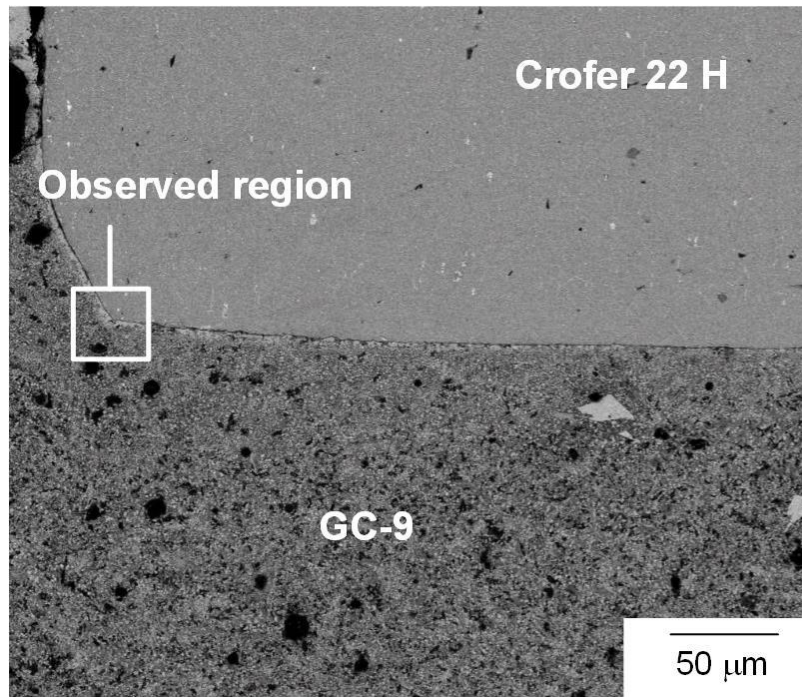
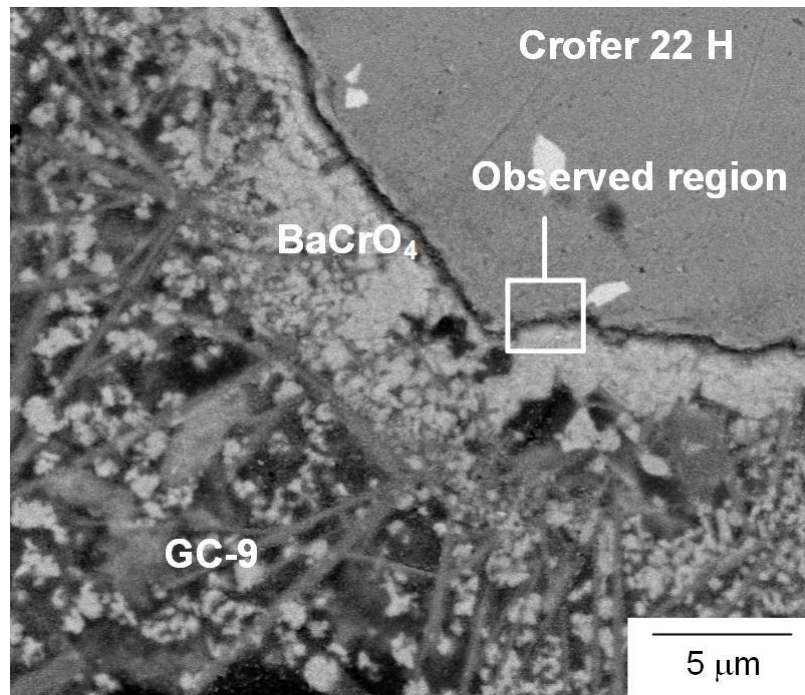


Fig. 20 A fracture surface region of the non-aged tensile specimen shown in the lower part of Fig. 16(b): (a) optical micrograph showing the observed region of SEM; (b) microstructure of GC-9 glass-ceramic.

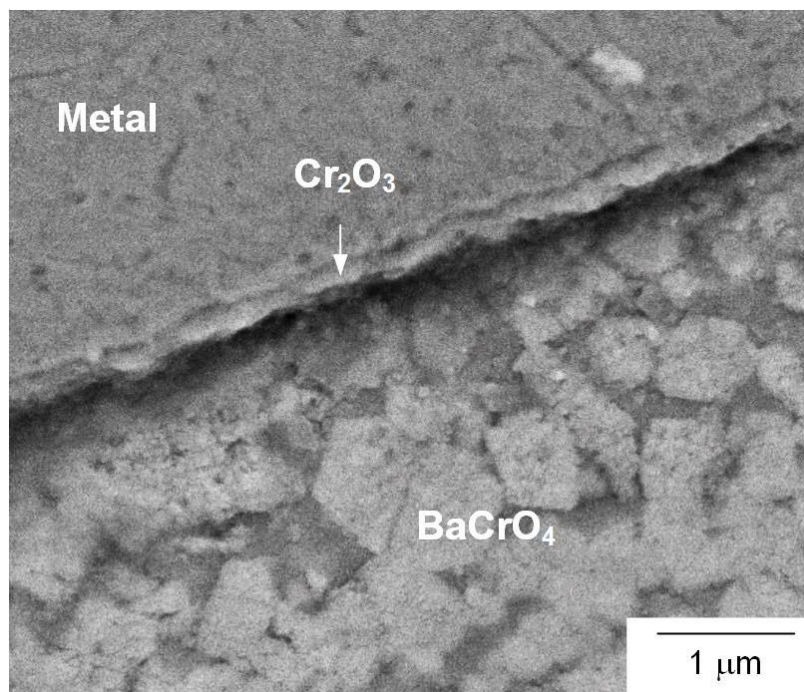


(a)



(b)

Fig. 21 SEM micrographs (BSE mode) of a cross section of an interface between the GC-9 and Crofer 22 H in a non-aged specimen: (a) low magnification view; (b) high magnification of outlined region in (a); (c) higher magnification of the outlined region in (b).



(c)

Fig. 21 (continued)

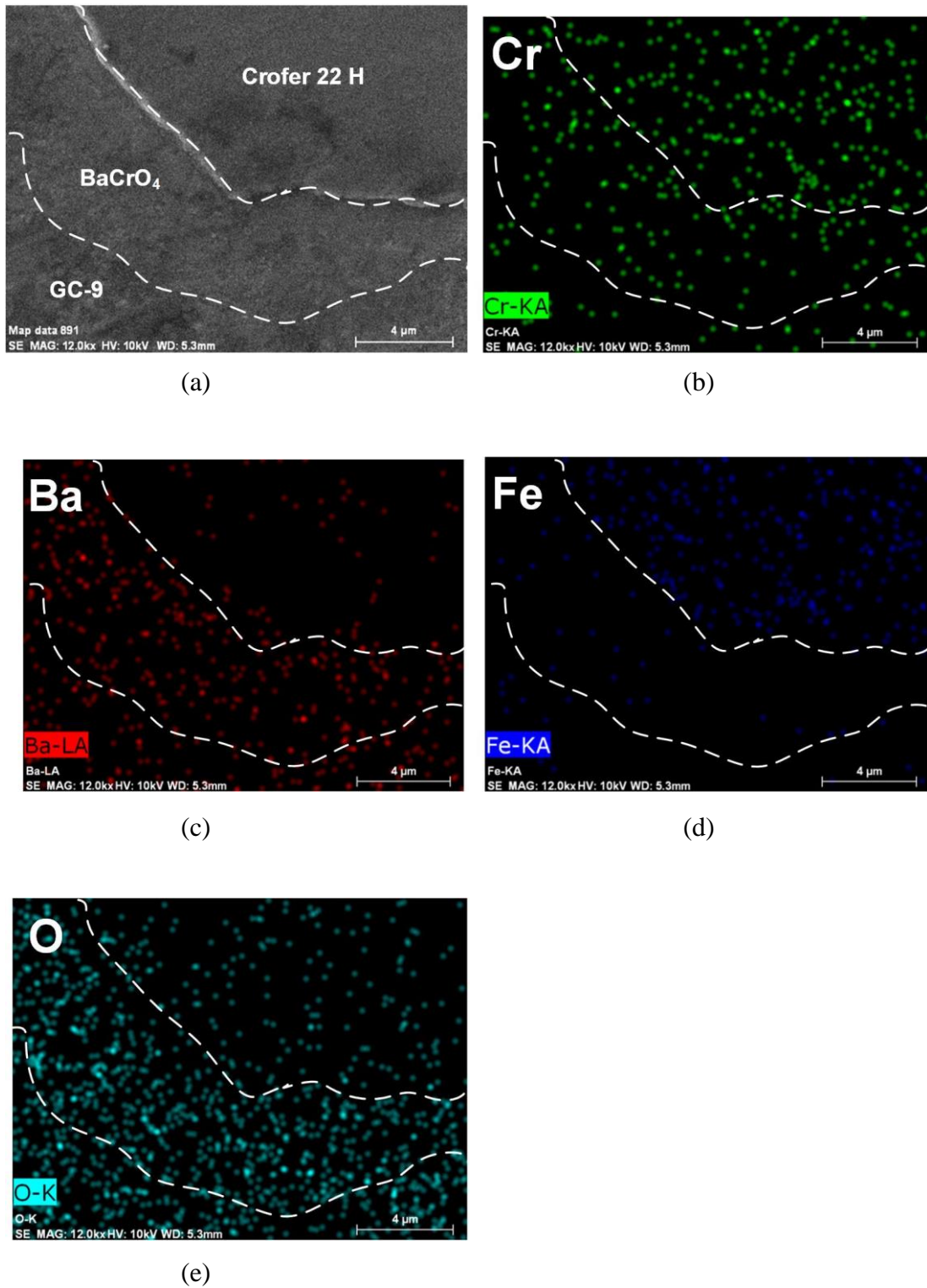


Fig. 22 EDS mapping of elements on the cross section of an interface between the GC-9 and Crofer 22 H shown in Fig. 21(b): (a) mapping region; (b) Cr; (c) Ba; (d) Fe; (e) O.

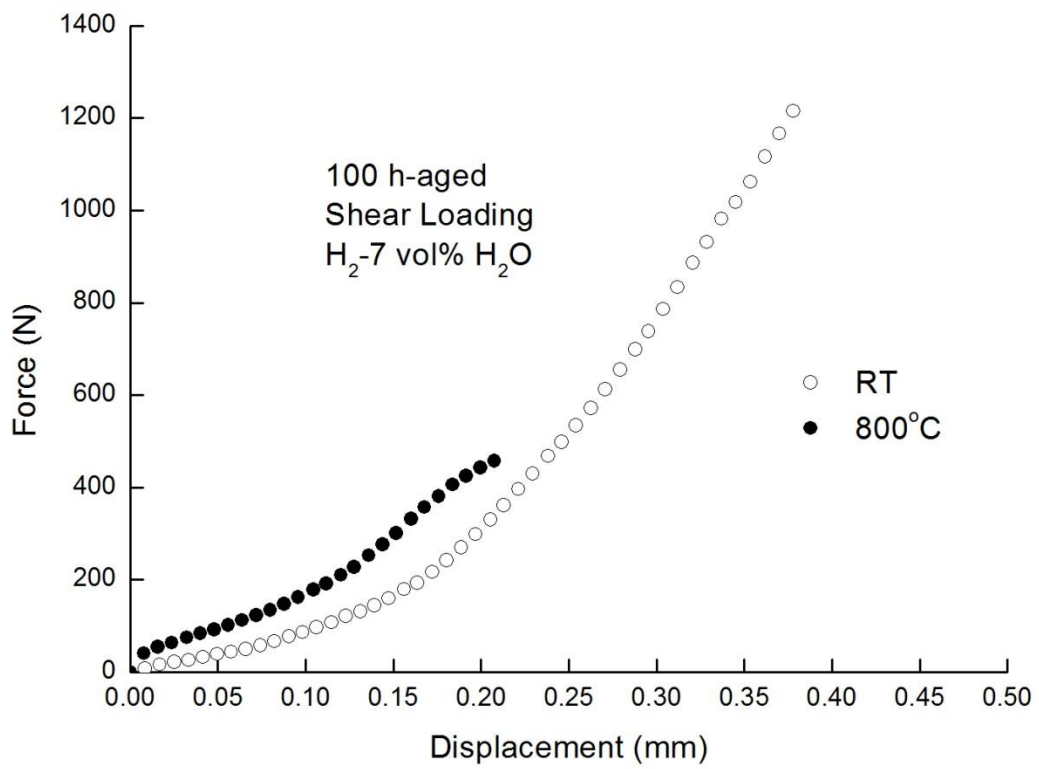


Fig. 23 Typical force-displacement curves of the 100 h-aged joint specimens tested under shear loading in H₂-7 vol% H₂O at room temperature and 800 °C.

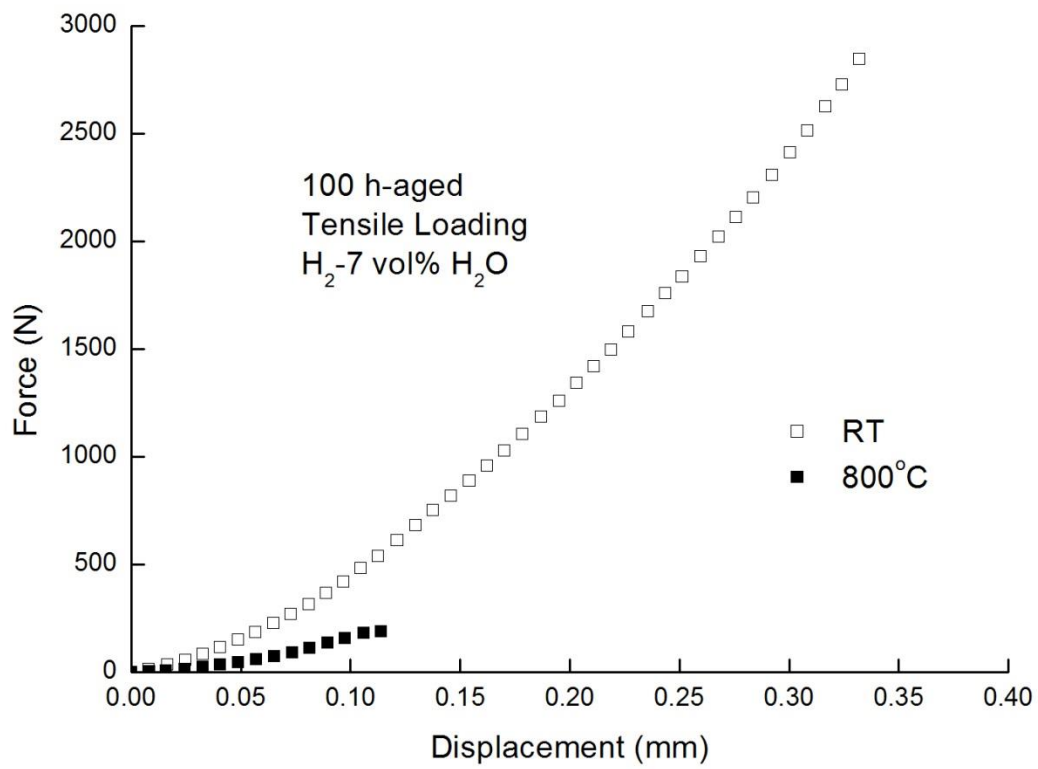


Fig. 24 Typical force-displacement curves of the 100 h-aged joint specimens tested under tensile loading in H₂-7 vol% H₂O at room temperature and 800 °C.

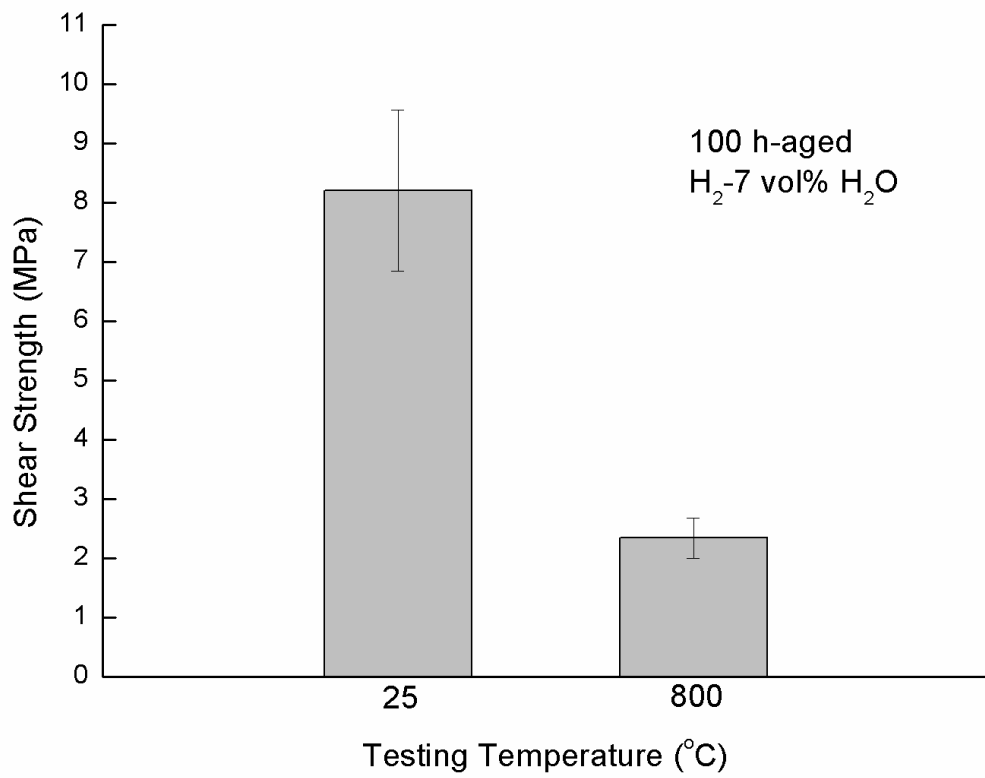


Fig. 25 Shear strength of 100 h-aged joint specimens tested in H₂-7 vol% H₂O at room temperature and 800 °C.

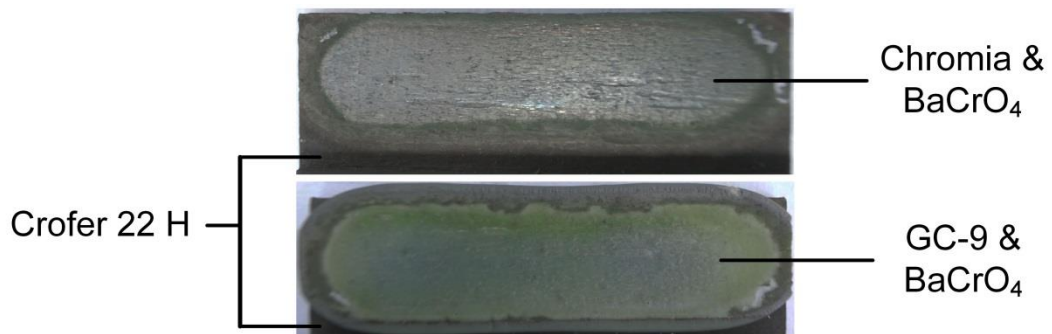
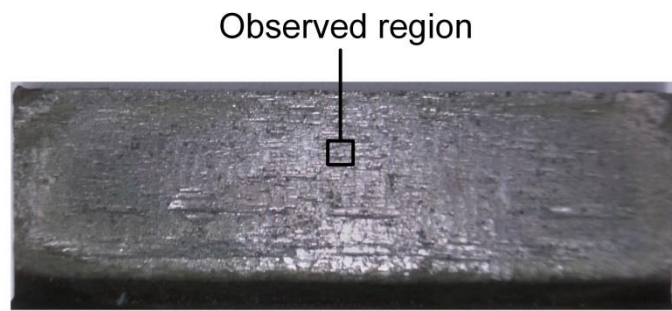
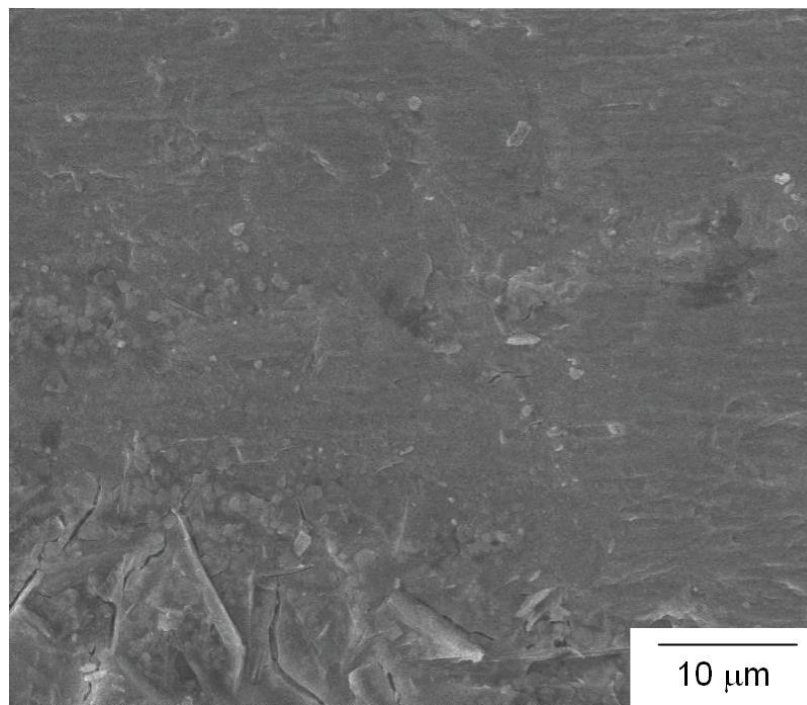


Fig. 26 Failure patterns of 100 h-aged shear specimens tested in H₂-7 vol% H₂O at (a) room temperature and (b) 800 °C.



(a)



(b)

Fig. 27 A fracture surface region of the 100 h-aged shear specimen shown in the upper part of Fig. 26(a): (a) optical micrograph showing the observed region of SEM; (b) microstructure of BaCrO₄ Chromate.

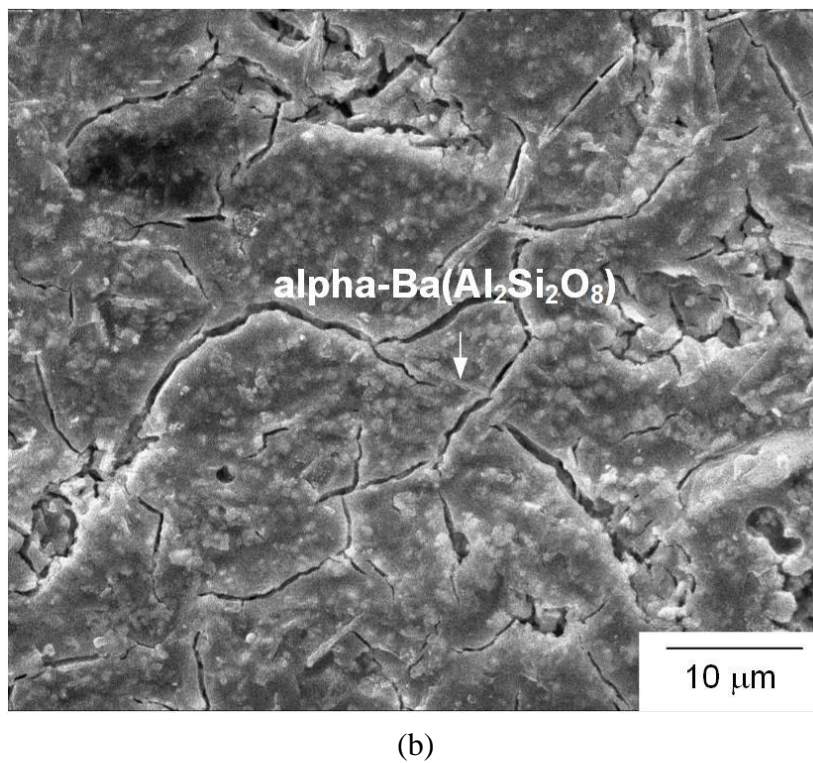
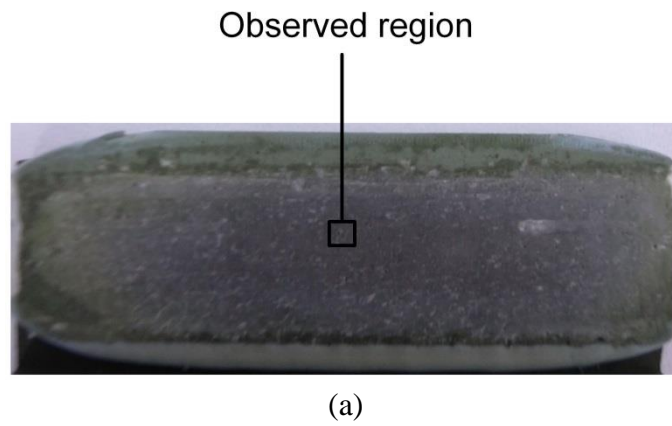
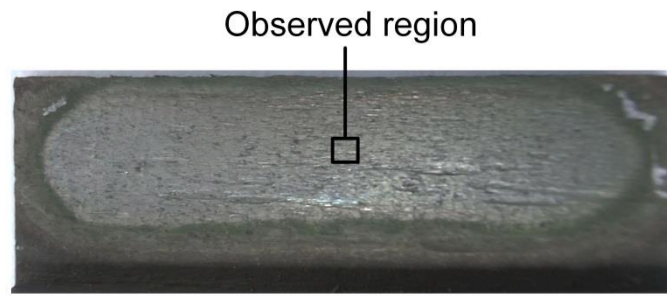
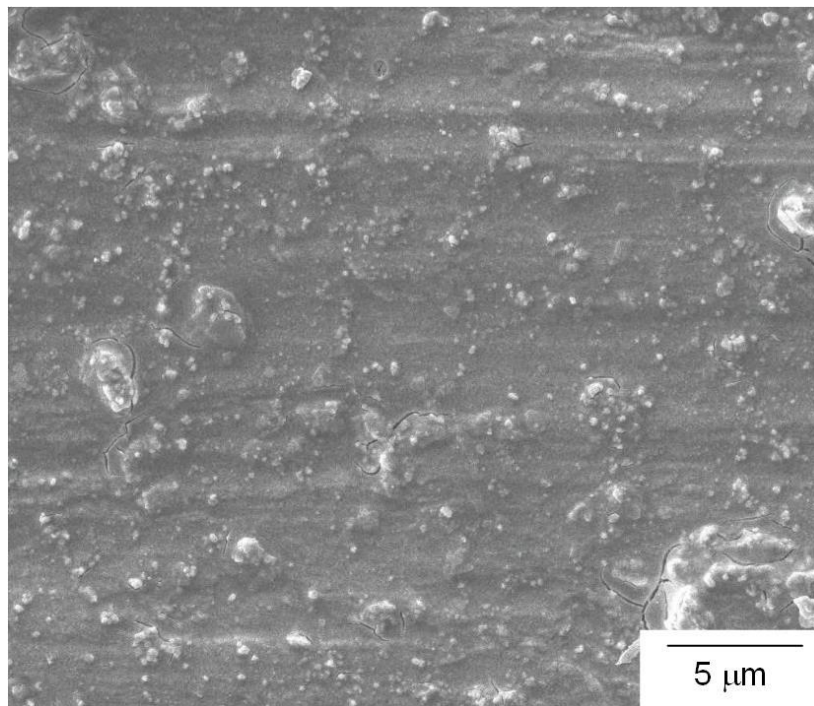


Fig. 28 A fracture surface region of the 100 h-aged shear specimen shown in the lower part of Fig. 26(a): (a) optical micrograph showing the observed region of SEM; (b) microstructure of GC-9 glass-ceramic.



(a)



(b)

Fig. 29 A fracture surface region of the 100 h-aged shear specimen shown in the upper part of Fig. 26(b): (a) optical micrograph showing the observed region of SEM; (b) microstructure of BaCrO₄ Chromate.

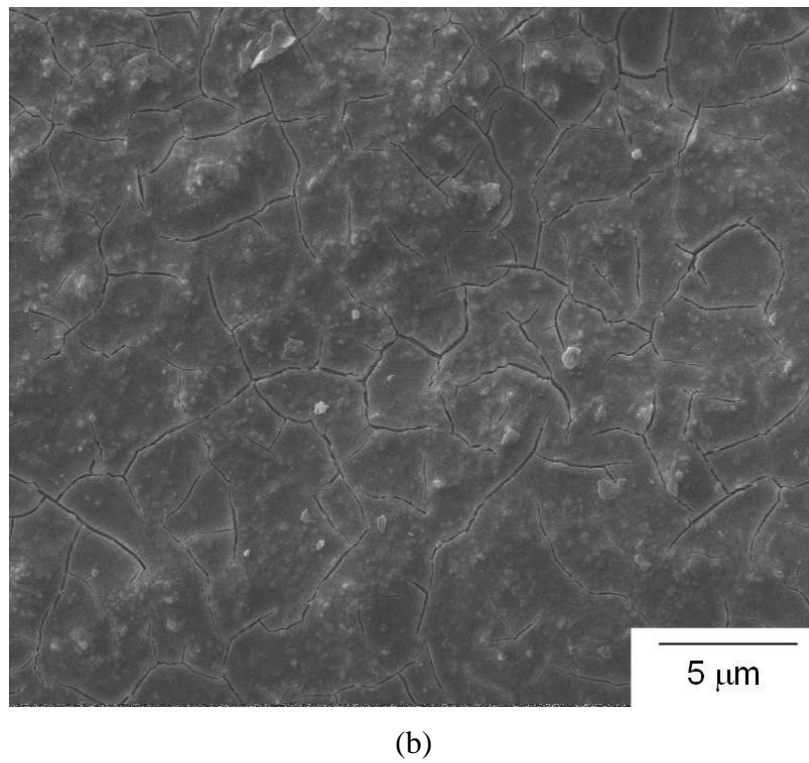
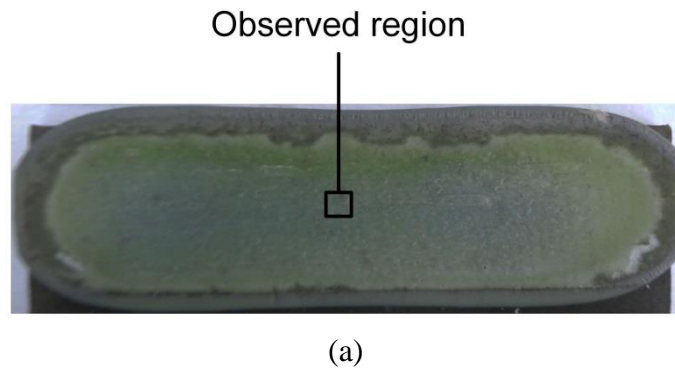


Fig. 30 A fracture surface region of the 100 h-aged shear specimen shown in the lower part of Fig. 26(b): (a) optical micrograph showing the observed region of SEM; (b) microstructure of BaCrO₄ Chromate.

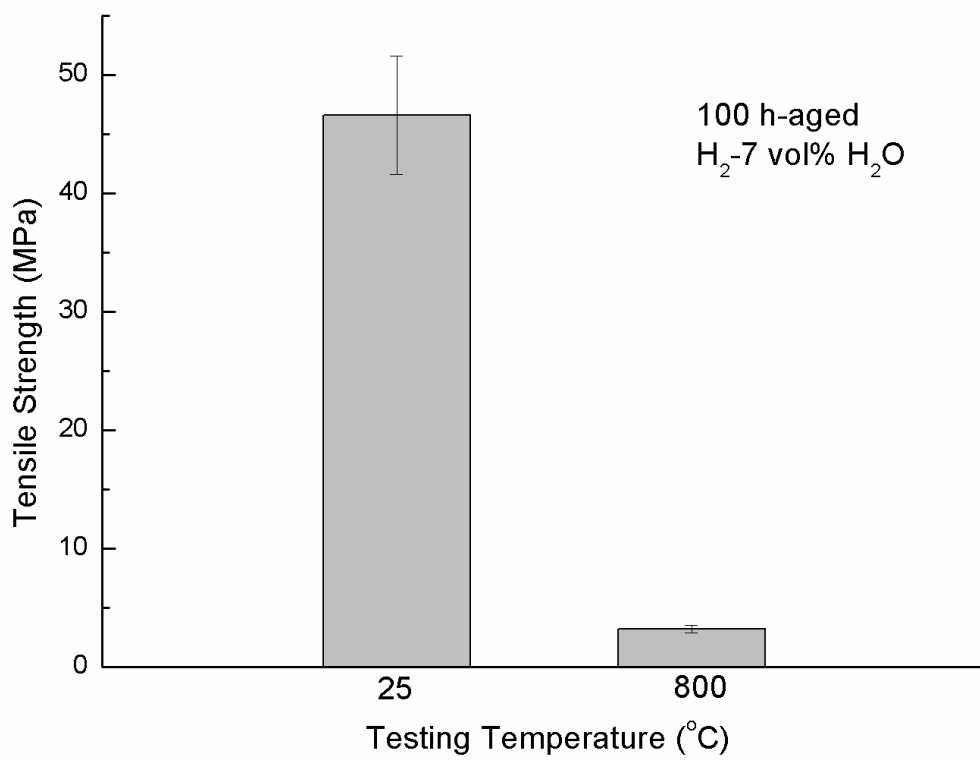
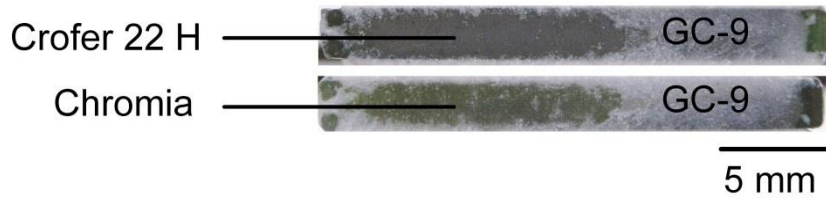


Fig. 31 Tensile strength of 100 h-aged joint specimens tested in H₂-7 vol% H₂O at room temperature and 800 °C.

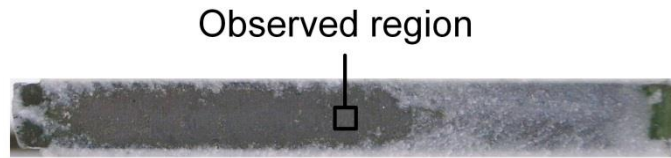


(a)

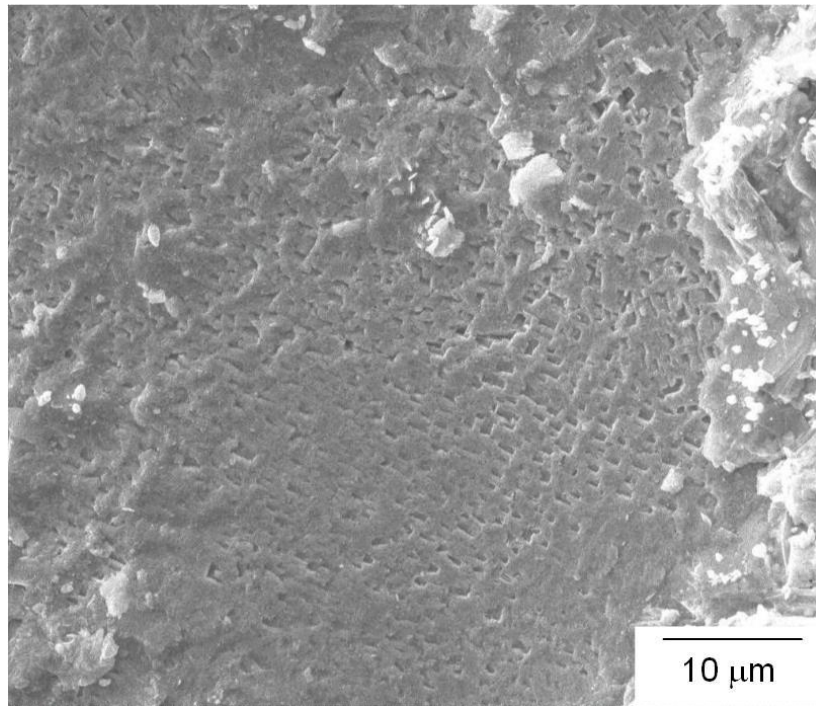


(b)

Fig. 32 Failure patterns of 100 h-aged tensile specimens tested in H₂-7 vol% H₂O at (a) room temperature and (b) 800 °C.



(a)



(b)

Fig. 33 A fracture surface region of the 100 h-aged tensile specimen shown in the upper part of Fig. 32(a): (a) optical micrograph showing the observed region of SEM; (b) microstructure of metal substrate.

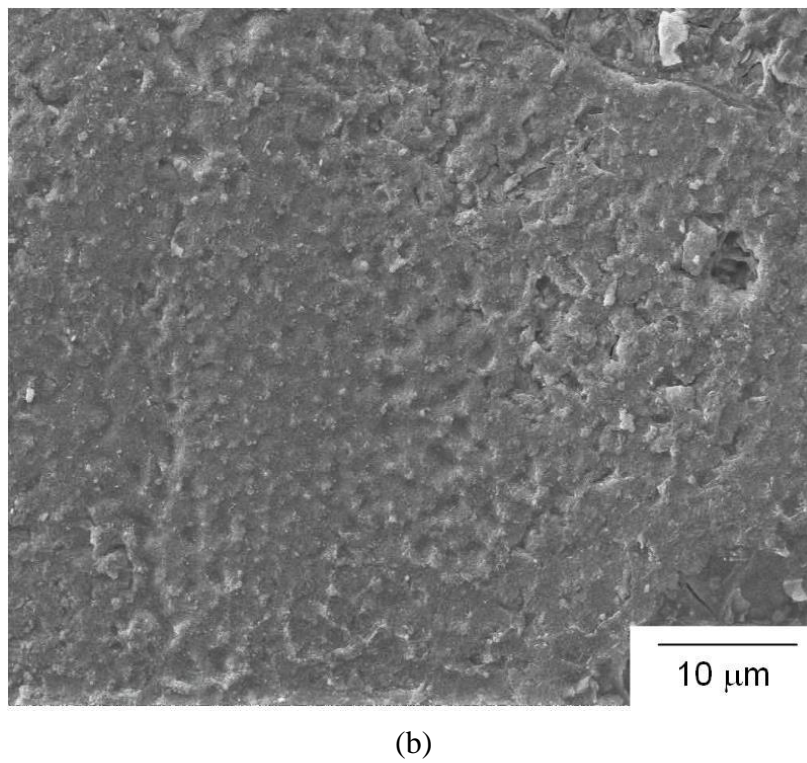
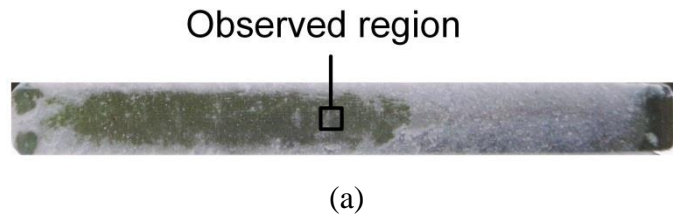


Fig. 34 A fracture surface region of the 100 h-aged tensile specimen shown in the lower part of Fig. 32(a): (a) optical micrograph showing the observed region of SEM; (b) microstructure of chromia.

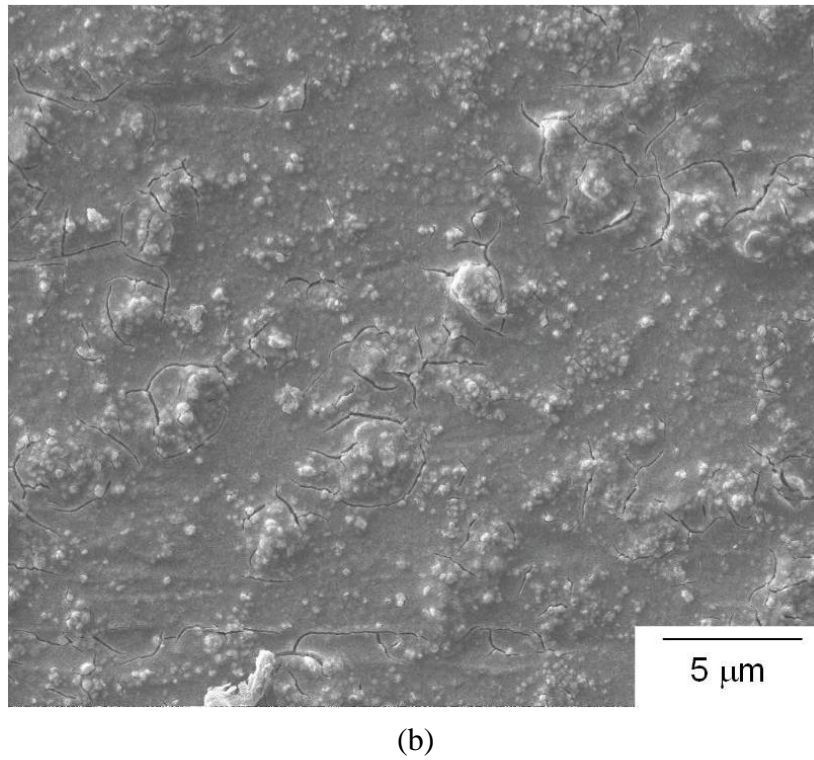
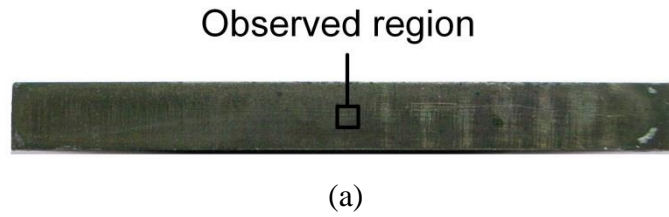


Fig. 35 A fracture surface region of the 100 h-aged tensile specimen shown in the upper part of Fig. 32(b): (a) optical micrograph showing the observed region of SEM; (b) microstructure of BaCrO₄ Chromate.

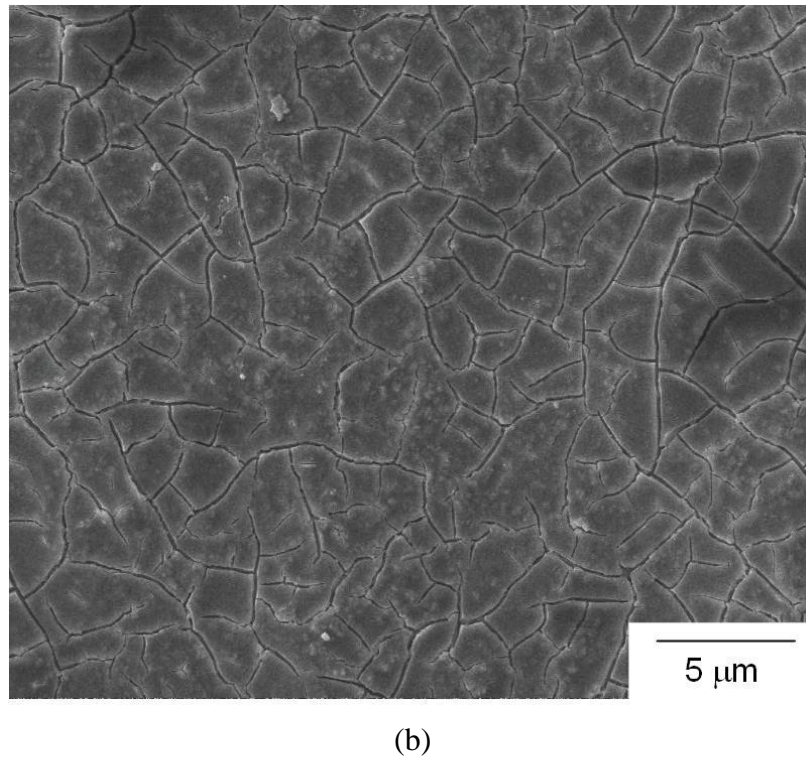
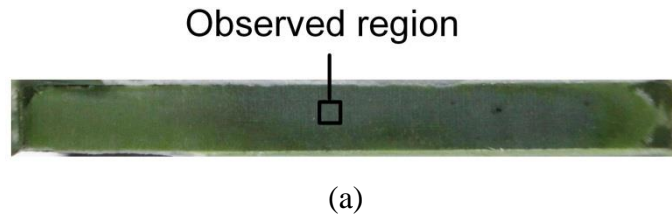
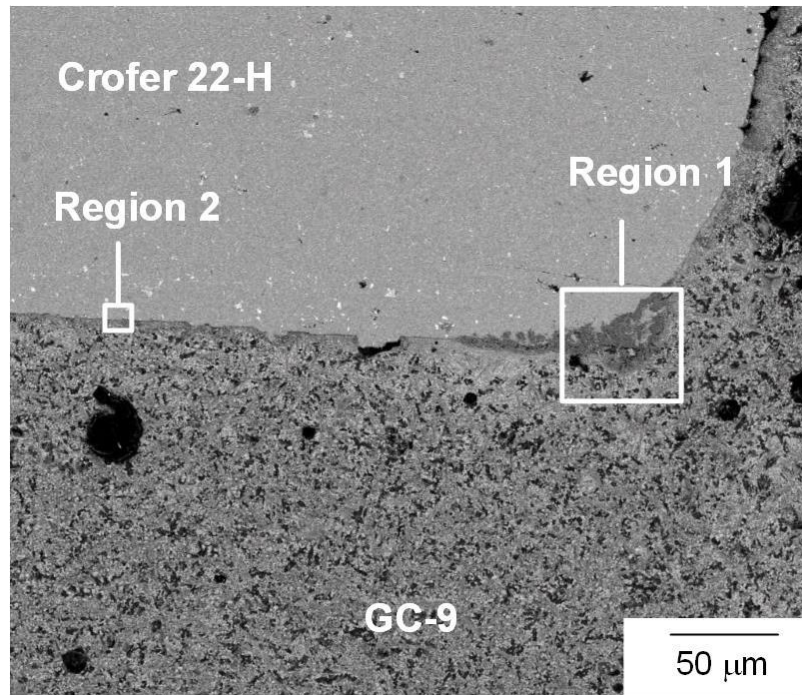
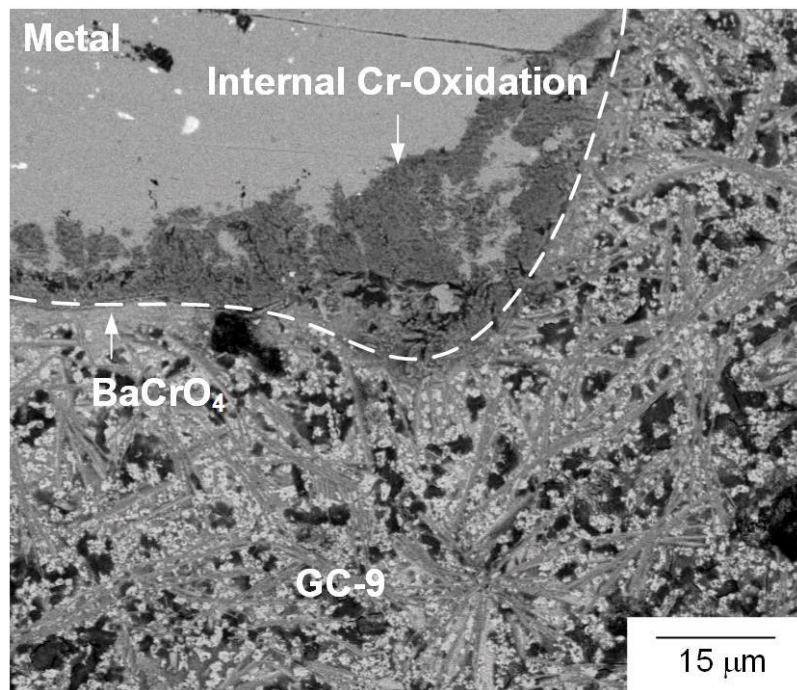


Fig. 36 A fracture surface region of the 100 h-aged tensile specimen shown in the lower part of Fig. 32(b): (a) optical micrograph showing the observed region of SEM; (b) microstructure of BaCrO_4 Chromate.

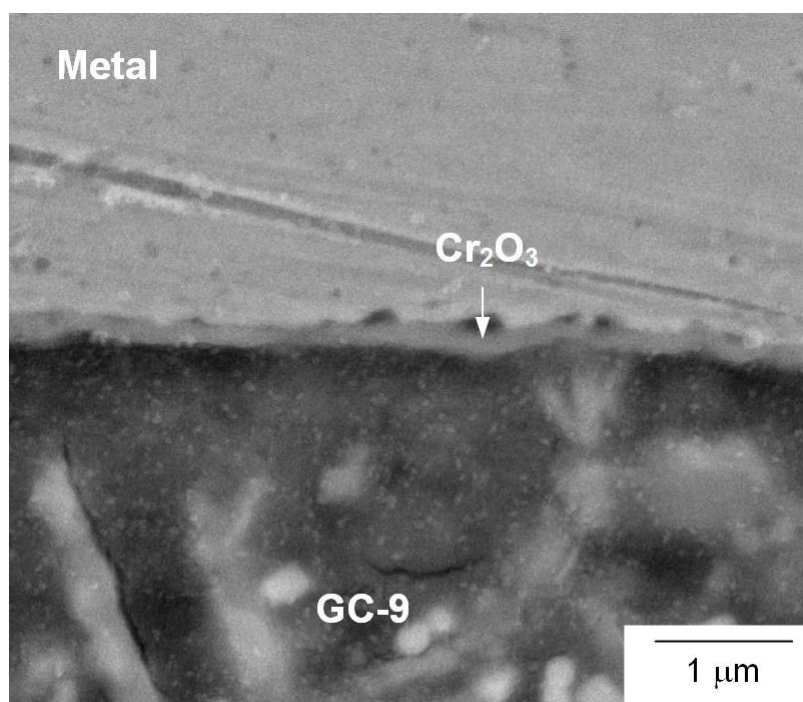


(a)



(b)

Fig. 37 SEM micrographs (BSE mode) of a cross section of an interface between the GC-9 and Crofer 22 H in a 100 h-aged specimen: (a) low magnification view; (b) high magnification of the region 1 in (a); (c) high magnification of region 2 in (a).



(c)

Fig. 37 (continued)

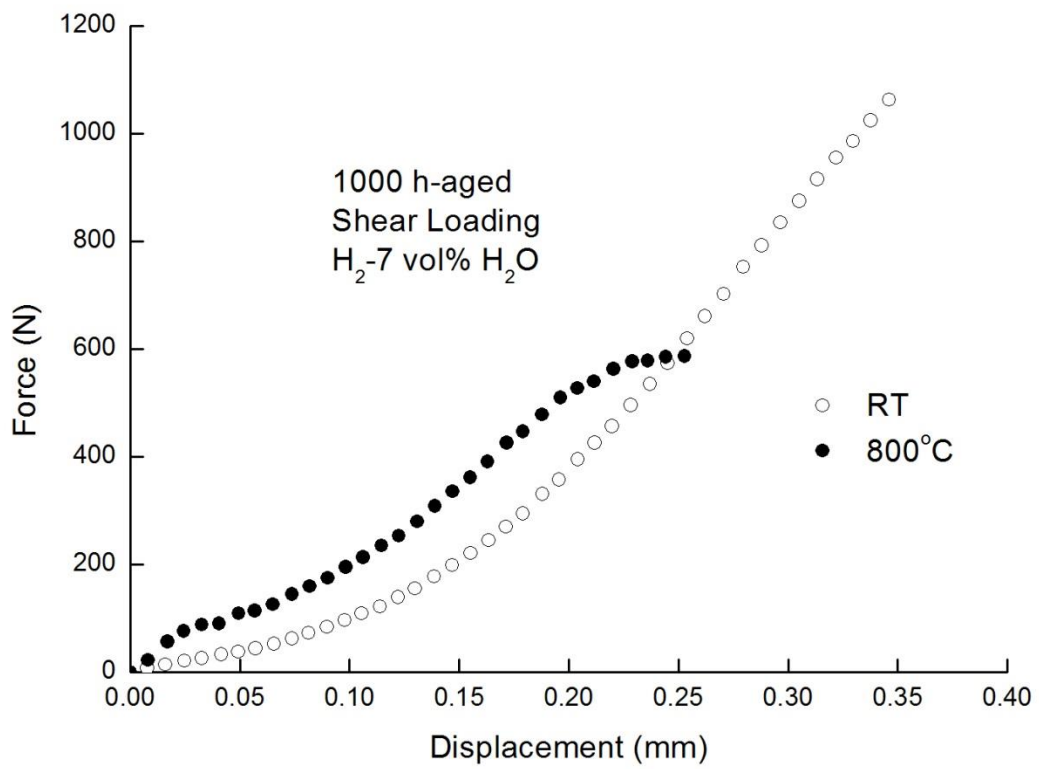


Fig. 38 Typical force-displacement curves of the 1000 h-aged joint specimens tested under shear loading in H₂-7 vol% H₂O at room temperature and 800 °C.

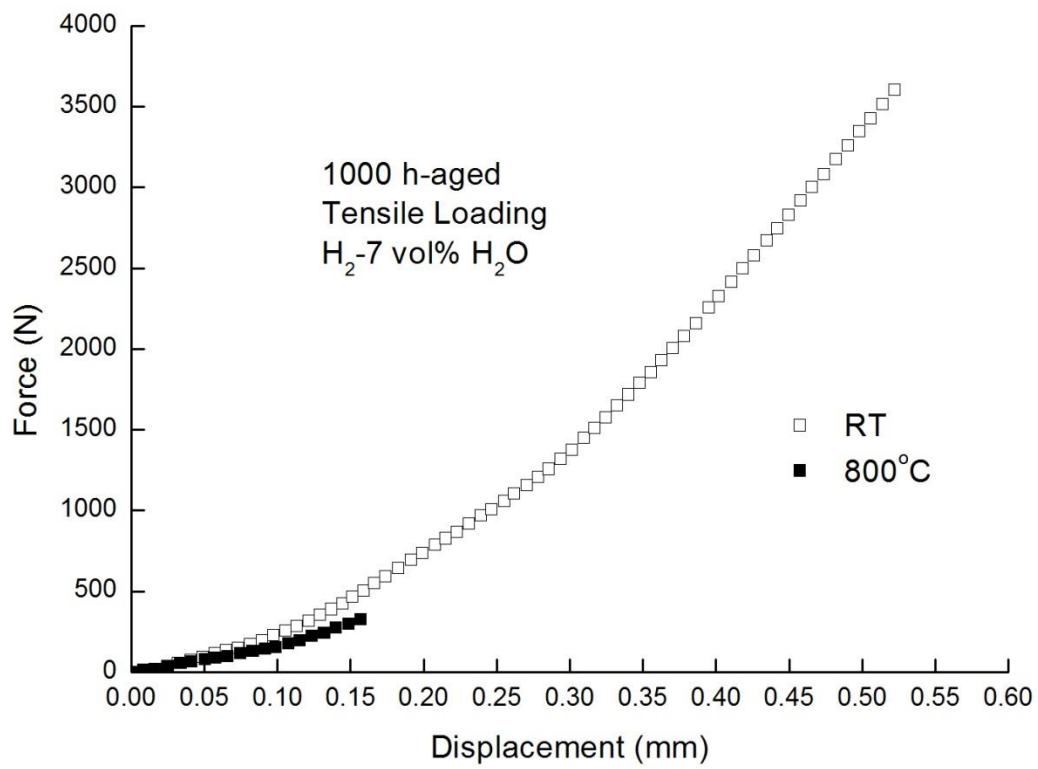


Fig. 39 Typical force-displacement curves of the joint specimens tested under tensile loading in H₂-7 vol% H₂O at room temperature and 800 °C.

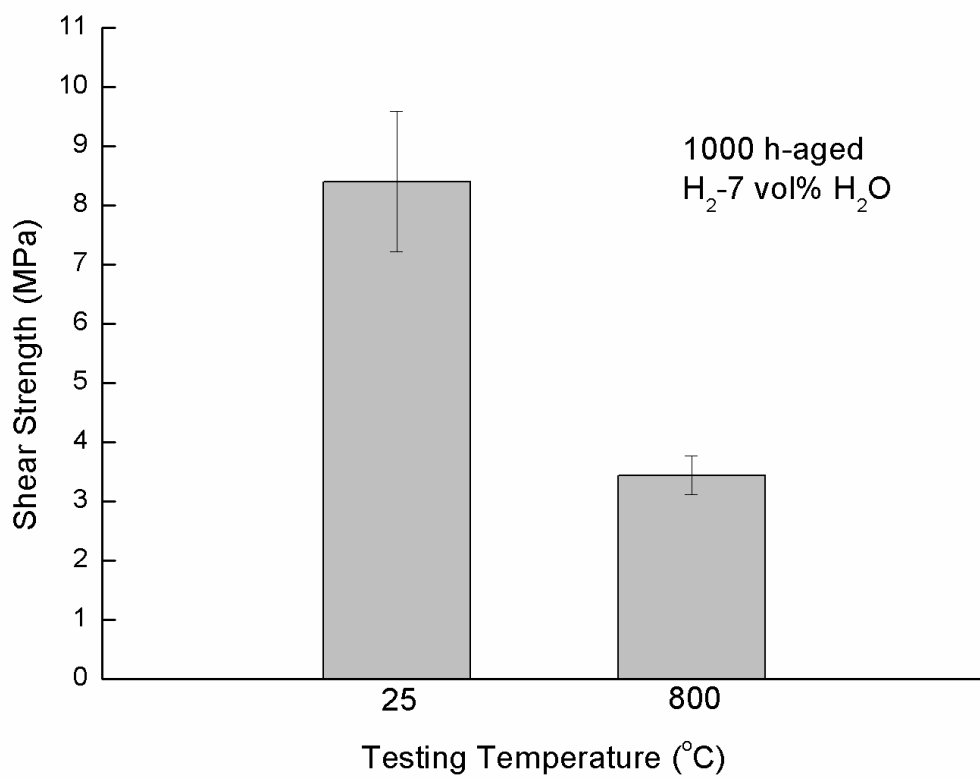
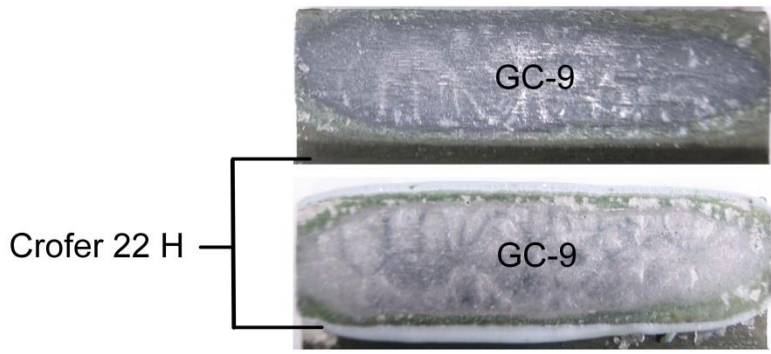
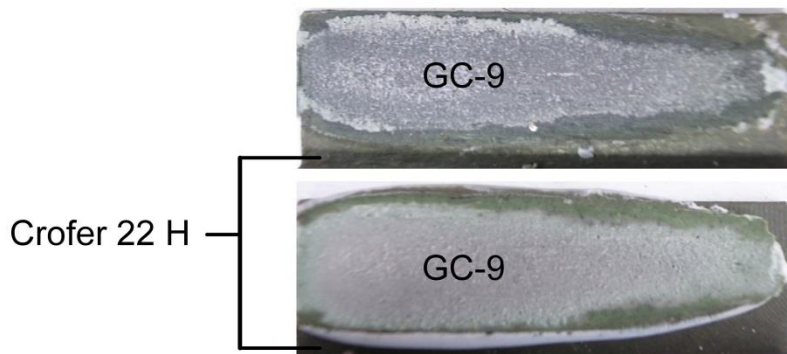


Fig. 40 Shear strength of 1000 h-aged joint specimens tested in H₂-7 vol% H₂O at room temperature and 800 °C.

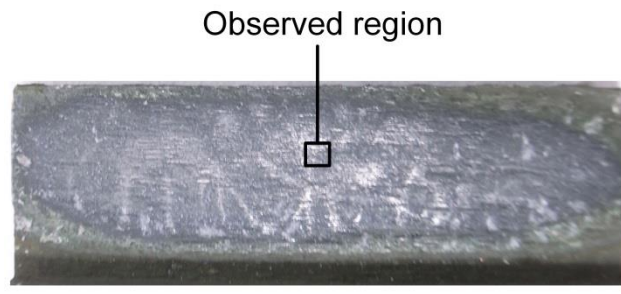


(a)

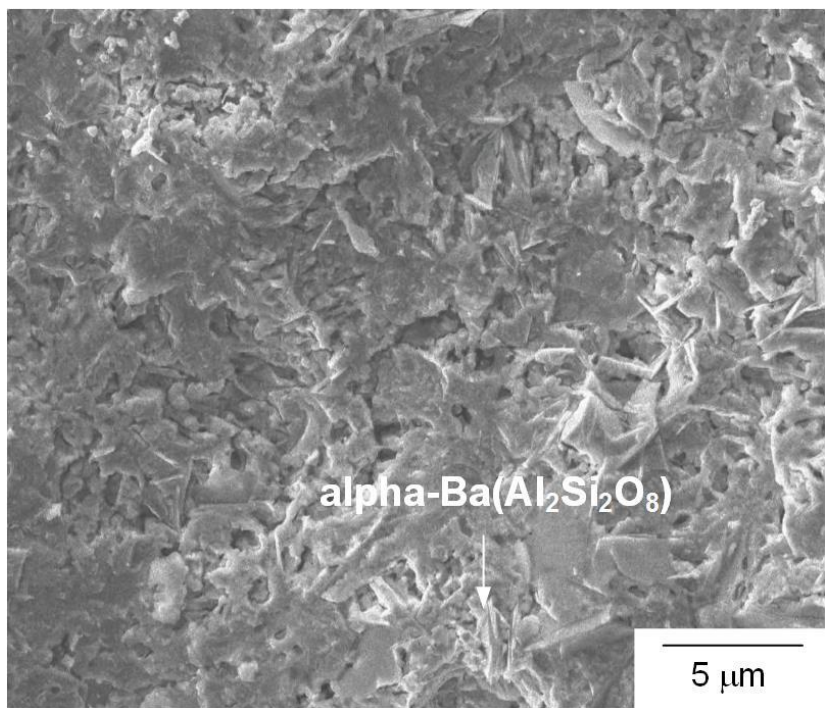


(b)

Fig. 41 Failure patterns of 1000 h-aged shear specimens tested in H₂-7 vol% H₂O at (a) room temperature and (b) 800 °C.

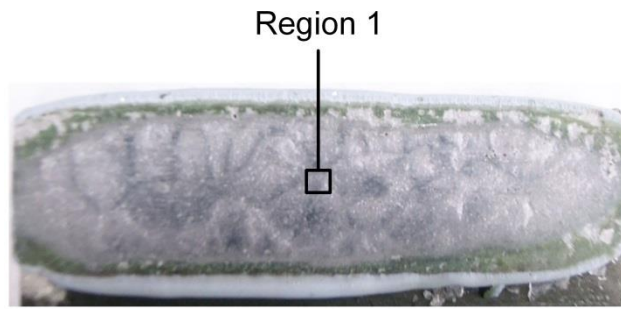


(a)

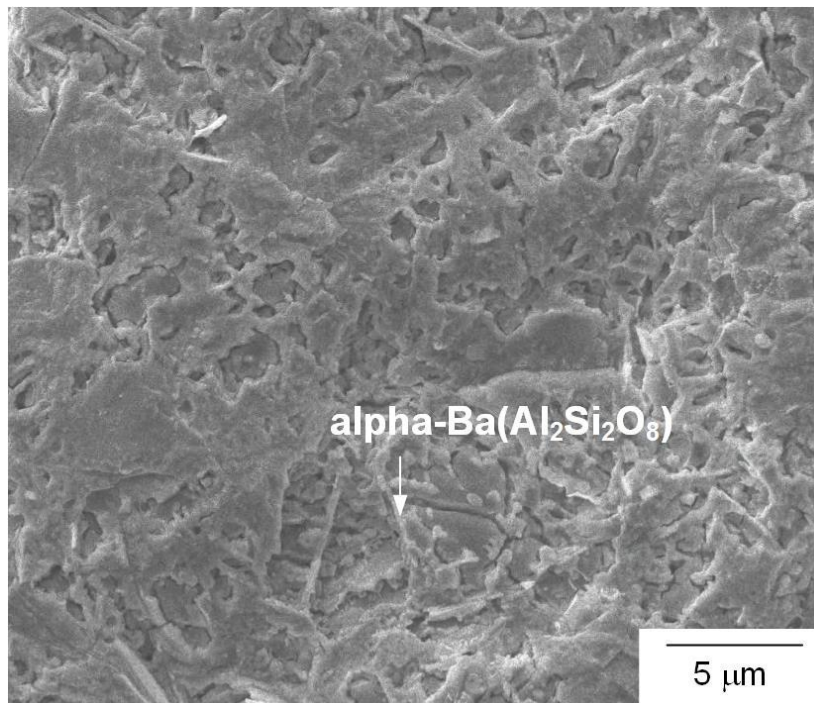


(b)

Fig. 42 A fracture surface region of the 1000 h-aged shear specimen shown in the upper part of Fig. 41(a): (a) optical micrograph showing the observed region of SEM; (b) microstructure of GC-9 glass-ceramic.

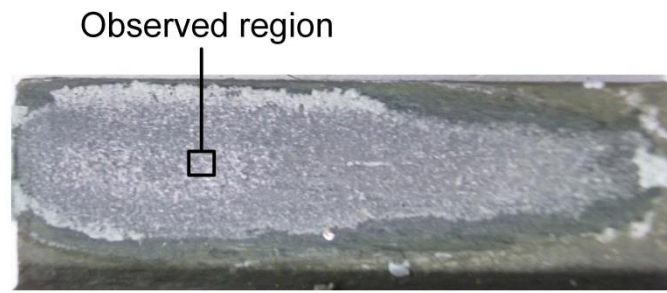


(a)

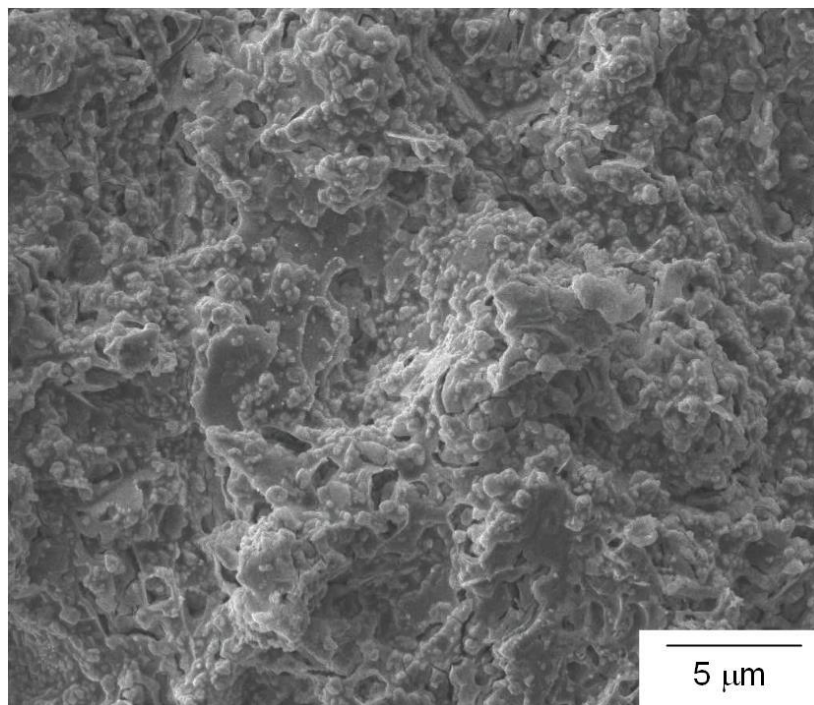


(b)

Fig. 43 A fracture surface region of the 1000 h-aged shear specimen shown in the lower part of Fig. 41(a): (a) optical micrograph showing the observed region of SEM; (b) microstructure of GC-9 glass-ceramic.

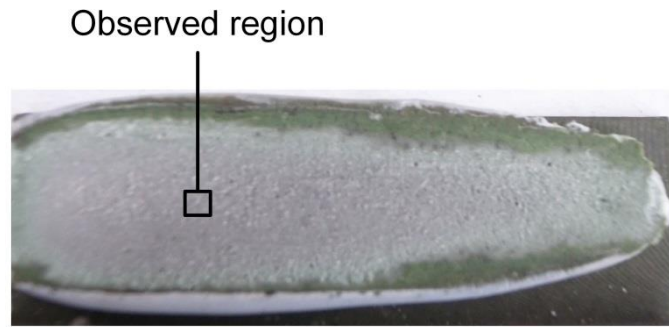


(a)

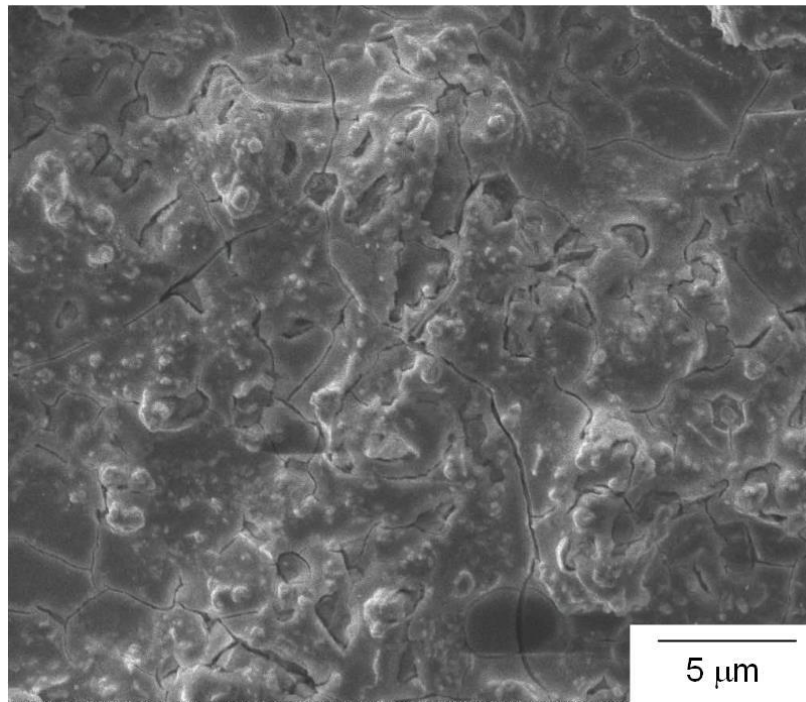


(b)

Fig. 44 A fracture surface region of the 1000 h-aged shear specimen shown in the upper part of Fig. 41(b): (a) optical micrograph showing the observed region of SEM; (b) microstructure of GC-9 glass-ceramic.



(a)



(b)

Fig. 45 A fracture surface region of the 1000 h-aged shear specimen shown in the lower part of Fig. 41(b): (a) optical micrograph showing the observed region of SEM; (b) microstructure of GC-9 glass-ceramic.

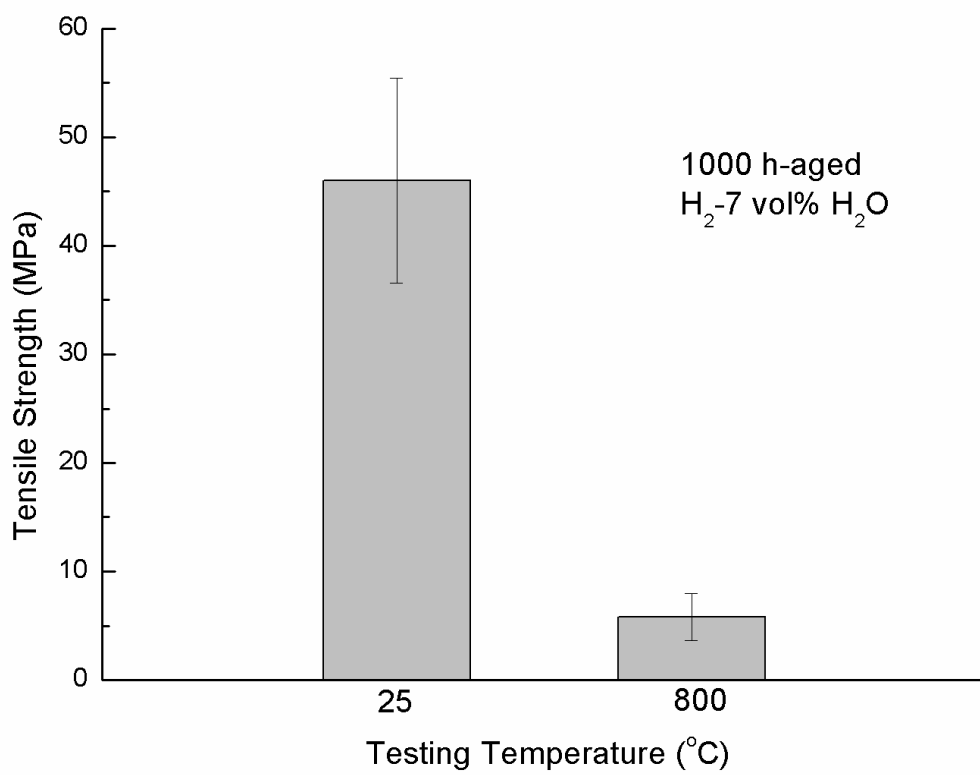
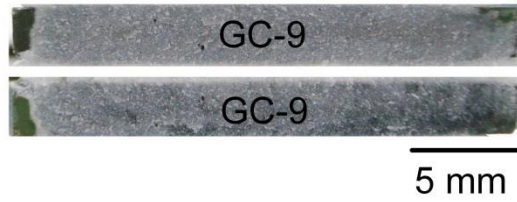


Fig. 46 Tensile strength of 1000 h-aged joint specimens tested in H₂-7 vol% H₂O at room temperature and 800 °C.

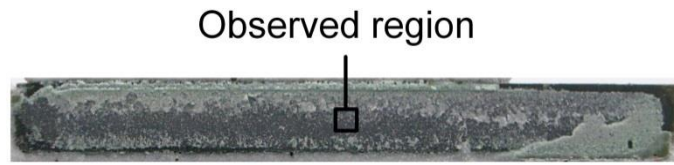


(a)

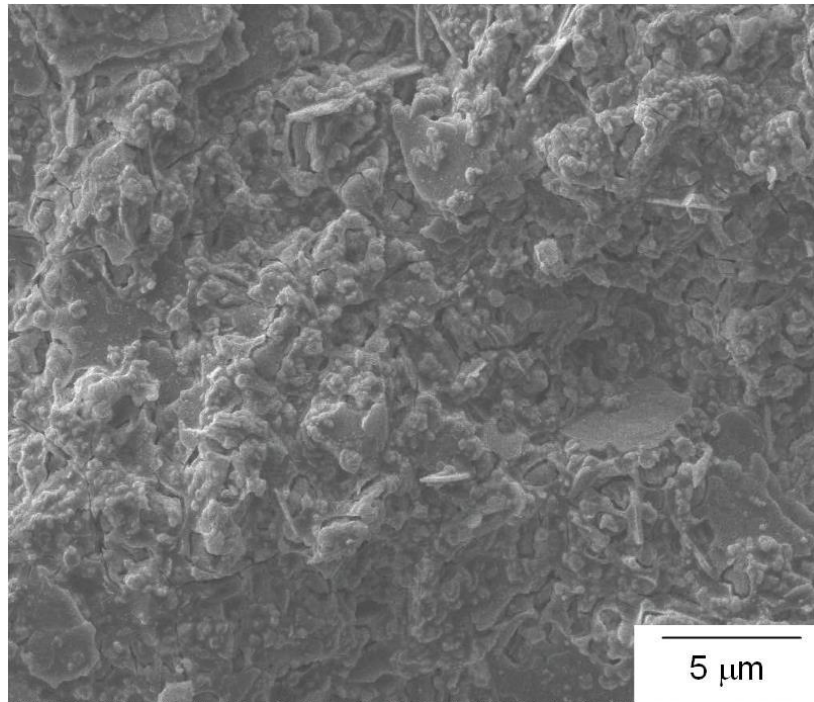


(b)

Fig. 47 Failure patterns of 1000 h-aged tensile specimens tested in H_2 -7 vol% H_2O at (a) room temperature and (b) 800 °C.

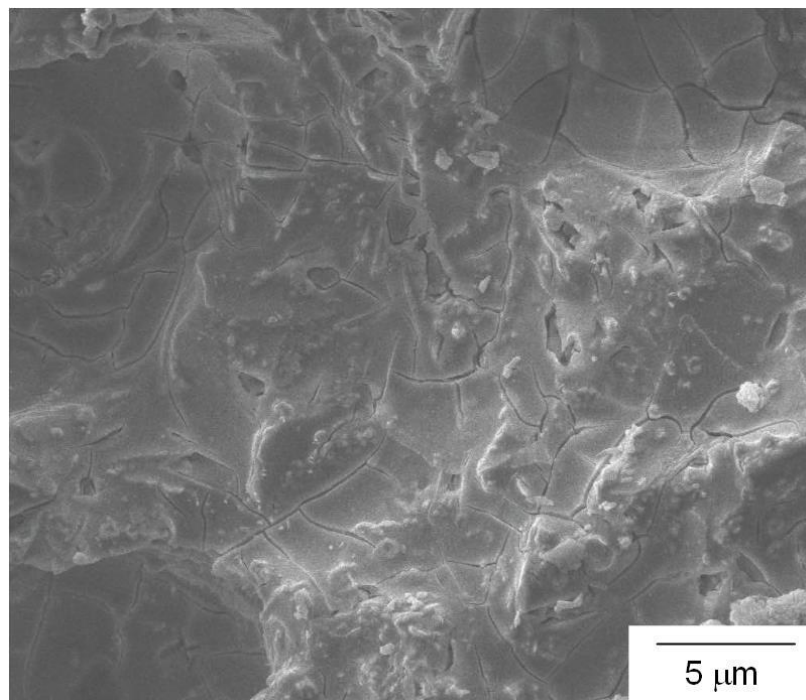
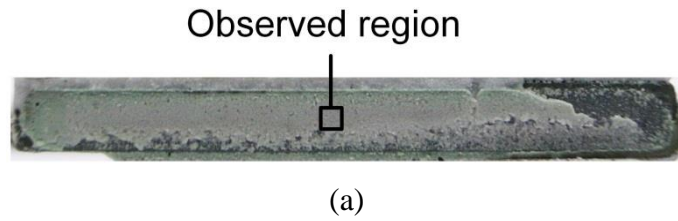


(a)



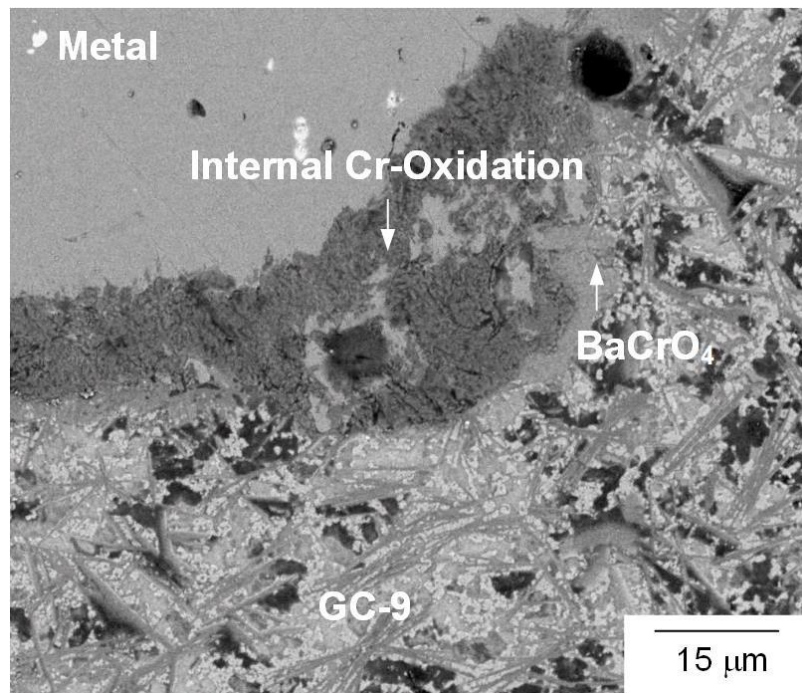
(b)

Fig. 48 A fracture surface region of the 1000 h-aged tensile specimen shown in the upper part of Fig. 47(b): (a) optical micrograph showing the observed region of SEM; (b) microstructure of GC-9 glass-ceramic.

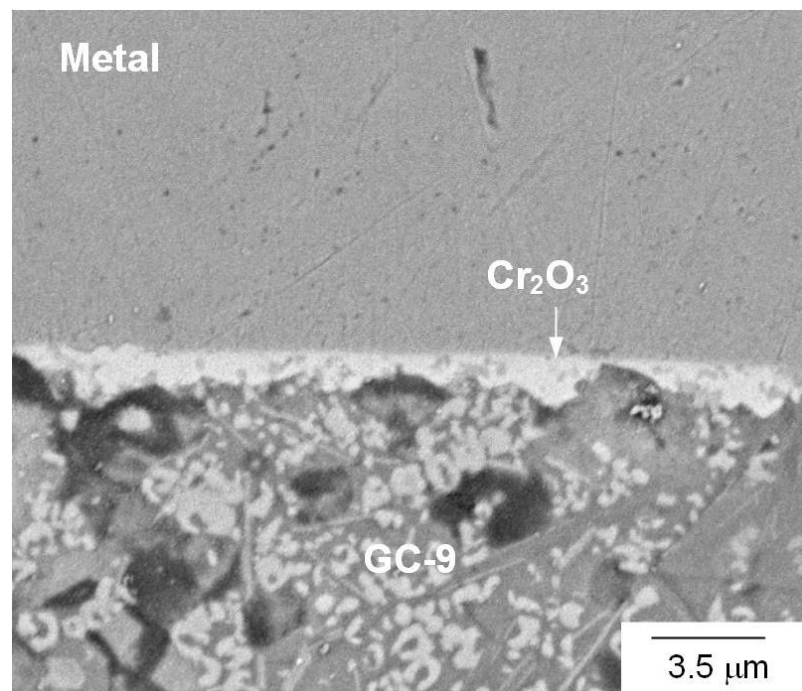


(b)

Fig. 49 A fracture surface region of the 1000 h-aged tensile specimen shown in the lower part of Fig. 47(b): (a) optical micrograph showing the observed region of SEM; (b) microstructure of GC-9 glass-ceramic.



(a)



(b)

Fig. 50 SEM micrographs (BSE mode) of a cross section of an interface between the GC-9 and Crofer 22 H in a 1000 h-aged specimen: (a) low magnification view; (b) high magnification view

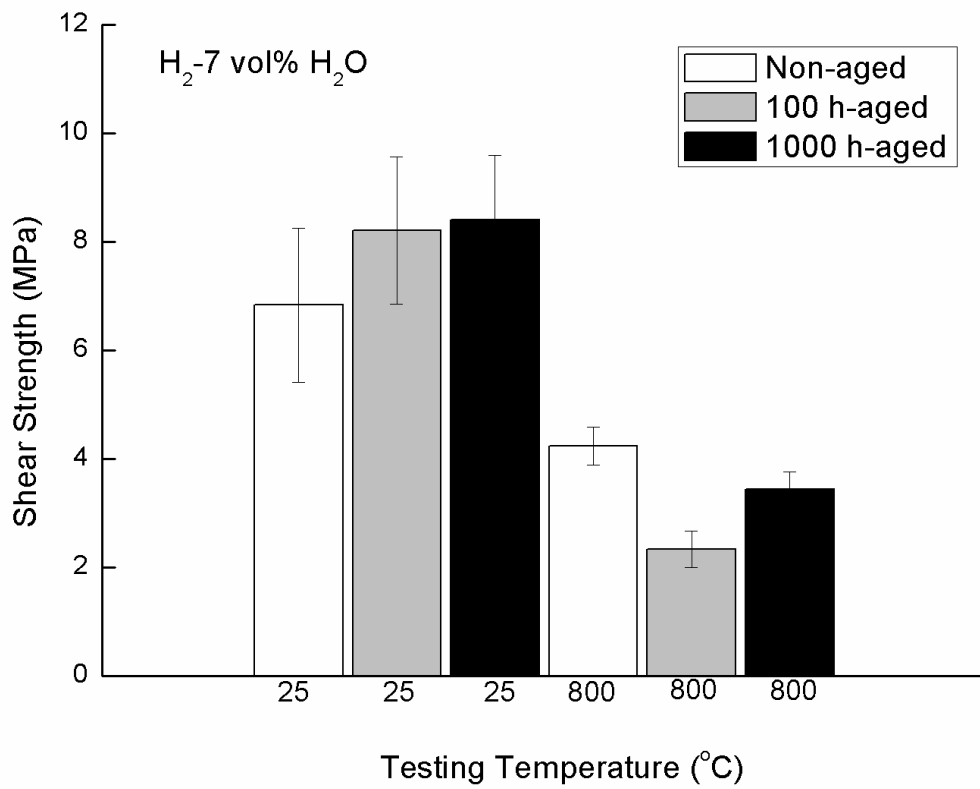


Fig. 51 Shear strength for variously aged specimens tested in H₂-7 vol% H₂O at room temperature and 800 °C.

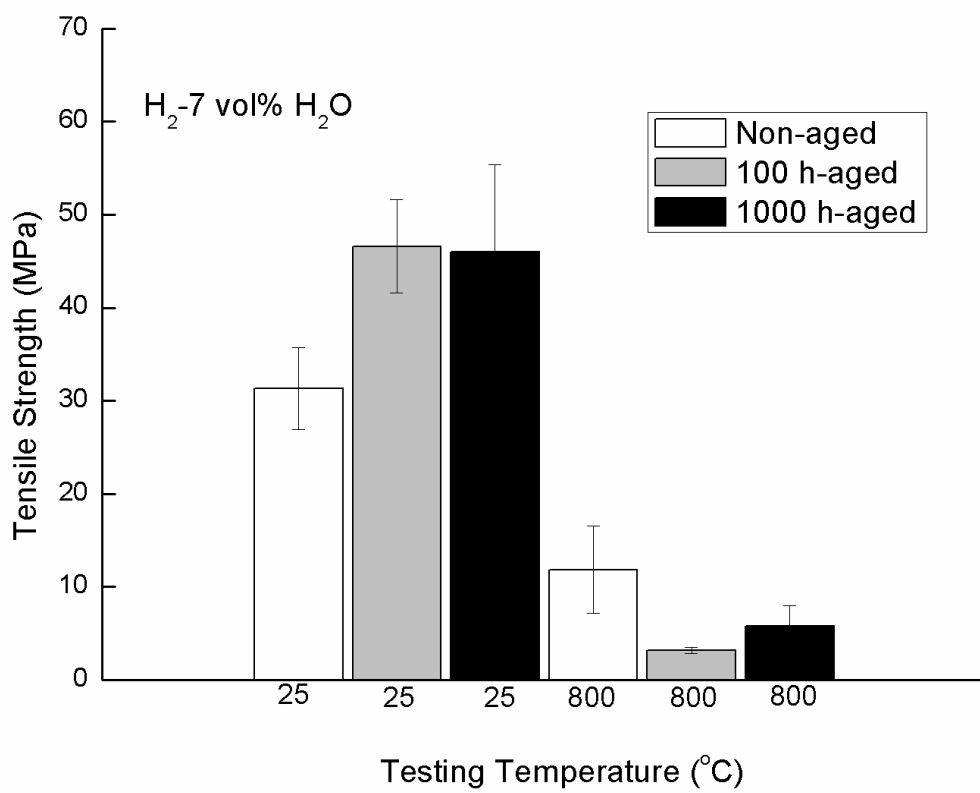
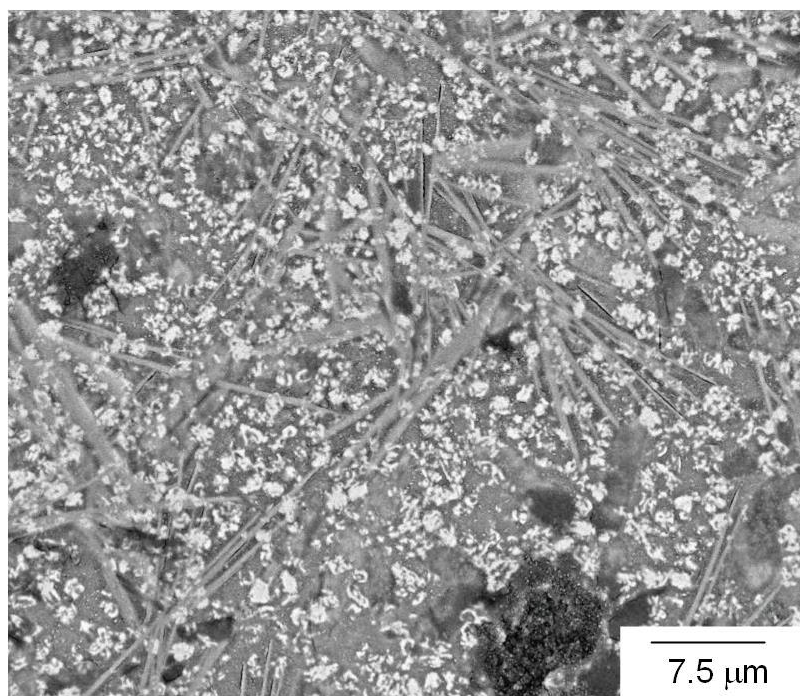
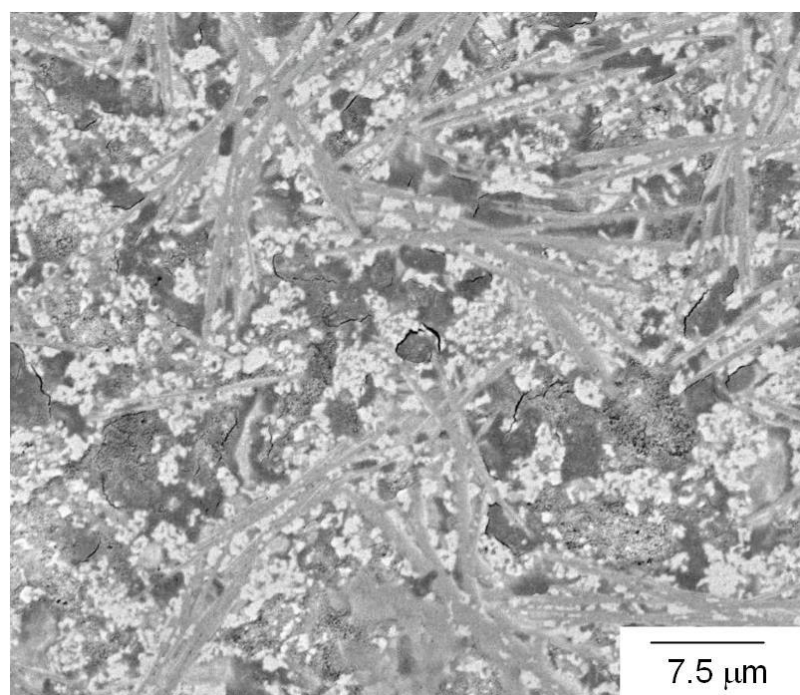


Fig. 52 Tensile strength for variously aged specimens tested in H₂-7 vol% H₂O at room temperature and 800 °C.

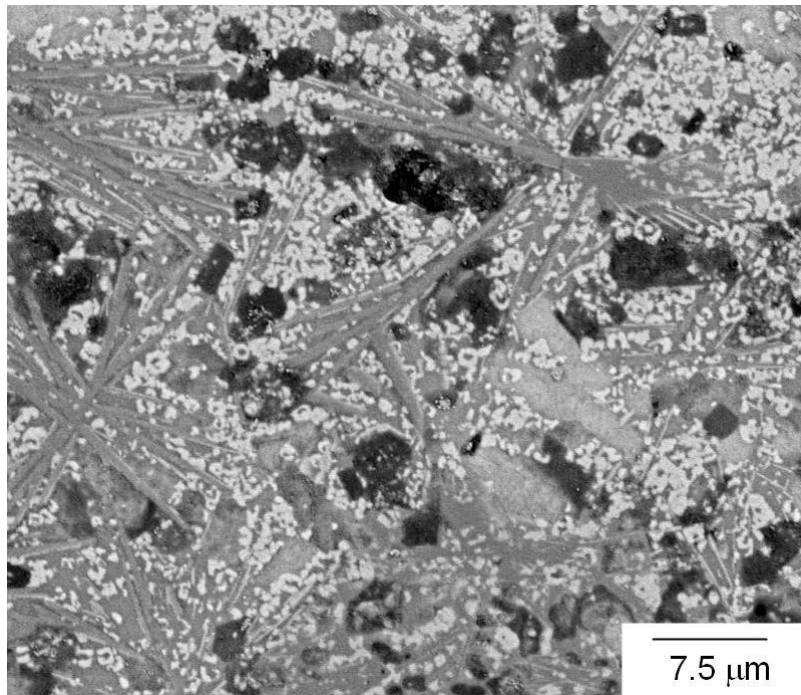


(a)



(b)

Fig. 53 SEM micrographs (in BSE mode) of variously aged GC-9 glass-ceramics: (a) non-aged; (b) 100 h-aged; (c) 1000 h-aged.



(c)

Fig. 53 (continued)

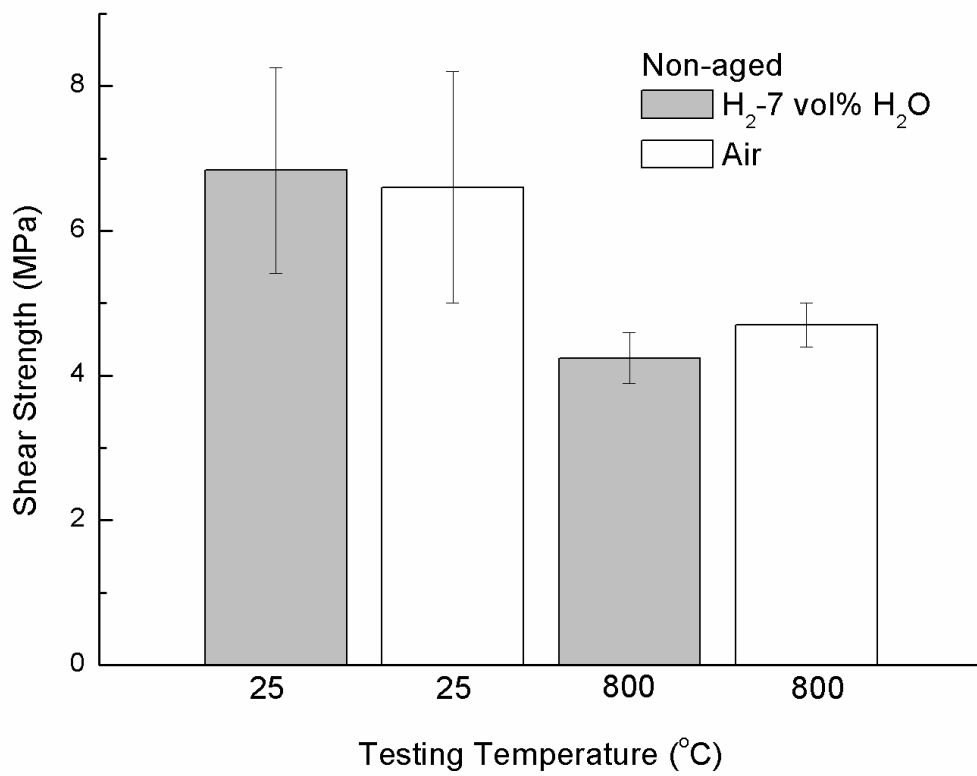


Fig. 54 Shear strength of non-aged joint specimens tested in H₂-7 vol% H₂O and air at room temperature and 800 °C. (Data of air are taken from Ref. [30].)

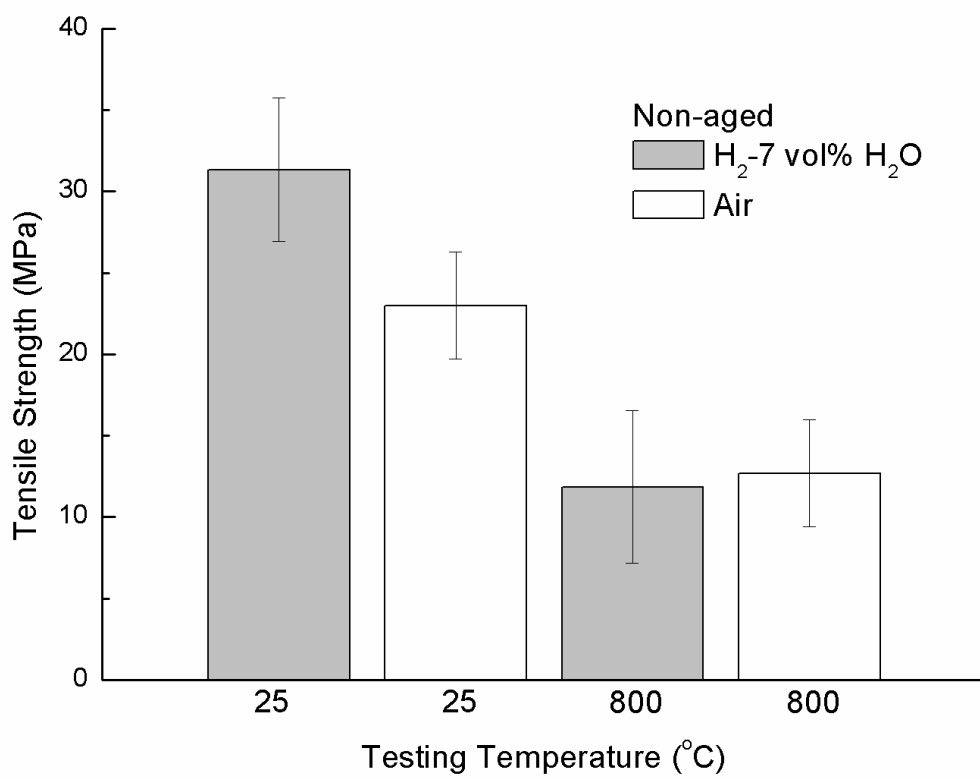


Fig. 55 Tensile strength of non-aged joint specimens tested in H₂-7 vol% H₂O and air at room temperature and 800 °C. (Data of air are taken from Ref. [30].)

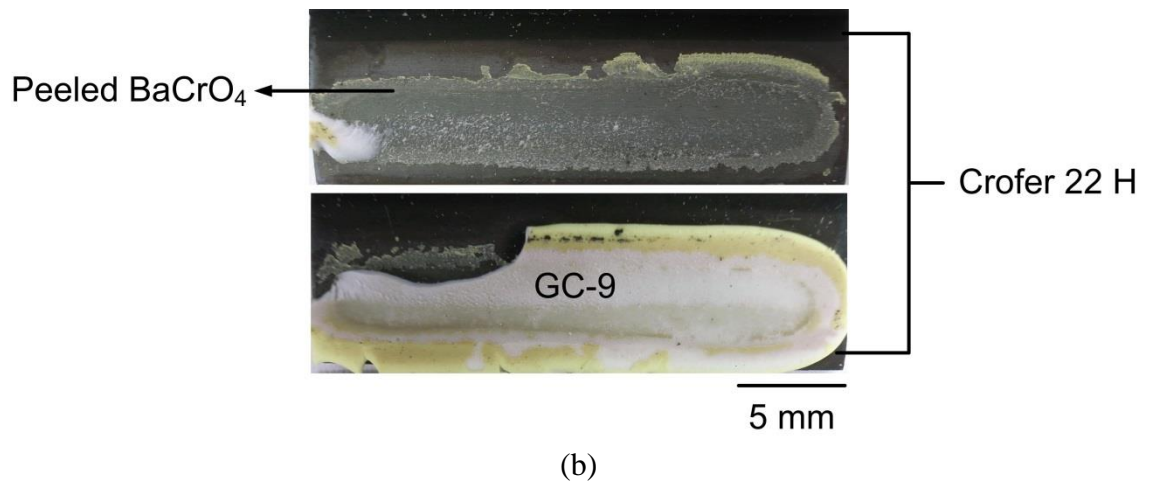
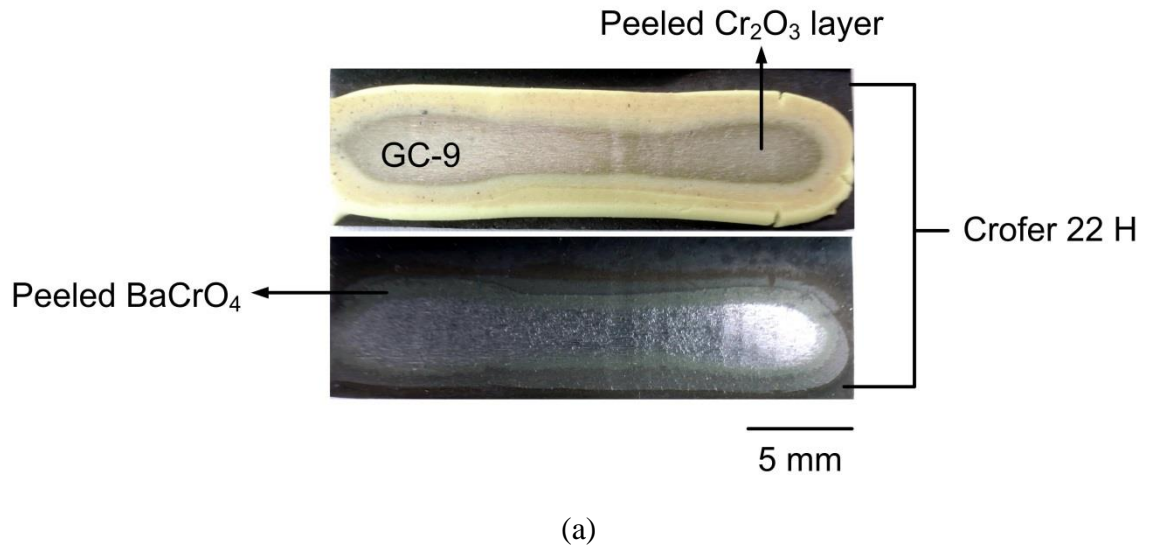
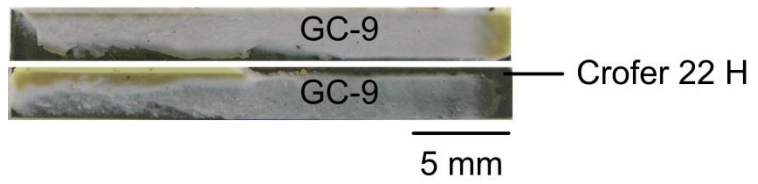
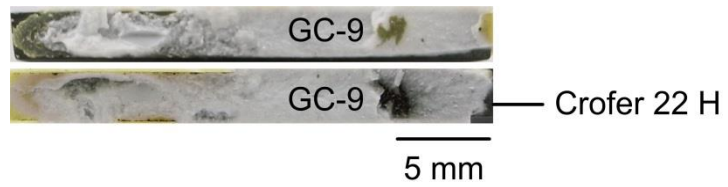


Fig. 56 Failure patterns of non-aged shear specimens tested in air at (a) room temperature and (b) 800 °C. [30]



(a)



(b)

Fig. 57 Failure patterns of non-aged tensile specimens tested in air at (a) room temperature and (b) 800 °C. [30]

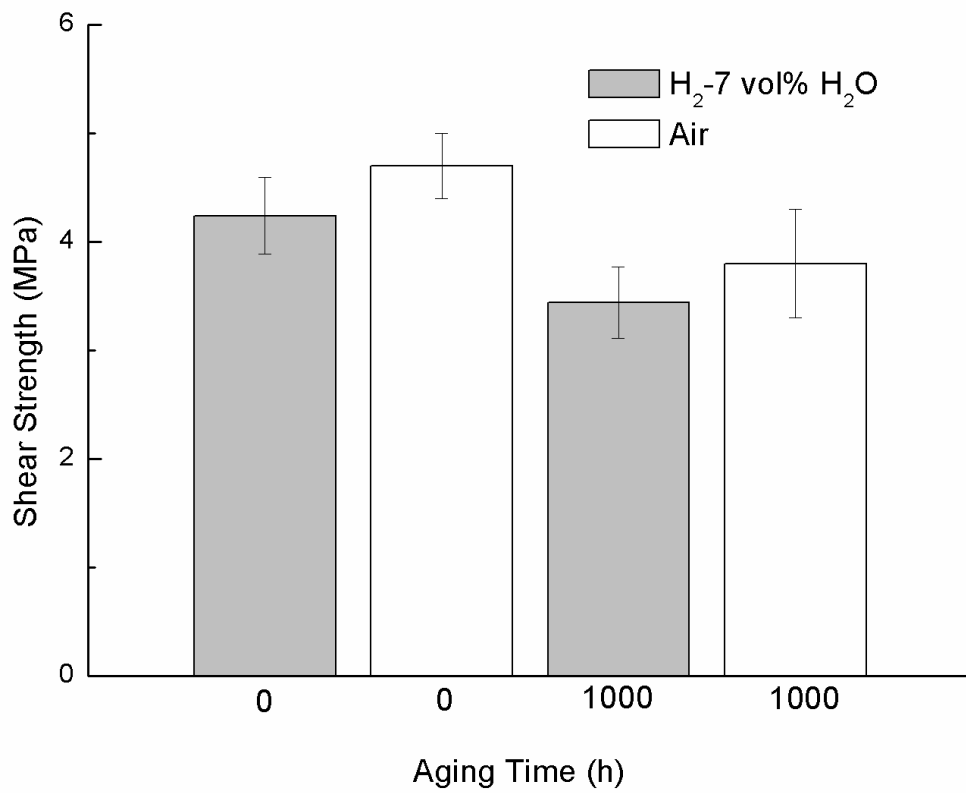


Fig. 58 Shear strength for variously aged specimens tested in H₂-7 vol% H₂O and air at 800 °C.